physics

Selected problems of condensed phase physics

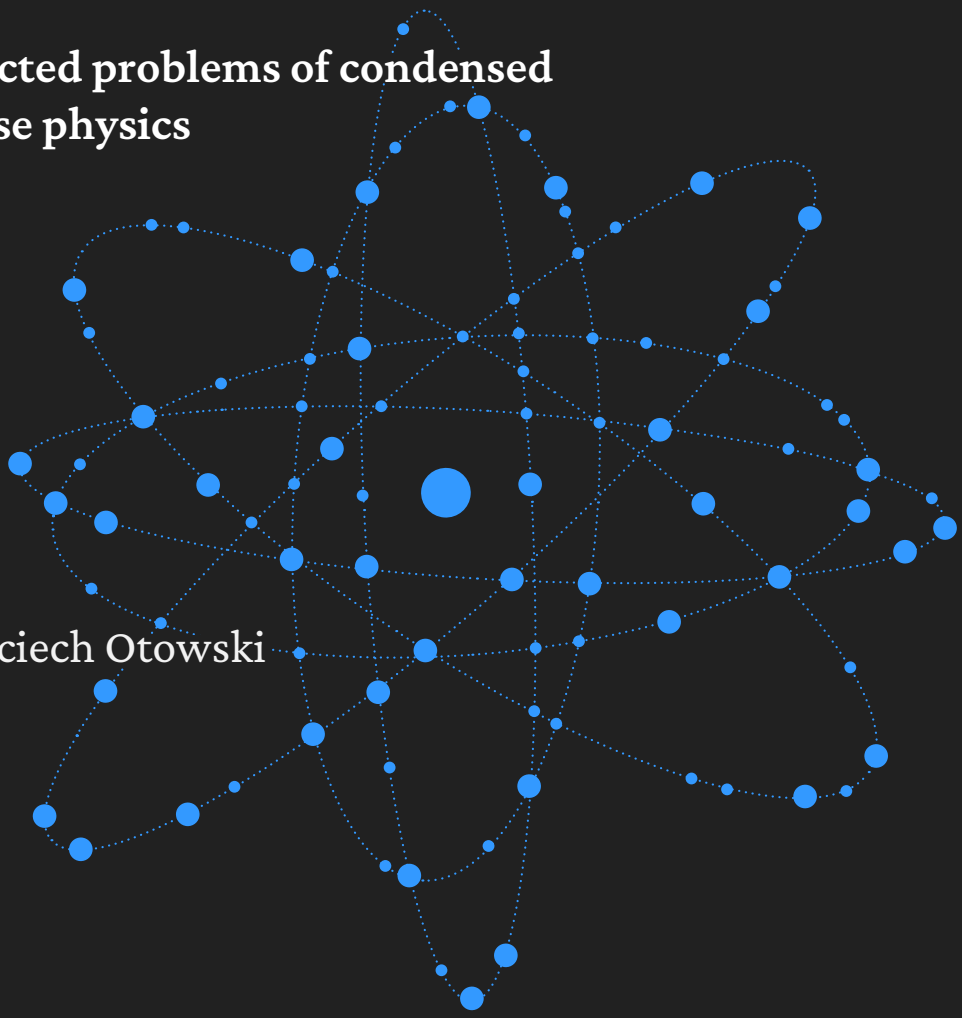

Wojciech Otowski

Kraków 2021

Cracow University of Technology

physics

Selected problems of condensed phase physics

Wojciech Otowski

Kraków 2021

This text was published as a part of the project 'Excellence programming – PK XXI 2.0 Cracow University of Technology development program for the years 2018–22'.
Funding from EU: 18,048,774.96 PLN

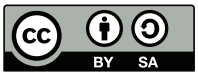

eISBN 978-83-66531-55-0

Online edition
5,5 publisher's sheets

Wydawnictwo PK, ul. Skarżyńskiego 1, 31-866 Kraków; 12 628 37 25, fax 12 628 37 60
wydawnictwo@pk.edu.pl
www.wydawnictwo.pk.edu.pl
Correspondence address: ul. Warszawska 24, 31-155 Kraków

CONTENTS

INTRODUCTION

The book presents basic information on selected issues of condensed phase physics. This field of study provides one with the possibility of specialising within many areas of "condensed matter physics", which is the largest branch of physics worldwide. As an elaboration designed for students (undergraduate and graduate), it contains elementary foundations of the issues discussed. The aim was to present a few topics showing the development of condensed phase physics.

Condensed phase physics is a field of physics that deals with the macroscopic and microscopic physical properties of matter. Thus, to understand many of the condensed phase issues and, in particular, the rapidly developing field of nanophysics, it is necessary to understand the basics of this field of physics.

For physicists, this handbook can be a way to understand how differently we analyse macroscopic physics relative to nanophysics. For engineers, this handbook can be helpful in understanding that the technology of tomorrow is constructed using materials from atoms via the nanoscale up to macroscopic phenomena and properties. And what interpretation difficulties introduce the world at the nano scale.

1. CRYSTALLINE STRUCTURE

Crystalline bodies are solids in which atoms, ions or molecules are arranged regularly in relation to each other.

Crystalline bodies, hereinafter referred as "crystals", i.e. systems in which the ordering includes the entire body, are called covalent crystals when they are composed of atoms, ionic crystals when they are composed of ions and molecular crystals when they are composed of molecules.

This specific structure is associated with many interesting optical, mechanical, electrical and magnetic properties. One of the basic attributes of crystals is anisotropy. Anisotropy is the dependence of analysed properties on the direction of observation. It is an experimental fact that all crystals exhibit anisotropy in elasticity and growth velocity. Other properties can be both anisotropic and isotropic (independent of the direction). Many crystals have the ability to twist the light polarisation plane.

From the microscopic point of view, regularity of the arrangement of atoms (ions, molecules) means that they retain their position in a three-dimensional space (showing a long-range order), determined in relation to other atoms. Such a spatial structure (a symmetrical arrangement of atoms) is invariant in time (except for phase transitions), despite the fact that atoms perform vibrations in relation to their positions of equilibrium. Symmetry results from the fact that atoms are arranged in a repetitive manner. It can be stated that any repetition operation can be represented by one of the three operations of symmetry: translation, rotation and reflection. This feature makes it possible to specify the symmetry rules that describe the structures that have been created. It is worth mentioning here that there are so-called quasicrystals, with a non-periodic lattice with, for example, a fivefold axis of symmetry[1].

The basic geometric solid that one can distinguish in the construction of crystals is a parallelepiped. By moving it in three dimensions, one creates a geometric lattice, which is a three-dimensional scheme of the internal structure of crystals. A spatial lattice defined in this way is an abstract concept. However, if one "superimposes" on the lattices a "base" containing physical elements of a crystal structure (atoms, ions, molecules) one will obtain a three-dimensional structure called a crystal lattice. The resulting elementary parallelepiped containing atoms, ions or molecules, being the smallest repeatable part of the crystal structure, is called an elementary cell

[1] In 2011, Dan Szechtman received the Nobel Prize in Chemistry for his discovery of quasicrystals in 1984.

(quasicrystals with a seemingly regular structure make it impossible to distinguish their elementary cells).

The basic feature of a crystal is its invariance in relation to the symmetry operation of translation $(\vec{T})$. Translation symmetry results from the fact that the same atoms in the same environment are repeated in different lattice nodes (lattice points) and that such a node (point) can be "superimposed" on another one as a result of symmetry operations. The elementary cells transformed by translation can be used to fill the entire space:

$$\vec{T} = n_1\vec{\mathbf{a}} + n_2\vec{\mathbf{b}} + n_3\vec{\mathbf{c}}, \tag{1.1}$$

where n_i are integers, and $\vec{\mathbf{a}}$, $\vec{\mathbf{b}}$, $\vec{\mathbf{c}}$ are translation vectors associated with elementary cells (lattice vectors).

A crystal does not change when we move it by any vector that is a linear combination of translation vectors.

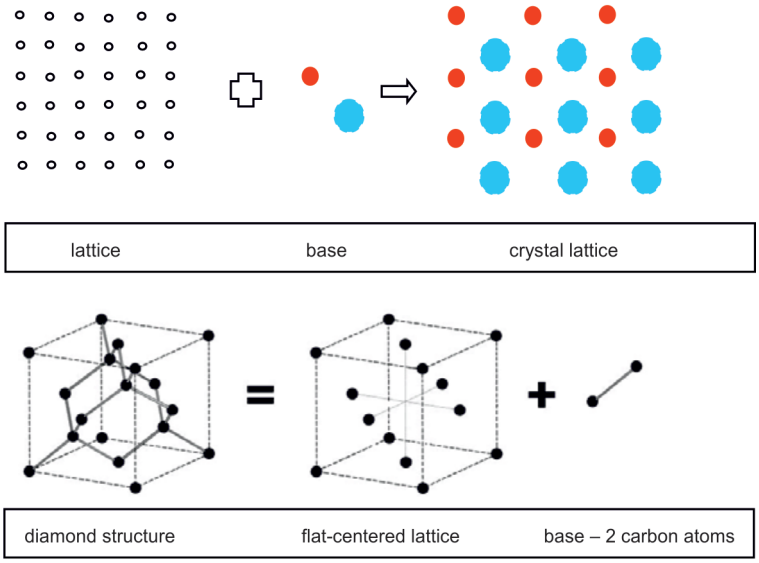

Fig. 1. Scheme of the "construction" of a flat (two-dimensional – top drawing) and spatial (three-dimensional – bottom drawing) crystal lattice. A spatial lattice is built using the example of a diamond structure

Rotary symmetry describes the fact that an identical image of a crystal is observed after its rotation around a selected axis. One can state that a crystal has an n-fold axis if, after a rotation around this axis by the angle $\frac{2\pi}{n}$ (radians), the crystal passes into itself. The multiplicity of the symmetry axis is limited to n equal to 1, 2, 3, 4 and 6. It can be demonstrated that no other axis of symmetry is compatible with the translation symmetry of the lattice.

This evidence leads to the formula:

$$\cos\alpha = \frac{1-N}{2}, \tag{1.2}$$

where N is an integer, and the angle $\alpha = 2\pi/n$.

Keeping in mind that $-1 \leq \cos\alpha \leq 1$ one gets $N = -1, 0, 1, 2, 3$, and thus $\alpha = 0, \frac{\pi}{3}, \frac{\pi}{2}, \frac{2\pi}{3}, \pi$ [1].

The centre of symmetry is a point which, as a result of the operation of inversion (transfer of a point from x, y, z to $-x, -y, -z$), makes it possible to obtain an identical arrangement of elements.

The plane of symmetry transforms the arrangement of elements into their image, created as if it were its mirror reflection.

The parallelepiped described by vectors $\vec{\mathbf{a}}$, $\vec{\mathbf{b}}$, $\vec{\mathbf{c}}$ forms an elementary cell. There is also the concept of a primitive cell built by vectors of the base but containing only one atom, i.e. the smallest elementary cell.

In 1850, August Bravais theoretically proved that crystals are made of parallelepipeds, which was confirmed by Laue[2] in 1912. According to Bravais, there are seven (non-equivalent) types of lattices in which atoms (ions, molecules) are distributed only in the corners. Since each corner is common to eight neighbouring cells, only 1/8th of each of these atoms belongs to a specific cell; as a result, the cell contains only one atom. The shape and size of an elementary cell are determined by the so-called lattice constants, which are the lengths of the cell edges a, b, c and angles α, β, γ between these edges; α – the angle between b and c, β – the angle between a and c, and γ – the angle between a and b. A cell defined in this way is called a primitive cell (Fig. 2a).

Apart from spatial lattices having nodes (points) only in the corners of cells, there are also lattices in which nodes (points) are located in the centres of walls or in the geometric centres of cells. Such arrangements are formed by the overlapping of two or more primitive cells.

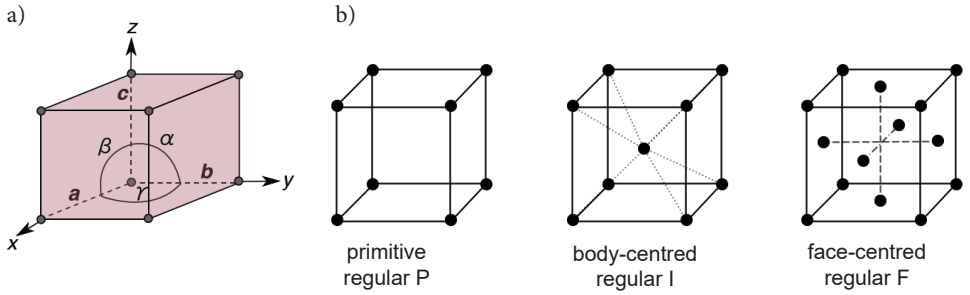

Fig. 2. a) a primitive cell [6], b) three types of a regular cell [7]

[2] In 1914, Max Theodor Felix von Laue received the Nobel Prize for Physics for discovering the phenomenon of X-ray diffraction on crystals.

The result is the following manner of distributing nodes (atoms, ions or molecules) in a cell:

- P – primitive, only corner knots, 1 atom per cell;
- I – body-centred, nodes in corners, an additional node in the centre of the cell, 2 atoms per cell;
- F – face-centred, nodes in corners, additional nodes on the cell walls, 4 atoms per cell;
- C – centred in the middle of the base, 2 atoms per cell.

Given the values of lattice constants *a*, *b*, *c* and angles α, β, γ seven crystallographic systems can be determined.

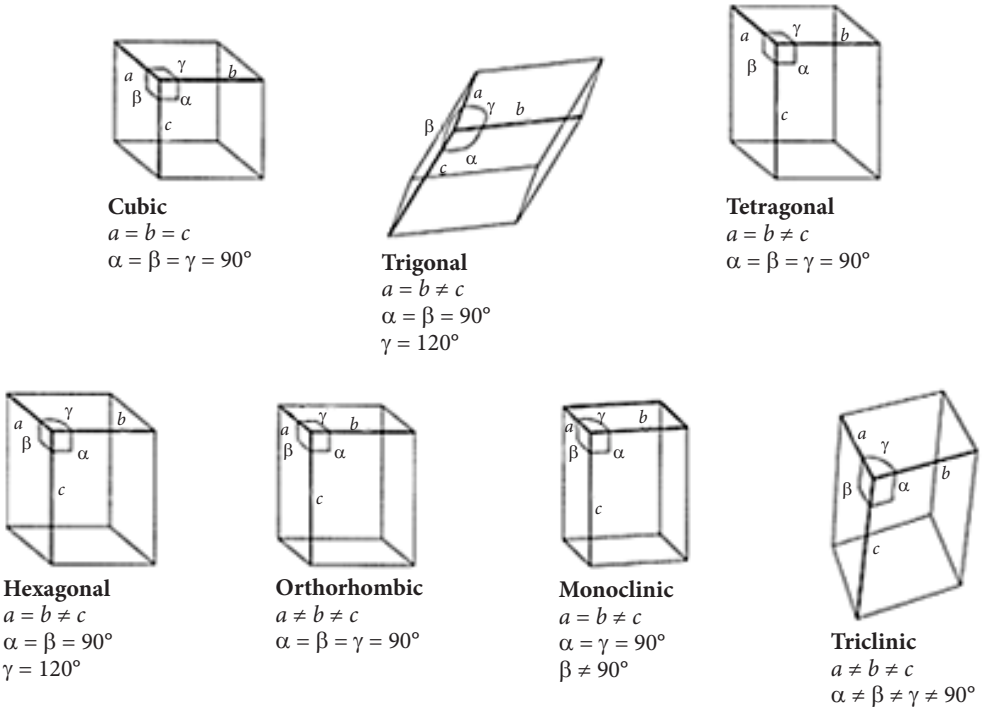

Cubic
$a = b = c$
$\alpha = \beta = \gamma = 90°$

Trigonal
$a = b \neq c$
$\alpha = \beta = 90°$
$\gamma = 120°$

Tetragonal
$a = b \neq c$
$\alpha = \beta = \gamma = 90°$

Hexagonal
$a = b \neq c$
$\alpha = \beta = 90°$
$\gamma = 120°$

Orthorhombic
$a \neq b \neq c$
$\alpha = \beta = \gamma = 90°$

Monoclinic
$a = b \neq c$
$\alpha = \gamma = 90°$
$\beta \neq 90°$

Triclinic
$a \neq b \neq c$
$\alpha \neq \beta \neq \gamma \neq 90°$

Fig. 3. Seven crystal systems [2]

Consequently, 28 Bravais lattices can theoretically be obtained by assembling seven crystal systems and four ways of centring (P, C, I, F – 7 x 4 = 28). It turns out, however, that in a three-dimensional (3D) space, there are only 14 different Bravais lattices [3]. In a two-dimensional space (2D), on the other hand, there are 5 different Bravais lattices.

Table 1

Crystal systems and possible 3D Bravais lattices

SYSTEM	P	C	I	F
regular	yes		yes	yes
tetragonal	yes		yes	
hexagonal	yes			
trigonal	yes			
rhombic	yes	yes	yes	yes
monoclinic	yes	yes		
triclinic	yes			

Simple (macroscopic) elements of the symmetry of crystal systems can be described as follows:

- a regular system – four triple axes along the diagonal of the elementary cell;
- a tetragonal system – the quadruple axis is always assumed to be parallel to the z axis, the lattice parameters a and b are equal;
- a hexagonal system – the x and y axes form an angle of 120° and are perpendicular to the six-fold axis parallel to the z axis;
- a trigonal system – one triple axis;
- a rhombic system – three axes twice perpendicular to each other;
- a single-axis system – one double axis;
- a triclinic system – no special elements.

Bravais space lattices are also called translation lattices, because they can be obtained by translating any node. For example, for a body-centred regular system (I), the permitted translations are:

$$a,\ b=a,\ b=c,\frac{a+b+c}{2}. \tag{1.3}$$

Other elements of symmetry are the same as those occurring in crystals (centre of symmetry, axis of symmetry and plane of symmetry). As mentioned above, the structure of a lattice does not change if we perform a rotation around one-, two-, three-, four- and six-fold axes of symmetry; analogously for rotations by 2π, $\frac{2\pi}{2}$, $\frac{2\pi}{3}$, $\frac{2\pi}{4}$, $\frac{2\pi}{6}$ radians. There is no lattice that can lead to a transition into itself through other rotations, especially by $\frac{2\pi}{5}$ radians (compare this with quasicrystals!). In 1619, Kepler showed that there is no seven-fold axis of symmetry (Fig. 4).

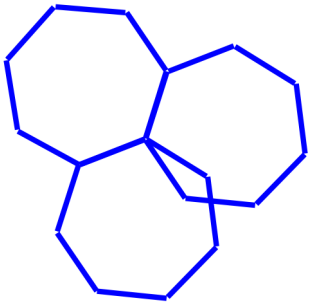

Fig. 4. Kepler's proof (1619) that there is no seven-fold axis of symmetry

Later works by Sohnke (1967), Schönflies (1891) and Fiodorov (1892) demonstrated that it is possible to create space lattices with certain special types of symmetry, such as screw axes or mirror-translation planes. In the case of a screw axis, the lattice passes into itself when we rotate it by 120° around the axis of symmetry and, simultaneously, move it parallel to the axis by ⅓ of the lattice spacing. Consideration of these additional elements of symmetry leads to 230 possible types of space lattices.

The choice of an elementary cell in the shape of a parallelepiped is not clear. Usually, it is chosen so that the shape of its walls reflects the symmetry of the lattice, and its volume is minimal, the number of right angles between the edges is maximal, and the nodes (points) are in positions conforming to one of Bravais' 14 cells. However, for any lattice with a Bravaisian-centred elementary cell, one can always create a primitive, non-centred cell. Such a cell is known as the Wigner-Seitz simple cell[3]. To create such a cell, a given node (point) of the space lattice must be connected with straight segments to the nearest nodes (points). The planes perpendicular to those segments are then guided though the centres of those segments. The intersecting planes form an area called the Wigner-Seitz cell. These are polyhedrons that can tightly fill the space.

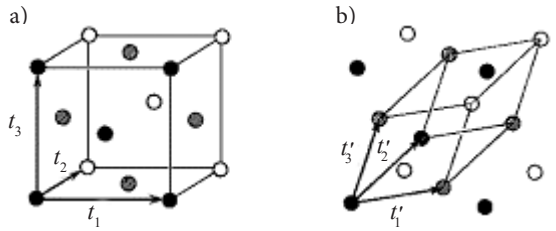

Two ways of selection of an elementary cell in a wall-centred cubic lattice:
a) high-symmetry cell, b) primitive cell

Fig. 5. Selection of a 3D elementary cell (upper part) and a 2D elementary cell (lower part) [4]

[3] Eugene Paul Wigner, an American physicist and mathematician, winner of the Nobel Prize for Physics; Frederick Seitz, an American physicist.

Using the definition of an elementary cell and primitive cell, the volume of these cells can be compared as described below (Fig. 6).

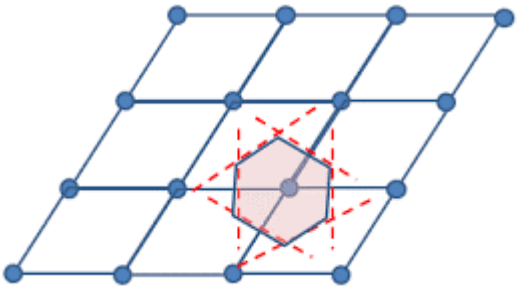

Fig. 6. Volume of primitive cells

In regular crystals, the directions that are three orthogonal axis directed parallel to the edge of the cube are usually determined by a notation composed of three natural numbers, as small as possible, one next to the other (in a row) placed in square brackets – [uvw]. Such a notation is called the Miller indices of *L* straight line (lattice straight line). These are the coordinates of the intersection point (node) of this line with one of the axes of the crystal in the reference system defined above. If the straight line passes through the origin of the coordinate system, the total coordinates of the first node (point) are the indices of the line. If the numbers are not integers, they must be reduced to a common denominator. The sense (the direction opposite to the one given) must be marked with a minus sign placed above the number. For example, [100] represents the direction parallel to one of the three axes (edges) of a cube. The notation [$\bar{1}$00] indicates the opposite direction (opposite turn). The notation [110] corresponds to the direction of the diagonal of the cube wall, and the notation [111] represents the direction along the diagonal of the cube.

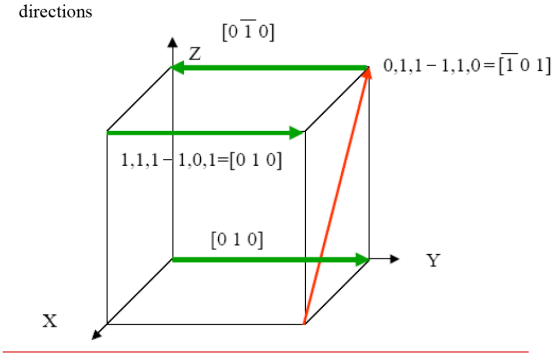

Fig. 7. Symbols for notation of the Miller indices of the lattice straight line

The orientation of planes in a crystal (Miller's indices for planes) is presented as a set of three numbers in round brackets (*hkl*). The position and orientation of planes is determined by three points in the plane which do not lie on a single line. If each point lies on a crystallographic axis, the plane can be determined by stating the position of these points along the axis in fixed units of the lattice. For example, if atoms defining a plane have the coordinates (4.0.0), (0.1.0) and (0.0.2) in relation to the axis vectors from the beginning of the system, the plane can then be defined as three numbers: 4, 1, 2. Using the inverse of these numbers, 1/4, 1 and 1/2 reduced to three first numbers relative to each other with a common denominator, one obtains the numbers *h*, *k*, *l*, i.e. the Miller indices of the plane:

$$(4,1,2) \rightarrow \left(\frac{1}{4},1,\frac{1}{2}\right) \rightarrow \left(\frac{1}{4},\frac{4}{4},\frac{2}{4}\right) \Rightarrow (142) = (hkl). \tag{1.4}$$

For an intersection at infinity (∞), the Miller index is zero (0). For example, symbolically:

$$m = \infty, n = 2, p = \infty \;\rightarrow\; \frac{1}{m} : \frac{1}{n} : \frac{1}{p} \;\text{ thus }\; 0,\frac{1}{2},0 \;\Rightarrow\; (hkl) = (010). \tag{1.5}$$

Therefore, the symbols (100), (110), (111) define three crystalline planes, perpendicular to three directions [100], [110], [111]. Thus, the zero index (0) in the symbol of a lattice plane indicates that this plane is parallel to the associated crystal axis (for example, the *h* indicator is related to the *X* axis). Miller indices in curly brackets {*hkl*} indicate that the described plane is the wall of the crystal.

The indices (*hkl*) define a single plane or a set of parallel planes. If the plane crosses the axis on the negative side, the corresponding index is marked with a minus sign above the number. The higher the Miller index value, the closer the given plane is located to the origin of the system. For example, if the plane *P* cuts the segments 3a, 2b, 2c on the crystallographic axes (i.e. $m = 3$, $n = 2$, $p = 2$), the inverse of these numbers is equal to 1/3, 1/2 and 1/2, respectively. The smallest common multiple is 6 – 2/6, 3/6, 3/6; as a result, the plane is (233) (see Fig. 8).

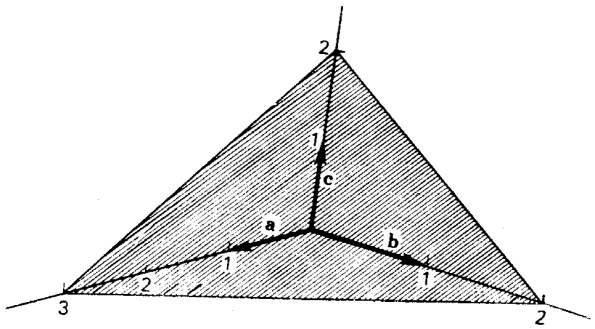

Fig. 8. Example: intersection points 3, 2, 2, the smallest common multiple of 6, plane (233) [5]

Base elements (atoms, ions or molecules) are considered in crystallography to be rigid spheres with the radius R. This assumption implies, for example, that for a regular simple lattice, the number of atoms per cell is one; 8 corners after 1/8th part of the sphere (atom) in the corner $\Rightarrow$ one atom. We further assume that atoms (spheres) come into contact with each other. There is a natural problem of how to pack the spheres in a three-dimensional space so that the free space is as small as possible; in other words, how can the packing density be the highest (packing factor $W_u = N \cdot \frac{V_{\text{atom}}}{V_{\text{cell}}}$ or the ratio of the volume of the crystal occupied by N atoms treated as rigid spheres to the total volume of the cell).

In a regular simple structure, the atoms "touch each other" along the diagonal of the cube wall; the radius of the sphere is equal to half the length of the wall length $\frac{a}{2}$:

$$W_u = 1 \cdot \frac{\frac{4}{3}\Pi r^3}{a^3} = \frac{4\Pi\left(\frac{a}{2}\right)^3}{3a^3} = \frac{\pi}{6} \cong 0.52. \tag{1.6}$$

In a body-centred structure, the atoms "touch each other" along the diagonal of the cube; the radius of the sphere is equal to 1/4th of the length of the diagonal of the cube $\frac{a\sqrt{3}}{4}$:

$$W_u = 2 \cdot \frac{\frac{4}{3}\Pi r^3}{a^3} = \frac{4\Pi\left(\frac{a\sqrt{3}}{4}\right)^3}{3a^3} = \frac{\pi\sqrt{3}}{8} \cong 0.68. \tag{1.7}$$

In a face-centred structure, atoms "touch each other" along the diagonal of the cube wall; the radius of the sphere is equal to 1/4th of the length of the diagonal of the cube wall $\frac{a\sqrt{2}}{4}$:

$$W_u = 4 \cdot \frac{\frac{4}{3}\Pi r^3}{a^3} = \frac{4\Pi\left(\frac{a\sqrt{2}}{4}\right)^3}{3a^3} = \frac{\pi\sqrt{2}}{6} \cong 0.74. \tag{1.8}$$

For comparison, the packing factor of a diamond is relatively small and equal to 0.34.

In 1912, Laue conducted an experiment that started X-ray crystallography. Crystals and photographic film were placed on the path of an X-ray beam. After developing the film, it turned out that apart from the trace of the incident beam, there were traces of beams deflected from the main beam. Laue asked himself where the deflected bundles came from. The answer contained a statement that they were created as a result of reflection of X-rays by mutually parallel (virtual) planes – the

so-called lattice planes of the crystal. This type of bent beam is created only in those cases where reflections from atomic planes of the crystal interfere[4].

This phenomenon is well illustrated by the following diagram:

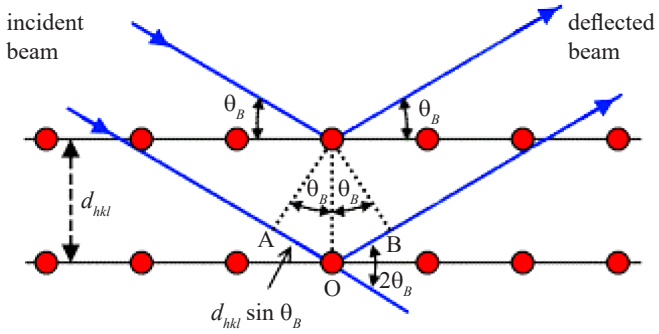

Fig. 9. Laue diagram (λ is the wavelength, θ_B is the angle of incidence and deflection, AO = OB = $d_{hkl} \sin\theta_B$ and d_{hkl} are the distances between planes

where λ is the wavelength, θ_B is the angle of incidence (and reflection); AO = OB = $d_{hkl} \sin\theta_B$ and d_{hkl} are the distances between planes. Regular structures are expressed by the formula (*a* is a parameter of the elementary cell of a crystal):

$$d_{hkl} = \frac{a}{\sqrt{h^2 + k^2 + l^2}}. \tag{1.9}$$

Therefore, under the condition of interference, one obtains:

$$n\lambda = 2d_{hkl} \sin\Theta_B. \tag{1.10}$$

The above formula represents Bragg's law. The law is fulfilled only for waves whose wavelength is equal to $\lambda \leq 2d$, which means that it is not possible to use visible light as an incident wave (*n* is an integer – so-called order of deflection).

Each X-ray beam reflected by the lattice planes can be characterised by the intensity and direction of propagation. The spatial distribution in the directions of reflected beams is determined by the symmetry and dimensions of the elementary cell. The number, the types and the mutual configuration of atoms in a cell influence only the intensity of the reflected beams. X-rays are the least sensitive to lattice defects (compared to electron and neutron radiation). Accurate measurements allow us to determine the relative positions of atoms within an elementary cell. This is due to the fact that only external electrons take part in the binding of atoms in the crystal. Most electrons are in energy states (energy shells), which are the same as in the isolated atom.

[4] Interference – the phenomenon of amplification and extinction of wave amplitude as a result of overlapping (superposition) of two or more waves. The prerequisite for interference is phase consistency (correlation) and frequency equivalence.

The following alkaline metals have a regular, spatially centred structure: Li, Na, K, Rb, Cs (at room temperature). The same type of structure: V, Cr, Nb, Mo, Ta and W, as well as Fe, Ti and Zr, was established within a certain temperature range. The lattice has one atom per node (point); the positions of the atoms are 0.0.0 and 1/2,1/2,1/2.

A hexagonal structure is formed by transition metals Sc, Ti, Y, Zr, Be, Mg, Zn, Cd and most rare-earth metals [1]. In many crystals, the symmetry of the distribution of external electrons not taking part in bonds is spherical.

Typical structures of metals, which constitute a majority of elements, have regular face-centred structures, regular body-centred structures and hexagonal structures [1].

Nobles metals, such as Cu, Ag and Au, higher-valence metals, such as Co, Ni, Rh, Pd, Ir and Pt, and nobles gases, such as Ne, Ar, Kr and Xe, have a regular wall-centred structure. The elementary cell contains four atoms in positions 0,0,0; 1/2,1/2,0; 1/2,0/1.2; 0,1/2,1/1. The elementary cell contains two atoms in positions 0.0.0 and 1/2.1/3.1/2.

Two specific structures are the diamond structure and the graphite structure. Si, Ge and Sn (in the α variety)[5], and of course crystalline carbon (C), have a diamond structure (which is an independent crystallographic structure). Each node (point) is assigned two atoms in positions 0.0.0 and 1/4,1/4,1/4. Graphite is a crystalline structure of C at room temperature. The hexagonal lattice consists of four atoms placed in the elementary cell at positions 0,0,0; 0,0,1/2; 1/3,2/3,0; 2/3,1/3,1/2.

References

[1] Kelly A. and Groves G.W., *Crystallography and Crystal Defects*, Longman Group, London 1970.
[2] http://www.expertsmind.com/questions/crystalline-solids-3016953.aspx [access: 23.04.19].
[3] Trzaska-Durski Z. and Trzaska-Durska H., *Podstawy krystalografii*, Wydawnictwo Politechniki Warszawskiej, Warszawa 2003 (in Polish).
[4] https://encrypted-tbn0.gstatic.com [access: 23.04.19].
[5] Kittel Ch., *Introduction to Solid State Physics*, John Wiley and Sons, New York 2004.
[6] https://www.doitpoms.ac.uk/tlplib/crystallography3/images/lattice_parameters.gif [access: 23.04.19].
[7] https://chemistryonline.guru/wp-content/uploads/2020/09/a3.png [access: 23.04.19].

[5] Tin forms allotropic varieties; the basic variety β (beta), known as white tin, durable at temperatures above 13.2°C, becomes the regular variety α (alpha) at lower temperatures.

2. TEXTURES

One can say that all substances have some physical and chemical properties. These different observed or measured characteristics make it possible to classify matter – in classical terms – as solids, liquids and gases. In the case of solids, one of the observed characteristics is texture. According to the definition provided in the Polish language dictionary published by the State Scientific Publishing House (PWN) in Warsaw in 2015, texture is "the internal structure of something, considered in terms of its characteristics and the way in which its components are arranged". By modifying this definition, depending on the examined object, let us analyse the relationship between observed textures and the physical properties of materials. However, it should be noted that in the case of so-called soft matter, due to optical birefringence, the observation of liquid crystal textures (in various thermodynamic states) is possible. While for condensed matter (e.g. Kevlar), the observation of a fibre pattern texture is possible without polarised light.

The ambiguity of the concept of texture is evident in many areas of life. In art, for example, the texture of a work of art is the features of its surface, derived from the materials used to make it. In music, the texture of a work determines its sound based on how different instruments mix their parts and the speed with which they are played. Even computer science uses the notion of texture. Texture mapping is a bitmap image applied to a surface in computer graphics.

In material science, the texture of a polycrystalline sample is defined as the image of the crystallographic distribution of grains. A sample with completely random grain distribution does not have a clear texture. If one can distinguish the preferred orientation, then one can observe a moderate or strong texture. Experience has shown that texture is visible in many engineering materials and is a "reflection" of the different properties of these materials.

Two extreme cases are total lack of texture (an isotropic sample on a scale larger than the size of crystallites) and an ideal monocrystalline texture (a clearly visible "geometry" of the image reflecting the degree of order).

The observation or measurement of texture can be classified into a group of measurements of the mechanical properties of solids performed with the senses (sensory tests such as touch to determine the extent to which something is rough or smooth, soft or hard).

Modern technological equipment is largely based on thin polycrystalline layers with a thickness at the level of nanometres or micrometres. This applies, for example, to all microelectronic circuits and most optoelectronic circuits, as well as to sensor and superconducting layers. Most thin-film textures can be classified as belonging to one of two different types:

1) in so-called fibre textures, the orientation of a certain plane of the grid is preferably parallel to the plane of the substrate;
2) in biaxial textures, the orientation of crystallites in the plane also tends to align with the sample.

The latter phenomenon is adequately observed in (almost) epitaxial growth processes, where certain crystallographic axes of crystals in the layer tend to align along a specific crystallographic orientation (single crystal) of the substrate.

Fig. 1. Kevlar carbon fibre pattern texture [1]

Examples of textures obtained in laboratories are presented in Figs. 1, 2 and 3. Obtaining a texture on demand is an important task in thin-film technology. For example, for oxide compounds intended for the production of transparent conductive films or surface acoustic wave devices (SAW), the polar axis should be aligned along the substrate; this effect should be visible in the image of the texture. Another example is cables made of high-temperature superconductors, which are formed as multilayer oxide systems embedded on metal strips. Obtaining a biaxial texture in the $YBa_2Cu_3O_{7-\delta}$ layers proved to be a decisive condition for obtaining sufficiently high critical currents [2]. *The SEM images in Fig. 3 indicate that $BaTiO_3$ promotes nucleation and assists the growth of Y211 faceted rods, which are observed on the top surface of the BaTiO seed crystal and melt-textured YBCO pellet. Both samples synthesized via route A and B. The $BaTiO_3$ epitaxial films were grown epitaxially on (100) $SrTiO_3$ substrates via pulsed laser deposition […]. The epitaxial $BaTiO_3$ was placed on the top of each of the Y123 pellets, with the film sur-face facing down. These sample assemblies were subjected to a series of thermal profiles that included initial heating to 940°C, followed by 960°C, before elevating to 1040°C and 1070°C for route A and B, respectively* [2].

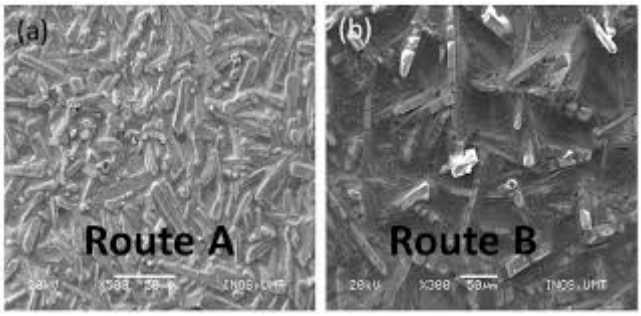

Fig. 2. Scanning electron microscope (SEM) images of YBCO textures

The degree of "clarity" of a texture frequently evolves, e.g. during the growth of a thin layer. The most pronounced textures are obtained only when the layer reaches a certain thickness. Thin film manufacturers need texture profile or texture gradient information to optimise the deposition process. However, the determination of texture gradients by e.g. X-ray scattering is not unambiguous, due to the heterogeneity of sample thickness.

It should be mentioned that modern technology has "forced" engineers to reproducibly and quickly produce micro cavities (grooves, holes) on the surface of machine elements, i.e. surface texturing. The primary objective of surface texture creation is to reduce frictional resistance and wear of mating parts. Surface texturing is used to give specific utility and aesthetic characteristics to the surface. It is used, among others, in polymer technology and in medicine (specialist medical elements). Surface texturing increases resistance to wear and tear and is used wherever the adhesive properties of surface layers (bonding, coating, printing techniques, biological and chemical activity of the surface) are important.

Laser micromachining is a surface texturing technique. It is a process where the thickness of the removed material is at a level of several micrometres or even millimetres with high accuracy.

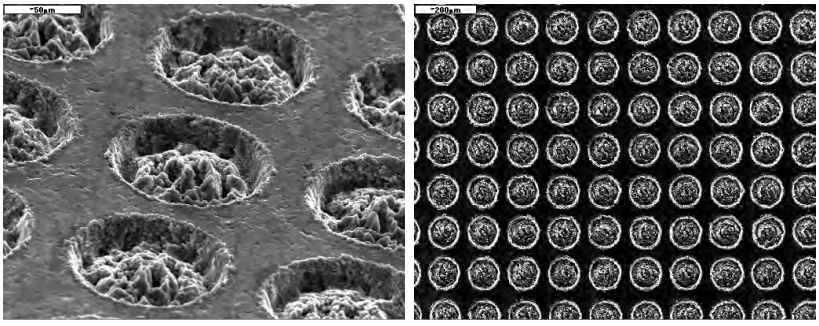

Fig. 3. View of a textured surface on an SiC ring: on the left – single recesses on the surface of the ring (magnification 500x), on the right – a set of textured recesses on the ring (darkness 42%, magnification 100x) [3]

In physical sciences, texture is a colourful interference image of a thin layer (a few micrometres) of material placed between glass plates, showing the degree of order (macroscopic orientation) of molecules in a given phase. These images, regardless of their cause, are characteristic, and if they are observed at a changing temperature, the phase can be identified. In other words, the texture is a localised topological defect. Particularly spectacular textures can be observed in the case of thin layers of liquid crystals. Substances capable of forming liquid crystalline phases due to their specific physical properties, such as refractive index anisotropy or birefringence, show, in polarised light under an optical microscope, characteristic spatial structures simply reflecting the symmetry of their structure. To date, about 80,000 different liquid crystalline compounds, including polymeric liquid crystals, have been synthesised. It should be emphasised, however, that proper image analysis requires a lot of experience, which is difficult to achieve in the case of new liquid crystal systems (families) in the initial phase of research. This condition is particularly important in the case of banana-shaped liquid crystals, where the effect of the thermal history of the sample described in literature is crucial. It is also relatively difficult to analyse phase textures (or, more correctly, phases texture) of the blue phases (three blue phases have been identified).

Another drawback of the method is the fact that, especially in the smectic phases, small differences in the structure within the layers are not always reflected in clear changes in the textures. Paramorphosis (pseudomorphosis) can also cause an interpretation error. Pseudomorphosis is the phenomenon of inheritance of an external form (texture in the case of liquid crystals) by the studied compound, despite the fact that a phase transition from one liquid crystal phase to another has taken place. The new phase should then be tested by other available methods. Usually, however, the texture image changes during the transition from one phase to another. Therefore, by observing a thin liquid crystal sample with a polarisation microscope, one can determine the temperature of phase transitions and determine the boundaries of the areas of occurrence of a given phase.

A polarisation microscope (the first one was built by H.F. Talbot in 1834) is an optical microscope used to observe anisotropic objects in polarised light [4]. Its operation is based on the phenomenon of birefringence of substances with a long-distance ordering of molecules. One must keep in mind that the limit of resolution of an optical microscope is 0.15 μm.

Polarisation microscopes have numerous applications, among others in mineralogy, crystallography and petrography, as well as in chemistry, ceramics, metallography and the textile and paper industry, for the observation of biological samples, tissue structures and cells.

A typical configuration of a polarisation microscope is shown in Fig. 4. The microscope consists of a light source, which is usually a halogen bulb emitting white light which, reflected upwards by the mirror, passes through the lens. The light is linearly polarised by a polariser, which can often be rotated by 360°. The design of the

microscope allows a white filter of a selected wavelength to be placed in the light path (if experiments depending on the wavelength are required). The light then enters the condenser, an optical system that is used to uniformly illuminate the sample.

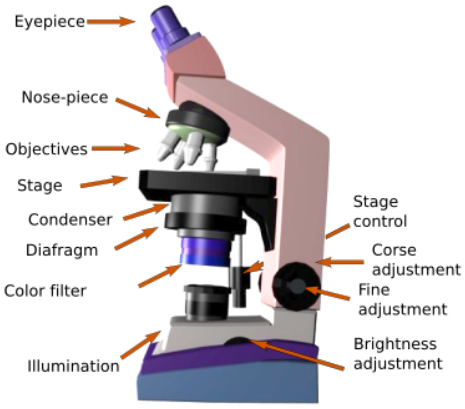

Fig. 4. Polarisation microscope [5]

A microscope for liquid crystal studies is normally equipped with a rotating table (on which the sample is placed). The table provides a rotation of the sample in a plane perpendicular to the direction of light propagation. The light then passes to the lens, which is crucial for the quality of the image. Three different lenses are often used for texture testing: 5x (red) for low magnification, 10x (yellow) and 20x (green) for medium magnification. The characteristic feature is that in addition to a typical orthoscopic observation, observation of the exit pupil of the lens, the so-called conoscopic observation, is possible. In this case, a 40x (40x – blue) zoom lens is used. The change from one form of observation to the other is made by switching between the eyepiece and the Bertrand lens.

After passing through the lens, the light passes through the analyser (the second polariser), which can be rotated by 360°. The polariser and the analyser transmit light with a strictly defined polarisation. When testing textures, the analyser and the polariser are rotated 90° in relation to each other (i.e. crossed), which results in a black field of vision if the sample does not exhibit birefringence. The polarisation plane of the analyser can be changed to blank and brighten the observed areas. Colour effects are caused by a change in the polarity at different light lengths.

The light then goes into the eyepiece, which further enlarges the image. A magnification of 10 (10x) is often used. Testing dynamic effects is performed using analogue or digital eyepiece cameras.

The polarisation microscope used in the study of liquid crystals is equipped with a heating table that can be used to change the temperature of the liquid crystal substance being tested, which is placed between two thin glass plates; the liquid crystal layer obtained in this way has a constant thickness, e.g. 5 μm or 10 μm (see Figs. 5 and 6) [6].

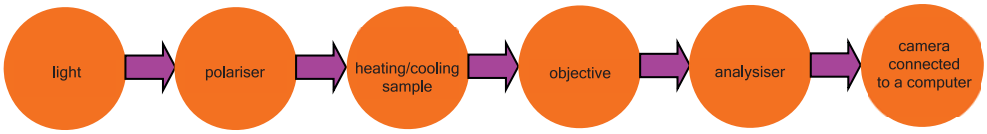

Fig. 5. Schematic diagram of the system for polarisation microscopy [6]

The image created in the measuring vessel can be observed directly (in real time) on a monitor screen, thanks to a digital camera (CCD) placed on the microscope eyepiece and connected to a computer (Fig. 6).

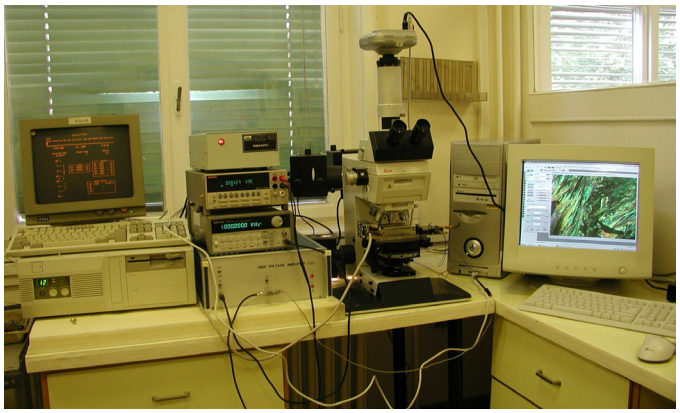

Fig. 6. Image created in the measuring vessel observed directly (in real time) on a monitor screen [7]

A thin layer of a liquid crystalline substance can be observed using a microscope in the so-called "sandwich" geometry (a flat-parallel layout), which consists of a mutual parallel arrangement of elements. Fig. 7 shows a measuring vessel with this geometry. The measuring vessel consists of two glass plates on which a transparent conductive layer of tin dioxide (SnO_2) is applied. Nylon separators are placed between the glass plates so as to form a flat parallel condenser. The thickness of the liquid crystal layer filling the vessel depends on the thickness of the spacers (usually at a level of several micrometres).

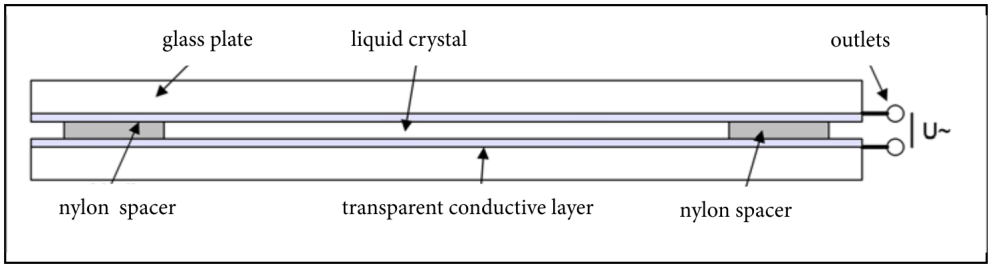

Fig. 7. Cross section of a measuring vessel – "sandwich" geometry [7]

The plates are glued to the surface using a conductive electrode adhesive so that the measuring cell can be supplied with alternating voltage. Before filling the vessel, its parallelism and thickness are checked by means of a measurement system using the laser beam interference phenomenon. After the measuring vessel has been prepared in this way, it is filled with the liquid crystal; the vessel is filled with liquid crystal in the isotropic phase using the capillary effect.

The liquid crystal molecules filling the measuring vessel can be oriented by creating two basic orders – *planar* and *homeotropic:*

- *planar orientation* is characterised by the fact that the long axes of the molecules lie in planes parallel to the plane physically bounding the thin layer of the liquid crystal and which are parallel to the selected edge of the surface. This orientation can be obtained by grinding the bounding surface (glass plate) in the desired direction;
- *homeotropic orientation* "sets" the long axes of the molecules perpendicular to the bounding plane (normal direction to the bounding plane). Many substances tend to orient themselves spontaneously on smooth glass or polymer surfaces. An additional element that ensures homeotropic orientation of the liquid crystal is the application of substances with an appropriate molecular structure, such as lecithin, on the surfaces of the glass plates.

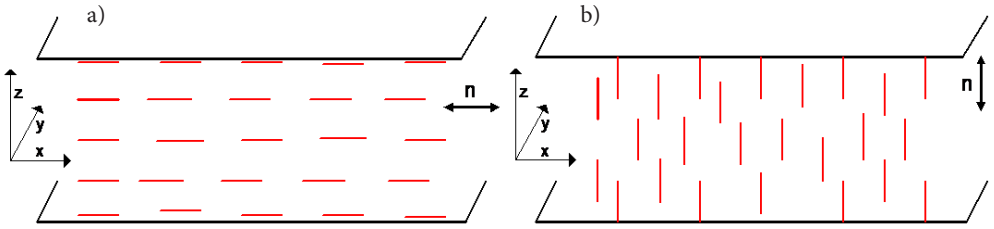

Fig. 8. Model orientations of a nematic liquid crystal: a) planar, b) homeotropic (symbol *n* states for director, a unit vector (axial versor)) [7]

There is also a combination of these two orientations called "a hybrid". In this case, one of the glass plates gives the liquid crystal a planar orientation, and the other – a homeotropic orientation. One must keep in mind that the molecular distribution shown in Fig. 8 is a model layout; in reality, it is disturbed by the thermal movements of molecules.

The nematic crystal in the planar phase (see Fig. 9) is transparent to light with polarisation in the direction of the molecules. It can easily be turned into an optically active element by rotating the bounding plates by a certain angle. The molecules adjacent to the upper plate are then arranged in a different direction to the molecules of the lower layer. The change of direction from one plate to the other is continuous (this an important feature of liquid crystals, indicating that the local orientation of the molecules can be extended to the entire macroscopic sample by the action of external factors (magnetic field, electric field, interaction with the surface), taking

advantage of the anisotropy of the physical properties of the material). Such a system will twist the light polarisation plane by exactly the same angle as the twisting angle of the plates. In this way, the polarisation plane can be twisted from 0° to 90°.

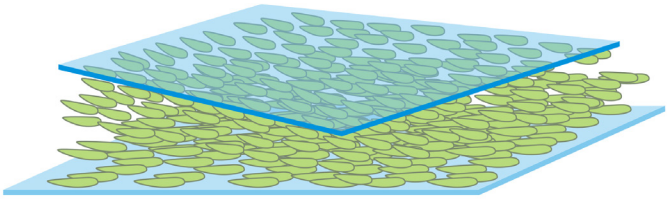

Fig. 9. Planar texture of a nematic liquid crystal after twisting of the plates [8]

If a liquid crystal has ferroelectric properties, the arrangement of the molecules can be controlled by an electric field, switching between planar and homeotropic textures. This is tantamount to changing the transparency of the liquid crystal layer. This effect has been used to develop liquid crystal displays.

The nematic phase is the least ordered mesophase (Fig. 10). Like all liquid crystals, it is made up of strongly anisotropic molecules. Liquid crystals ordered in this way are called nematics – the nematic phase is marked with the capital letter N. The name of this phase comes from the Greek word *nema*, which means a thread. The texture of the N-phase is visible under a polarising microscope in a way that resembles thin, elongated streaks. The nematic phase has been observed in more than 20,000 compounds.

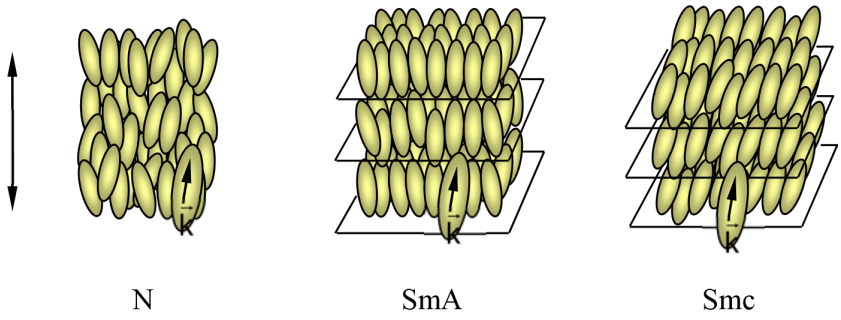

Fig. 10. Schematic image of a nematic, smectic A phase and a tilted (oblique) smectic C phase. The nematic uniaxial phase is characterised by quasi-parallel positioning of long molecular axes (described by the long axis vector $\vec{\mathbf{k}}$). The microscopic direction of orientation of the molecules is described by the unit vector (axial versor) $\vec{\mathbf{n}}$, called *a director*. The figure shows the smectic A phase planes (an additional planar arrangement of the centres of gravity of molecules; the long axes of the molecules are perpendicular to the layer). The tilted (oblique) smectic C phase shows the molecules tilted with respect to the layers [9, 10]

The nematic phase is characterised by quasi-parallel positioning of long molecular axes (described by the long axis vector $\vec{\mathbf{k}}$) of the neighbouring molecules. This leads to the distinction of the average, local, microscopic direction of orientation of the

molecules of the so-called *director* described by the unit vector (axial versor) $\vec{\mathbf{n}}$. The N-phase is a uniaxial phase (a crystallographic group of symmetry $D_{\infty h}$). The vector $\vec{\mathbf{n}}$, which defines the rotary axis of symmetry, does not have a distinguished sense, i.e. vectors $\vec{\mathbf{n}}$ and $-\vec{\mathbf{n}}$ are equivalent. The phase is not polar, even though the molecules can be polar. The lack of a long-range correlation of the centres of mass of the molecules enables them to translate almost freely. As a result, the nematic phase has low viscosity. The phase transition from nematic phase to isotropic phase is seen in Fig. 11.

It should be emphasised that in addition to the nematic phase described above, the occurrence of the chiral nematic phase has been observed. The chiral phase is made up of optically active mesogens, so-called chiral molecules (i.e. molecules that can exist in the form of two optical isomers that are mirror reflections of each other). Chirality eliminates the mirror plane but leaves the non-polarity of the director (directions $\vec{\mathbf{n}}$ and $-\vec{\mathbf{n}}$ are equivalent). The chiral phase was observed by Ch. Maugilin in cholesteric esters; hence its historical name – *cholesteric* phase.

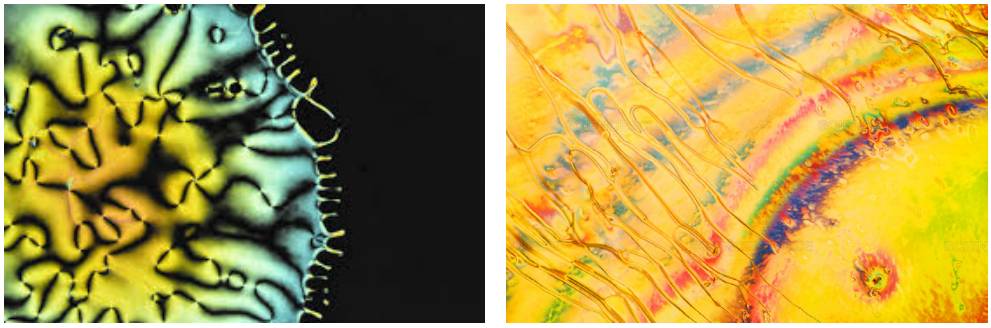

Fig. 11. Phase transition from nematic to isotropic phase (left side) and nematic phase (right side – nematic "threads" can be seen). In the left image, the nematic phase is seen as a colourful patchwork, while the isotropic phase is seen as a black stain [11]

It is characterised, in addition to the long-range orientation order of the molecules, by the twisting of the vector $\vec{\mathbf{n}}$, so that the structure becomes a chiral. The chiral pitch of such a helix ranges from 200 nm to infinity. It can be assumed that a nematic phase is a borderline case of a cholesteric phase with a chiral pitch equal to infinity $Ch_{(\infty)} \equiv$ N. The cholesteric phase has reduced symmetry – D_{∞}. Like nematics, *cholesteric* liquid crystals have loosely spaced molecules. Chirality refers to subsequent layers – molecules lie parallel to each other, but only in a certain plane. The next plane also contains molecules arranged parallel to each other, but in relation to the molecules located under and above it, it is twisted by a certain angle (at a level of 1°). The value of the angle depends on the type of the substance, the dopants, the temperature and the external fields. The pitch of the helix of a twisted nematic has a length comparable to the wavelength of light (a few to several hundred nanometres), which results in the phenomenon of selective reflection of light. It is assumed that there are two types of

cholesteric phases defined by the direction of rotation of the helix: right-handed or left-handed. Most cholesteric materials exhibit a decrease in the pitch of the helix as the temperature rises [12, 13].

Smectic phases (Sm) – we now know several dozen of them – are more ordered liquid crystalline phases (Fig. 10). Apart from arranging the directions of long molecular axes (as in the nematic phase), in the smectic phases, there is also an additional planar arrangement of the centres of gravity of molecules – a translational order in virtual layers. Elongated molecules have limited translation freedom – they can move by the length of the molecule at most. The basic division of smectics results from the slope of the molecules in relation to the smectic layer; we have distinguished orthogonal or oblique phases. When the long axes of the molecules are perpendicular to the layer, the smectics are orthogonal (SmA, SmB). When the long axes of the molecules are tilted with respect to the normal to the layer, the smectics are oblique (SmC, SmI, SmF). Modifications of smectic phases are also connected with periodical ordering of molecules in planes (crystalline smectic phase E) or correlations between planes (crystalline smectic phase L).The simplest smectic is the type A smectic (SmA). The difference between a nematic and a type A smectic is that in a smectic, there is a translation order along the director. The symmetry group remains unchanged ($D_{\infty h}$), but the translation symmetry is broken at the N $\Rightarrow$ Sm phase transition point. At certain intervals, which are constant for a given substance but do not necessarily commensurate with the length of the mesogen, there are virtual layers whose normal is parallel to the director. A typical thickness of the smectic layer is about ~30Å. In the case of a type *A* smectic, the molecules in each layer are arranged in a quasi--parallel order so that their long axes, on average, are perpendicular to the layer. Thus, this is an orthogonal-type smectic.

Most liquid crystal phases, such as N and SmA, are optically positive, which means that the refractive index parallel to the optical axis $n_{\parallel}$ is greater than the refractive index perpendicular to the optical axis $n_{\perp}$; $\Delta n = n_{\parallel} - n_{\perp} > 0$. For optically negative liquid crystals, such as most of the cholesteric phases (*Ch*), where the optical axis coincides with the helix axis and not with the (local) director the anisotropic refractive index is negative; $\Delta n < 0$.

A common feature of all liquid crystals is the phenomenon of double refraction of light (birefringence), which is typical of some crystals (solids). Birefringence is the ability of optical media to double split the light beam into two beams: an ordinary beam n_o that fulfils the Sneullius law, and an extraordinary beam n_e that does not fulfil the Sneullius law. The measure of this phenomenon is the difference of refraction coefficients n_e and n_o; $\Delta n = n_e - n_o$. The birefringence of the nematics decreases monotonously with an increase in temperature to zero at the point of phase transition to an isotropic liquid.

The existence of a birefringence in a crystal results from the settings of anisotropic molecules along a selected direction, i.e. along a well-defined optical axis. In a uniaxial crystal, during refraction, the beam entering the crystal is divided into two beams: n_e and n_o. In a biaxial crystal, both beams behave like extraordinary rays.

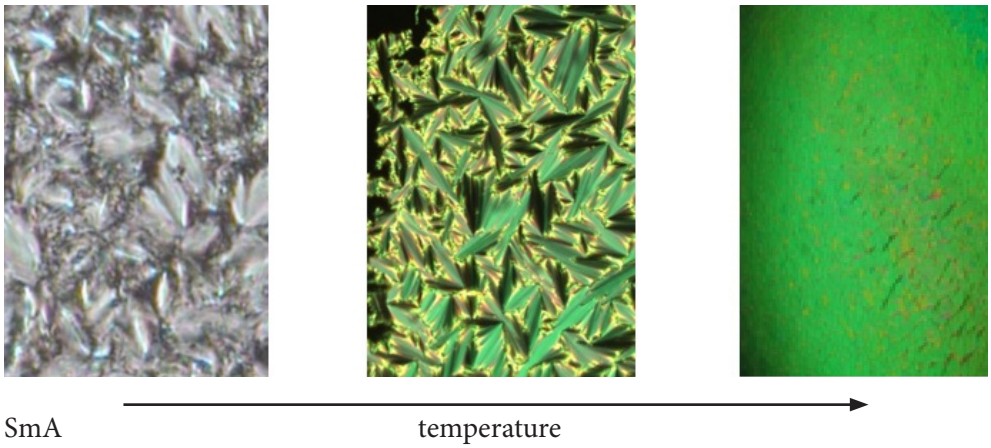

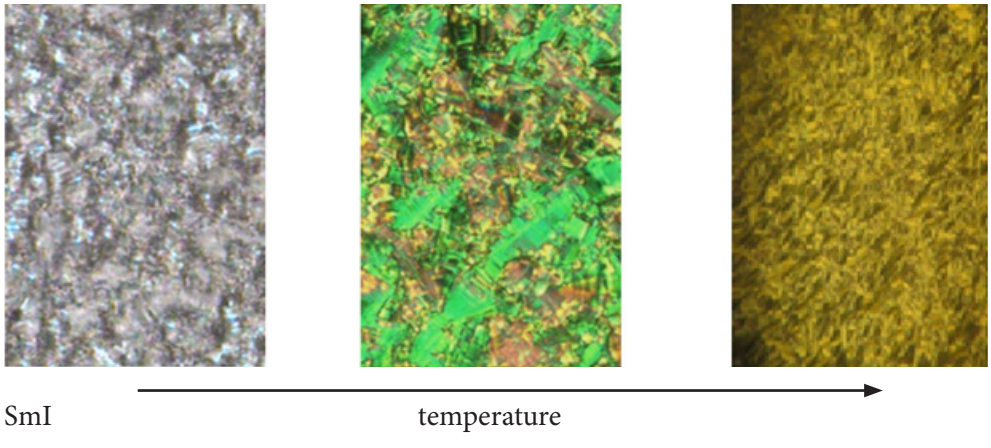

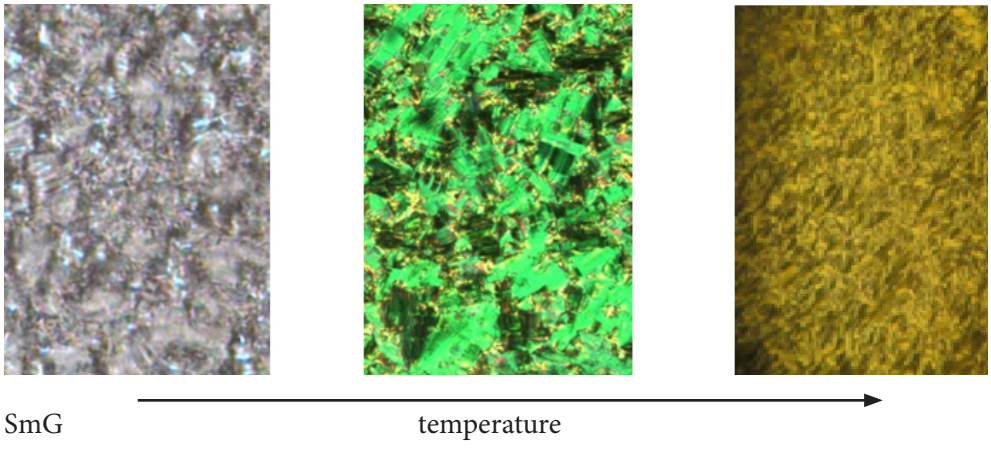

Fig. 12. Temperature modification of SmA, SmI and SmG textures [6]

Let us analyse the example of an uniaxial nematic or smectic type A liquid crystal placed between crossed polarisers. In the homeotropic orientation, the direction of light propagation coincides with the optical axis. In this case, the angle between the optical axis and the direction of light propagation is zero. Consequently, $\Delta n = n_e - n_o = 0$, and thus the intensity of the passing light, is equal to zero – the image is black.

In the planar orientation $n_o = n_\perp$ and $n_e = n_{||}$ or $\Delta n = n_\perp - n_{||}$, the intensity of the passing light changes as $\sin^2(2\varphi)$, where φ is the azimuthal angle or angle between the analyser and the projection of the optical axis on the surface of the sample. The "sinus square" function reaches the maximum for φ = 45° and the minimum for φ = 0° and φ = 90°. The image is dark as soon as the optical axis becomes parallel to one of the directions of the main axes of the polariser, and the emerging texture exhibits a periodicity of 90° as the sample rotates between the polarisers.

Because of the interlayer interactions, we can distinguish between liquid-like and crystal-like smectics. Liquid-like smectics, such as SmA and SmC, do not exhibit an arrangement of the centres of gravity of the molecules inside the layers – in this respect, they resemble a two-dimensional liquid. In crystal-like smectics (SmB, SmD, SmE, SmI, SmG, etc.), within the layers, there is an arrangement of centres of gravity of molecules. They are more like a two-dimensional crystal. The crystalline smectic E (see Fig. 13) exhibits an orthorhombic arrangement. In the B smectic, the molecules are arranged perpendicularly in the vertices of regular hexagons (pseudohexagonal). Phases I and G have a similar arrangement, except that the molecules are inclined in phase I to the corner of the hexagon and in phase G to the wall of the hexagon. It was observed that the some smectic phases, such for instance smectic E, form partially ordered glasses. A partially ordered glass is formed by the cooling of an orientationally disordered crystal [12, 13].

By giving up the condition of axial symmetry along the normal to the smectic layer, we may set the mesogen so that the direction of its long axis forms a non--zero angle to the normal to the layer – the SmC mesophase (Fig. 10). Such geometry requires entering not only a tilt angle, but also an azimuthal angle, determining the momentary position of the mesogen on the tilt cone, into the description of the direction of the selected molecule. However, the occurrence of a tilt angle is a necessary and sufficient condition to reduce the symmetry of the SmC phase with respect to the SmA phase. The symmetry of the smectic phase C is C_{2h}. Lowering the symmetry usually means an increase in the order. Thus, the phase transition SmA $\Rightarrow$ SmC (the second order transition) is connected with an increase in the order. This is confirmed by the fact that the SmC phase always occurs at a lower temperature than the SmA phase (for mesogens that have both phases). However, it is not necessary for the SmC phase to be followed by the SmA phase and then the nematic phase. Nevertheless, such a sequence of phases suggests that the translational order appears simultaneously with the deviation of the director. The formation of a tilted smectic structure directly from the nematic phase is probably connected with the

"transverse" interaction of the nearest molecules. This type of interaction can occur, for example, between side dipoles (electric) of polar neighbours. When the system reaches the energy minimum with a mutual interaction of the "ends" of the nearest molecules, a layer structure of the SmA type is formed. However, if the optimal interaction is a correlation such as the neighbouring molecules' central dipole – end dipole, then this is a tilted SmC phase. The angle of tilting will depend mainly on the steric interactions or the best possible packing of molecules resulting from their chemical structure. It can be expected that the tilting angle does not depend on the temperature. Such smectics can be divided, depending on the tilting angle of the molecules, into high-angle smectics (tilting angle greater than 40°) and low-angle smectics (tilting angle within 26–30°) [6].

Fig. 13. Texture of the E smectic and of the glass phase[6] of this smectic (right side) [12, 13]

At the end of the 1970s, liquid smectic crystals made of chiral molecules appeared, exhibiting ferroelectric properties in the SmC phase. It is customary to mark this phase with the symbol C^* (SmC*). The property typical of *cholesteric* phases is the twisting of the polarisation plane; these are optically active liquid crystals. This means that the molecules forming the SmC* phase rotate the polarisation plane and thus change the polarisation state of the incident light. The angle by which the polarisation plane rotates is proportional to the optical path of the passing beam.

A decrease of the symmetry of the SmC (C_{2h}) phase (in comparison to the N or SmA – $D_{\infty h}$ phases) implies the appearance of biaxiality, and thus three different refractive indexes. The smectic C* is a chiral variety of the smectic C (see Fig. 14). The phase is characterised by a tilting from the normal to the layer (an angle θ) changing from layer to layer.

[6] Glass is a nonequilibrium, non-crystalline state of matter that appears solid on a short time scale but continuously relaxes towards the liquid state. The liquid crystalline phases can be supercooled and frozen-in like isotropic liquids. As the nematic or smectic liquid crystalline structure freezes-in, and can be conserved by this process, glasses with anisotropic properties are obtained. These glasses show e.g. a high optical birefringence [20].

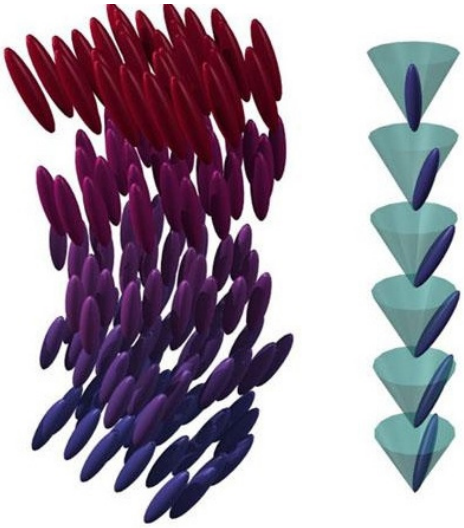

Fig. 14. Smectic C* – a model [6]

The optical properties are similar to those of the cholesteric phase. When considering the transition of light along the axis of the helix, the effect is identical to that of twisted nematics.

Due to the chirality of the molecules, there is no planar symmetry (which is present in SmC). The only element of symmetry is a double axis parallel to the layers and to the normal to the direction of the long axis of the molecules.

Textures of the smectic C* are presented in Fig. 15.

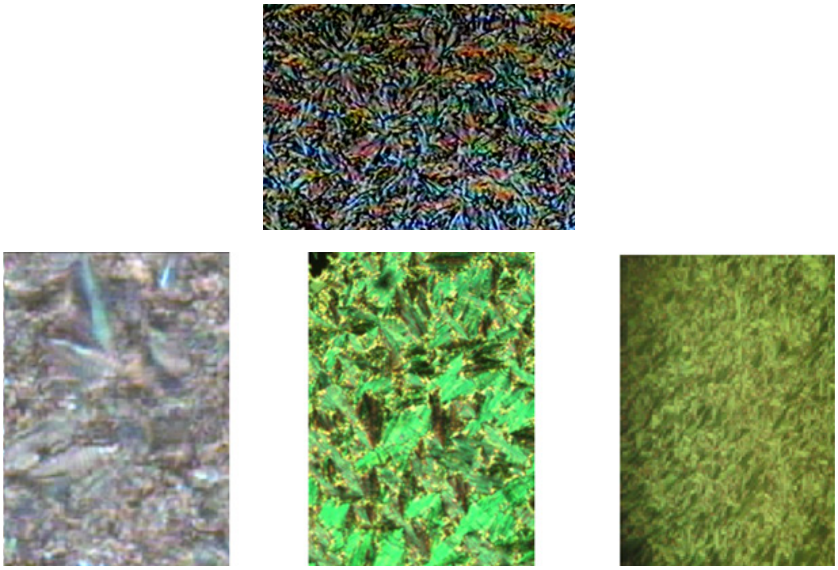

Fig. 15. Textures of the smectic C* [12, 13]

The phase transition between SmC* and SmA can be either of the first or of the second order. The angle of inclination and the pitch of the screw are temperature dependent.

There are also more characteristic textures, such as streak texture (German: schlieren) (Fig. 16) and "fingerprint" texture (Fig. 17).

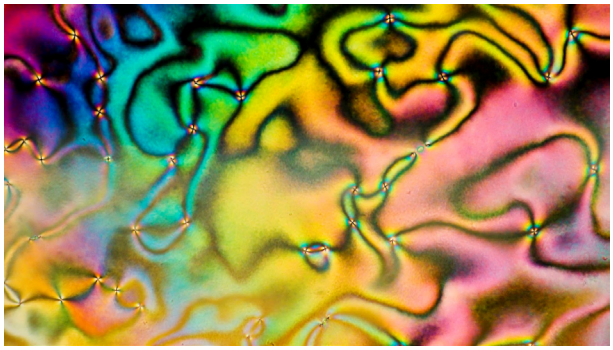

Fig. 16. Streak texture (German: schlieren) of the 5CB nematic [16]

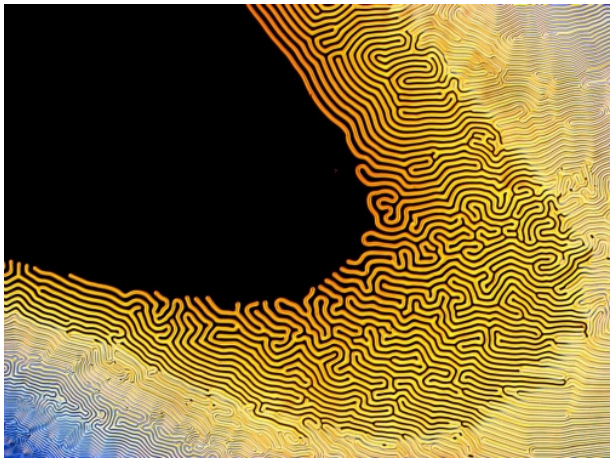

Fig. 17. Fingerprint texture of a cholesteric crystal [17]

Blue phases

The traditional phase diagram that is present when the temperature rises is the sequence:

$$\mathrm{Cr} \Rightarrow \mathrm{Sm} \Rightarrow \mathrm{N/N^*} \Rightarrow \mathrm{Iso}$$

Slow cooling, however, can result in a phase(s) that is observed only in chiral materials, the so-called blue phase(s) (BP). The blue phase was previously observed

by Lehmann in the first period of development of liquid crystal physics. He noted that below the transition to isotropic liquid, some cholesterol derivatives have a bluish phase. Its most common texture is bright blue tiles. The blue phase is separated from the cholesteric phase by a phase transition with a specific transition warmth – thus, there is no doubt that it is a separate phase and not a peculiarity (textural). It is present in a narrow temperature range of approx. 1°C but can easily become supercooled. The blue cholesteric phases occur in substances for which the cholesteric phase has a relatively small helix pitch – approx. 5,000 Å (1 Å = 0.1 nm). Liquid crystalline substances with a helix length greater than 1 μm do not produce blue phases.

The width of the temperature range in which the blue phase occurs depends on the pitch of the cholesteric helix (the larger the pitch of the helix, the narrower the range). The nature of the arrangement of molecules is not fully understood. One of the characteristic features of the blue phases is the defect lattice.

The three blue phases are abbreviated as BP_I, BP_{II} and BP_{III}. They are clearly separated by phase transitions of type I. The blue phases BP_I and BP_{II} are characterised by a cubic structure with an elementary cell with the size of the helix pitch length. The size of the elementary cell of the BP_I phase decreases with temperature, and the elementary cell in the BP_{II} phase does not change with temperature. Phase BP_{III} is not well-known. This phase is called a "blue fog" and occurs just before the isotropic phase (see Fig. 18). It includes helix elements and is not periodic. One must keep in mind that phases B_I, B_{II} and BP_{III} are not "seen" by X-ray spectroscopy due to the fact that the existing three-dimensional arrangement with a lattice constant of 500 nm is not detected by X-ray diffraction (no X-ray scattering). Thus, one of the very important techniques for the analysis of the blue phase is polarising microscopy. The blue phases have a number of optical properties (mostly typical of liquid crystalline phases): such as optical activity with simultaneous isotropy and selective light reflection. The blue phases exhibit selective reflection of circularly polarised light.

Fig. 18. Left to right: phase transition between the cholesteric phase (left-hand side, top corner) and the blue phase (right-hand side side); the texture of the cholesteric phase; the texture of the cholesteric phase with the texture of the blue phase BP_{II} and BP_{III} [6]

The stable phase of BP_{III} is also known as "fog phase" and "grey texture". It is an almost amorphous structure with the same symmetry as in the isotropic phase, which, however, reflects the circularly polarised light, which indicates the existence of a kind of spiral superstructure. Its chirality increases with temperature (the same as in the case of BP_I). It usually occurs in the range of 0.1°C, at a temperature higher than that of the BP_I and BP_{II} phases; the texture of the blue phase BP_{II} is shown in Fig. 19 [6].

The "structural" element of phases BP_I and BP_{II} are the so-called double-twisted cylinders, as shown diagrammatically in Fig. 20, which represent a local structure with minimum free energy. In a double-twisted cylinder, the local director rotates around any cylinder radius. In the middle of the cylinder, the director is parallel to the cylinder axis. Moving outside the cylinder, the local director turns until it reaches an angle of 45°. The double-twisted cylinders are spatially perpendicular to each other. Taking into account the elasticity coefficients, it is the only structure forming a lattice of topological defects.

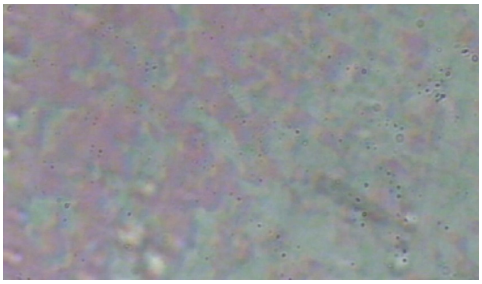

Fig. 19. Texture of the blue phase BP_{II} [6]

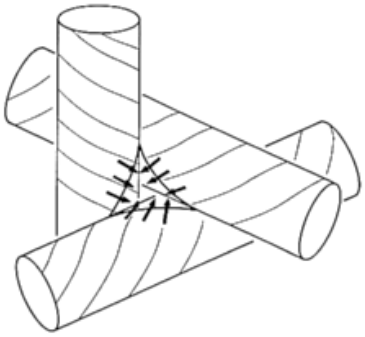

Fig. 20. Suggested structure of the cubic lattice of a blue phase consisting of twisted cylinders. The "exclusion" area with a tetrahedral arrangement is marked [14]

The blue phase BP_I is characterised by a long-range order with three-dimensional cubic symmetry bcc (body-centred cubic) [$I4_132$]. The blue phase BP_{II}, like the phase BP_I, exhibits a cubic structure – it is a "single cubic" structure [$P4_232$] (in international short symbol notations: the letter symbol describes the centring of the Bravais lattice (P is simple cubic, I is body-centred cubic), the first digital symbol (4_1 or 4_2) denotes

the symmetry along the major axis (c-axis in trigonal cases), the second (3 in this case), along the axes of secondary importance (a and b) and the third symbol (2 in this case), the symmetry in another direction) [6]. Both structures with lattice parameters are at the level of several hundred nanometres, i.e. the wavelength of visible light. The blue phases are therefore optically isotropic, i.e. they do not exhibit birefringence. For temperatures where the BP_{II} phase is stable, we usually observe a texture consisting of different coloured plates (usually blue, but also green, red and others).

The transformation between the structure of the cholesteric phase (helix) and the cubic structure cannot occur without defects. The disclination lines of the blue phases BP_{I} and BP_{II} create a unique three-dimensional structure. These structures are shown in Fig. 21. In the case of the blue phase BP_{I}, chirality increases with temperature, while in the case of the blue phase BP_{II}, it does not change.

The textures of the blue phases obtained in a polarising microscope are known as "plate textures". The different colours are due to the different orientations of the double-twisted cylinders (see Fig. 22).

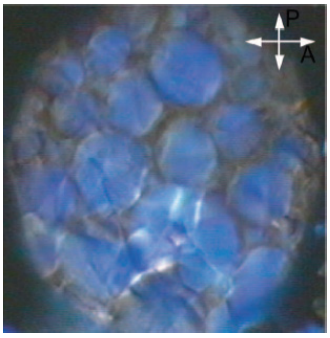

Fig. 21. Texture of the smectic blue phase [6]

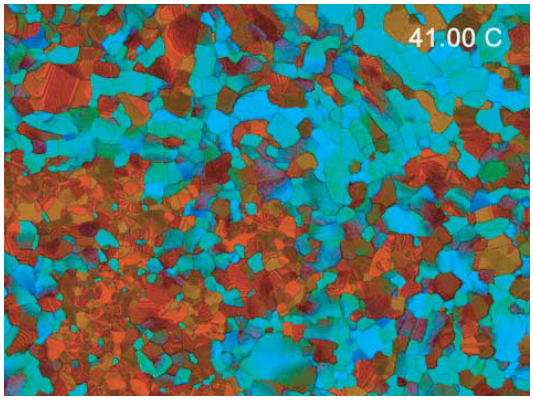

Fig. 22. Typical texture of the blue phase BP_{I} (41°C) [6]

The blue smectic phases BP_{Sm} were discovered in a chiral compound, nBTMHC, where n is the length of the aliphatic chain. They are similar to the blue cholesteric

phases but are characterised by the translation symmetry typical of smectics. The smectic blue phases can be examined by X-ray diffraction. The smectic arrangement is connected with a three-dimensional orientation, and as a result, information about the symmetry of the elementary cells of the smectic blue phases was obtained. The structure of the blue phase BP_{Sm1} is characterised by cubic symmetry, and that of the BP_{Sm2} – by hexagonal symmetry. The size of the cell makes it impossible to test for visible light, which is commonly used in the case of cholesteric blue phases (ultraviolet range) [6].

Due to their narrow range of occurrence, the blue phases could not be used in liquid crystal displays. Given the interesting properties of the blue phases, an attempt has been made to increase the functionality of this type of material. In 2002, Kikuchi discovered the possibility to stabilise the blue phase with polymers.

The first implementation of the blue phases with a wide temperature range was published in the journal "Nature" [6]. The publication describes the results of research on a mixture created on the basis of a liquid crystal exhibiting the existence of the blue phase. The used dopants caused that the range of blue phase occurrence, increased from the typical (about 1°C) to over 40°C (for the obtained substance, the blue phase was stable in the range of 16–60°C). The mixtures obtained were examined using polarising microscopy, light diffraction, differential scanning calorimetry (DSC) and electro-optical spectroscopy.

Banana-shaped liquid crystals: the name of these types of liquid crystals is derived from the shape of the molecules from which it is made; the molecules are bent in a characteristic way and resemble a banana (Fig. 23). Sometimes the term "boomerang" is also used in literature to describe the shape of a characteristic molecule.

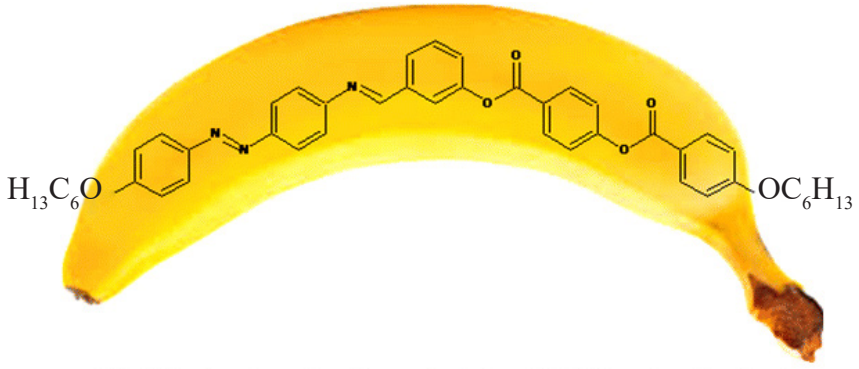

Fig. 23. Artistic drawing explaining the name [6]

Banana liquid crystals have been of particular interest to researchers since 1996, when Teruki Niori and his colleagues reported the discovery of ferroelectric properties in smectic phases composed of bent molecules [14]. This was a significant

discovery, because until then, ferroelectricity had only appeared in mesomorphic phases of sufficiently low symmetry and were necessarily made up of chiral molecules. However, the history of banana-shaped liquid crystals began earlier. It was initiated by Vorländer, who first noticed in 1929 that liquid crystal phases can be formed by molecules of nonlinear shape. It should be mentioned here that two years before Niori's publication, Matsunaga and his collaborators synthesised a liquid crystal compound made up of nonchiral, curved (banana-shaped) molecules revealing the SmC phase.

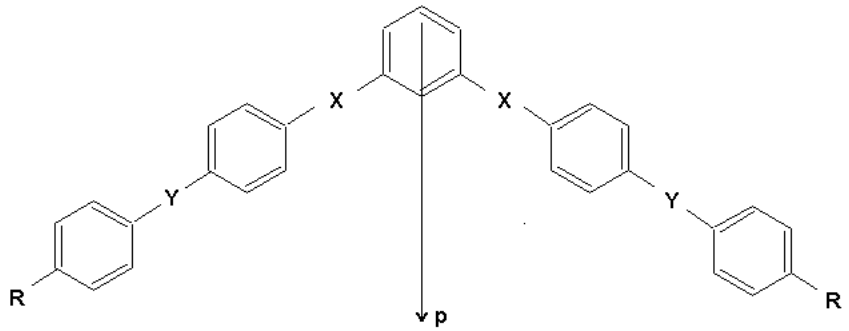

Fig. 24. Typical banana-shaped liquid crystal molecule (R – end group, X, Y – bridge groups, p – electric dipole moment)

Banana-shaped liquid crystals represent a new, separate class of thermotropic liquid crystals. Banana-shaped phases created by bent molecules have no equivalent among calamitic liquid crystals, whose mesophases are made of rod-like molecules, or among discotic liquid crystals, which have column phases. These new modifications to the liquid crystal phases are the result of the specific packing of banana-shaped molecules. The designation of banana-shaped phases with the letter B (phases B_i) with an index (digits from 1 to 7) was proposed, and later adopted by scientists all over the world, at the "Chirality by Achiral Molecules" workshop on bent liquid crystal molecules held in Berlin in December 1997 [6]. Currently, we know eight modifications of banana-shaped smectic phases: from B_1 to B_8. The special arrangement of molecules in these phases causes them to exhibit ferro-, ferri- or antiferroelectric properties. Liquid crystalline phases composed of banana-shaped molecules are chiral, despite the fact that individual molecules are achiral [15].

A typical banana-shaped molecule is made up of five benzene rings – compare with Fig. 24. Some molecules are also known to be made up of six and seven rings. The curved shape is obtained by chemists by attaching the molecule's "branches" to the phenyl ring in position 1,3. The resulting curvature between the molecular chains has an angle in the range of 120–130° [6].

Banana-shaped molecules form smectic phases with near-reach positional arrangement in the layer. These phases differ significantly from smectic phases formed by rod-like particles such as SmA and SmC. While the rotation around the

long axis in SmA is free, the rotation of the banana-shaped molecule around the axis connecting its two ends (the rotation around the long axis) is very difficult. In substances composed of banana-shaped molecules, the nematic phase occurs rarely.

According to preliminary X-ray studies, phase B_1 seems to indicate a perpendicular column phase. A phase is formed for relatively short alkyl tails. There are usually 6 to 10 molecules per elementary cell. Under a polarising microscope, phase B_1 presents a mosaic texture. Observations demonstrate that B_1 appears as a high-temperature phase of phase B_2. However, when the temperature decreases, phase B_1 appears as a low-temperature phase of phase B_6. Phase B_2 is an inclined smectic mesophase exhibiting a polar arrangement – the texture of B_2 phase is shown in Fig. 25. The long molecular axis is inclined towards the normal layer (similar to SmC). However, chirality in phase B_2 is not a result of a superhelical organisation, like in phase SmC* [6].

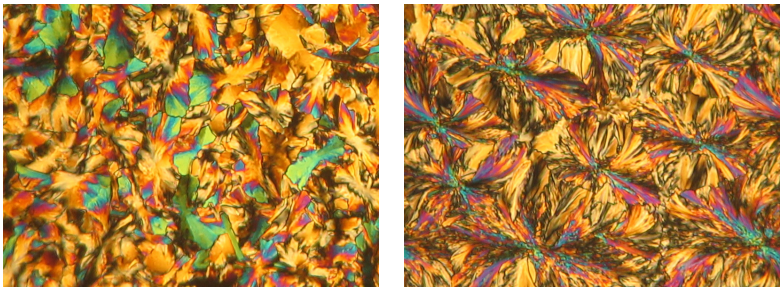

Fig. 25. Phase B_2 at 68°C and 60°C [13]

Phase B_3 (see the Fig. 26) is an inclined lamellar crystalline phase that does not exhibit a switching effect. It occurs below phase B_2 [15].

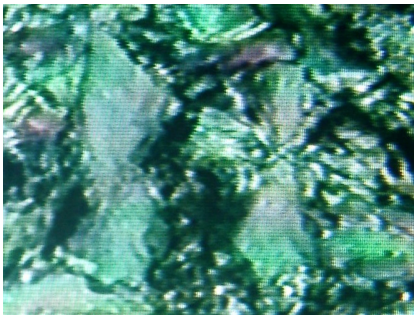

Fig. 26. Phase B_3 (81°C) [15]

Phase B_4 (like B_3) is a crystalline phase; thus, from the formal point of view, it is not a mesophase. The molecules in phase B_4 exhibit a helix (a spiral system). Seen with a polarising microscope, phase B_4 has an intense blue colour. The texture of the crystalline phases B_3 and B_4 are shown in Figs. 26 and 27, respectively. The B_3 to B_4 phase transition is shown in Fig. 28.

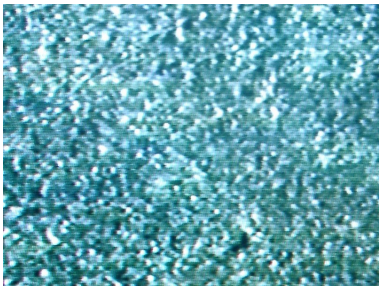

Fig. 27. Phase B_4 (51°C) [15]

Phase B_5 is observed as phase B_2 cools down. The two phases are very similar to each other. For example, the observed textures and symmetry of the arrangement are almost identical. The $B_2 \Rightarrow B_5$ phase transition is visible in X-ray measurements by clearly sharpening the observed spectrum [15].

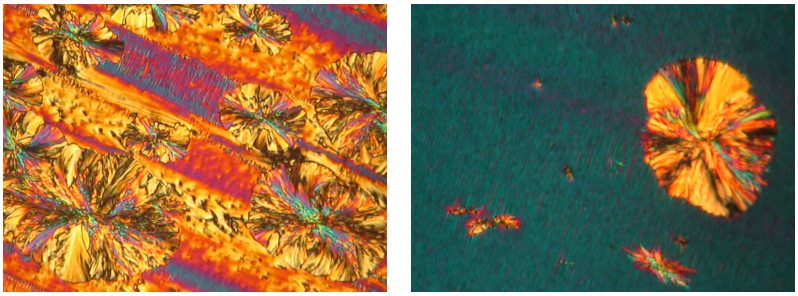

Fig. 28. B_3 (53°C) $\rightarrow$ B_4 (50°C) phase transition. The blue colour appearing in the background confirms the suggestion that this is a transition to phase B_4 [15]

According to the X-rays tests, B_6 is an intercalated, inclined smectic phase devoid of order in the smectic planes. It is formed by cured molecules with very short end chains. Phase B_6 (as well as B_1) is formed by a "collapse" of polar smectic layers in B_2. Seen with a polarising microscope, phase B_6 has a fan-shape texture.

Phase B_7 is a liquid-like polar smectic. The observed textures suggest the existence of a double helix (left- or right-turn). The phase is a switchable phase (like B_2), but with a much higher amplitude of electric field than phase B_2 [15].

The comparison of the appearance of smectic and banana-shaped phases as a function of increasing temperature is presented in Fig. 29.

SmH – SmK – SmE – SmG – SmJ – SmL – SmF – SmI – SmB – SmC – SmA

$B_4 – B_3 – B_5 – B_2 – B_1 – B_6$ temperature

B_7 – a phase appearing in monomorphic compounds

Fig. 29. The typical order of occurrence of the smectic (SmY (Y ≡ A, B, C, E, F, G, H, I, J, K, L) and banana-shaped phases (B_i (i ≡ 1–7))

When the influence of the bounding surfaces on the arrangement of molecules is small, a confocal texture is formed. Confocal domains, referred to as Dupin cyclides, appear. Liquid crystals forming this texture, due to their layered structure, tend to group into macroscopic objects of quite complicated structures and shapes, usually resulting from the confocal connection of the ellipses and the hyperboles. Confocal domains sometimes create regular arrangements visible under the microscope in the form of the so-called polygonal texture, visible as a lattice of separated polygons. A subgroup of confocal textures is fan textures typical of A, C, and F type smectics and cholesteric liquid crystals (see Fig. 30) [12, 13].

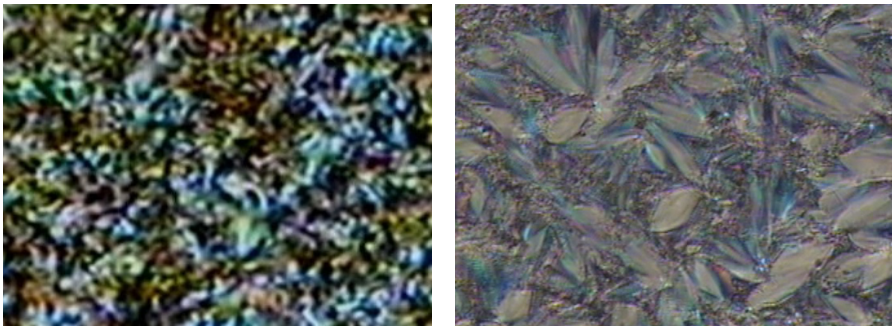

Fig. 30. Confocal (left side – 138°C) and fan (right side – 81°C) textures of the A smectic [12, 13]

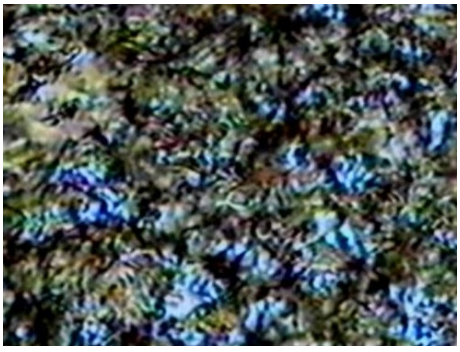

Fig. 31. Smectic mosaic texture – 66°C [6]

Mosaic texture (see Fig. 31) is the name used to describe a specific type of image seen in a polarising microscope. It is often not possible to clearly determine the mesomorphic structure from observations of this type of texture. It is necessary to perform e.g. a structural X-ray analysis.

A unique form of phase transition analysis is direct observation of the change in the microscopic image. In addition to the transition kinematics, one can observe the dynamics of the change in the phase transition area (observe the near-transition effects). Photographs of such changes are shown in Fig. 32.

a) b)

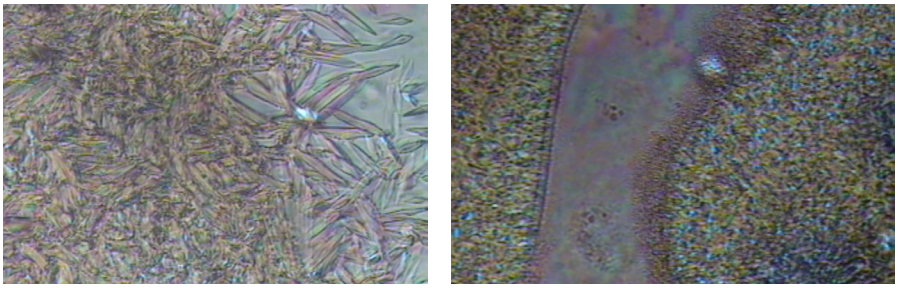

Fig. 32. Dynamics of the change in the phase transition area of the blue phase. Fig. 32a presents the transition from the blue phase (left hand side of the drawing) throughout the cholesteric phase (centre) to the "needles" from the smectic A (fan texture) (right-hand side of the drawing) – a "double" transition at 141°C at a cooling rate of 0.2°C per minute [14]. Fig. 32b presents the transition from the blue phase (central part of the drawing) to the cholesteric phase – a transition at a temperature of 140.5°C at a cooling rate of 0.2°C per minute [14]

Anisotropy, i.e. the dependence of different physical properties on the direction of research, is a feature which, by its nature, disappears in fluids. Thus, it is especially interesting to observe anisotropy in liquid crystals. It is anisotropy that makes the flow of liquid crystals so different from the flow of ordinary liquids. The flow of a liquid crystal between two closely arranged parallel plates results in an orientation of molecules (in combination with the flow), which in turn results in dendritic patterns. By applying an alternating voltage of an amplitude above the critical value to a flat parallel capacitor filled with a liquid crystal, one will cause the fluid to move. This electrohydrodynamic process is called electro-convection and can be observed under a polarising microscope. A schematic image of electro-convection rolls suggested by Ralf Stannarius is presented in Fig. 33 [18].

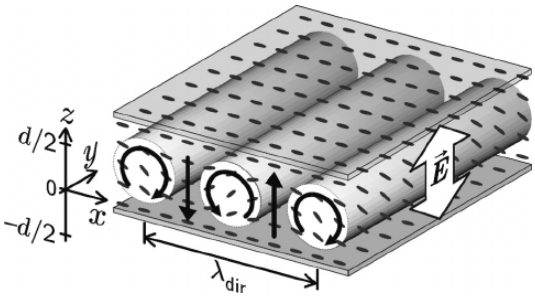

Fig. 33. Schematic image of electro-convection rolls suggested by Ralf Stannarius [18]

Given the variety of the liquid crystal phases, the boundary conditions and the amplitude and frequency variants of the external electric field, it is easy to imagine the variety of electro-convection images that one can observe. Example photos are shown below (Figs. 35–39).

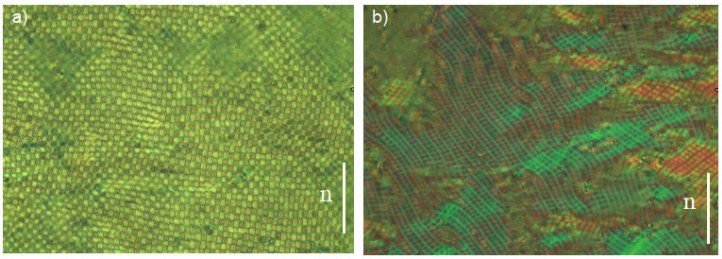

Fig. 35. Lattice image of a nematic liquid crystal created for the planar orientation as a result of the overlapping of "rolls" in four different directions (a) and the image of a smectic type created as a result of the influence of the smectic phase on the nematic phase (b) (actual dimension of the photograph: 350x150 mm; *n* – director) [7]

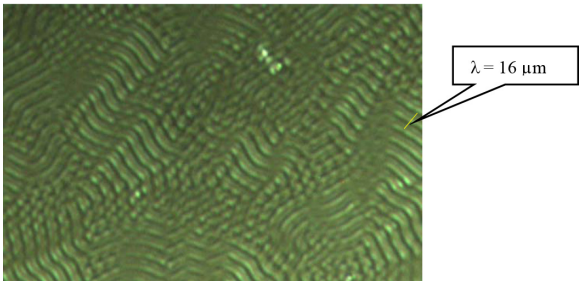

Fig. 36. Image of rolls and squares of a nematic liquid crystal created for the homeotropic orientation [own elaboration]

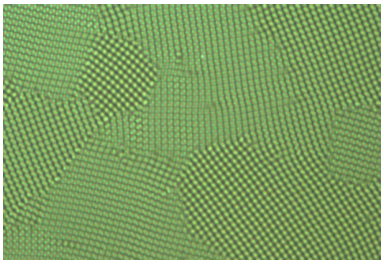

Fig. 37. Image of domains of squares of a nematic liquid crystal created for the homeotropic orientation [19]

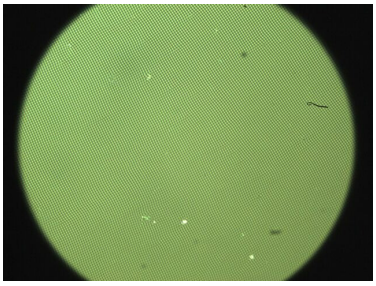

Fig. 38. Image of a domain built of squares of a nematic liquid crystal created for the homeotropic orientation [own elaboration]

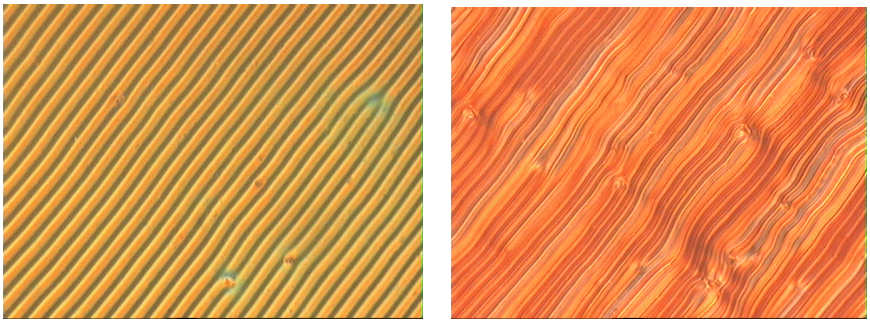

Fig. 39. Images of the pattern of rolls (left hand side) and stripes (right hand side) of a nematic liquid crystal created for the planar orientation [own elaboration]

References

[1] https://image.freepik.com [access: 07.02.19].

[2] Jawari1 M.S.A., Chen S.K., Halim S.A., Talib Z.A. and Lee O.J., *Structural Manipulation of YBa2Cu3O7–δ(YBCO) Superconductors via Melt-textured Growth with $BaTiO_3$ Epitaxial Seed*, ASM Sci. J.J., Special Issue 2018(1), 1–7.

[3] Sęk P. and Antoszewski B., *Powierzchnia z teksturą – topografia i energia powierzchniowa*, Postępy Nauki i Techniki, nr 6, 2011, 88–95 (in Polish).

[4] https://pl.wikipedia.org/wiki/Mikroskop_polaryzacyjny [access: 07.02.19].

[5] http://chomikuj.pl/lulka26/Dokumenty [access: 07.02.19].

[6] Gabriela Lewińska, PhD thesis, IFJ PAN, Kraków 2012.

[7] Elżbieta Kochowska, PhD thesis, IFJ PAN, Kraków 2007.

[8] https://commons.wikimedia.org/w/index.php?curid=4054829 [access: 07.02.19].

[9] Otowski W., *Dynamika molekuł termotropowych ciekłych kryształów w świetle badań relaksacji dielektrycznej*, Cracow University of Technology Kraków 2008 (in Polish).

[10] Adamczyk A., *Niewzwykły stan materii. Ciekłe kryształy,* Wiedza Powszechna, Warszawa 1991 (in Polish).

[11] https://www.flickr.com/photos/76862526@N03/8547996174 [access: 07.02.19].

[12] Otowski W. and Pabian G., *Tekstury termotropowych ciekłych kryształów*, "Czasopismo Techniczne", 1-NP/2009, 95–107 (in Polish).

[13] Dierking I., *Texture of Liquid Crystals*, Wiley-VCH Verlag GmbH&Co., KGaA 2003.

[14] Otowski W. and Lewińska G., *Molecular dynamic of (4-(4'oktylobiphenyl)carboksylan) 4-(2-methylobuthyl) phenol liquid crystal having blue phase seen via the dielectric spectroscopy method*, "Acta Physica Polonica A", Vol. 125, No. 5, 2014, 1152–1158.

[15] Agnieszka Dobrowolska, PhD thesis, IFJ PAN, Kraków 2007.

[16] http://1.bp.blogspot.com/Schlieren.jpg [access: 07.02.19].

[17] https://c1.staticflickr.com/4/3820/11379927384_27f6831fd6.jpg [access: 07.02.19].

[18] Rietz F. and Stannarius R., *Pattern formation in a flat rotating box*, AIP Conference Proceedings 1542, 763, 2013, https://doi.org/10.1063/1.4812043

[19] Buka A., Dressel B., Otowski W., Camara K., Toth-Katona T., Kraker L., Lindau J., Pelzl G., and Pesch W., *Electroconvection in nematic liquid crystals with positive dielectric and negative conductivity anisotropy*, "Physical Review E" 66, 051713, 2002, 1–8.

[20] Rehage G. and Frenzel J., Lecture given at the Conference "Thermal and Mechanical Properties of Polymers", 6–7 January 1982, Wiley Online Library, https://doi.org/10.1002/pi.4980140408

3. CONDENSED PHASE PHYSICS – ELEMENTS OF THE BASIC TENETS OF THE THEORY OF FREE ELECTRON GAS

One of the specific types of solids are crystalline bodies. They include a group referred to as metals. Most of the elements in the periodic table are metals.

Metals are elements characterised by the presence of so-called free electrons in the crystal lattice.

Let us consider a metal atom with one valence electron – a sodium atom, Na (Latin name: *Natrium*). Sodium has 11 electrons (Na – $1s^2\ 2s^2\ 2p^6\ 3s^1$), of which, as one can see, only one valence electron is on the 3s shell. It surrounds the sodium ion Na^+ with an electron cloud – a core composed of 10 electrons filling states 1s, 2s and 2p. If, by bringing two sodium atoms close to each other, one forms an Na_2 molecule, the valence electrons will move freely in the "area" of the entire molecule. If we bring a larger number of atoms close to each other to form a sodium crystal with a metallic bond, the valence electrons will still be delocalised and will move throughout the volume of the entire crystal. This is due to the fact that in such a crystal, the mutual proximity of atoms causes the splitting of energy levels into sublevels. Electrons stay in the narrow energetic states 1s, 2s and 2p for a long time, while in the state 3s, they stay for a very short time (10^{-16}s). This is a consequence of Heinserberg's indeterminacy principle. Consequently, the short lifetime of electrons in the 3s state means that they can move freely through the entire crystal and take part in the transport of electricity. One of the parameters characterising a conductor is work function; in sodium, the work function is equal to 2.36 eV.

The radius of the free ion Na^+ is 0.98 Å, while the distance between the nearest neighbours is equal to 3.71 Å. Thus, the sodium metal consists of a lattice of positive ions (it is a regular, body-centred lattice) immersed in the gas of freely moving valence electrons. This gas forms a form of "glue" permeating the interior space, which, by electrostatic interaction, "pulls" positive ions into itself and densely packs them (relative density 0.97 g/l (20°C)). This interaction of ions and the electron gas is a metallic bond.

Quantum electron gas

Let us consider the highest energy band corresponding to valence electrons (e.g. the 3s band in a sodium atom). In a crystal composed of N atoms, the band contains N quantum states. According to the Pauli exclusion principle[7], for a single atom in a given state, there can be at most two electrons described by the same quantum numbers (they differ by the spin number). Quantum states of electrons in a solid originate from the electron structure of the atom. If atoms are very distant from each other, their states are undisturbed, and, for example, in sodium, each atom has four independent energy values associated with states 1s, 2s, 2p and 3s. However, when the lattice constant decreases and reaches values close to the interatomic distance, there is an interaction between atoms that causes each electron level to split into sublevels (a split effect). Thus, a band of energy states is created from each level. Energy bands can overlap. The width of an energy band increases as is the greater, the greater the number of atoms interacting with each other increases (at distances commensurate with the atom radius).

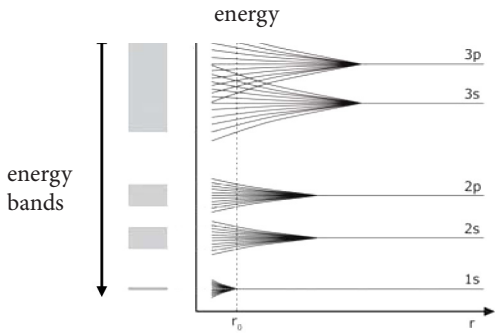

Fig. 1. Diagram showing a split of atomic energy levels; interatomic distances (r) are marked on the axis of abscissa, and energy values are marked on the axis of ordinates (r_0 – equilibrium separation, s, p – electron energy states)

The splitting of the energy levels of the sodium atom is shown in the figure on the next page (Fig. 2).

As one can see, the 3s and 3p levels associated with the electrons furthest from the nucleus are the easiest to split. These levels have been so strongly split that for certain values of interatomic distances, they form a single common band. It is only partially filled with electrons, because in the unexcited sodium atom, on the 3s level, there was only one electron, and the 3p level was empty.

An additional effect of the formation of energy bands is the appearance of areas of energy inaccessible to electrons – these are the so-called energy gaps. The number of

[7] According to the Pauli exclusion principle, there can be no two electrons in the atom with the same values of all four quantum numbers.

electron states within a band is equal to the number of elementary cells in the crystal. Because the concentration of atoms in a solid is at a level of $10^{23}/cm^3$, the energy states lie so close to each other that the values of energy inside the bands can be considered (in practice) as a continuous set.

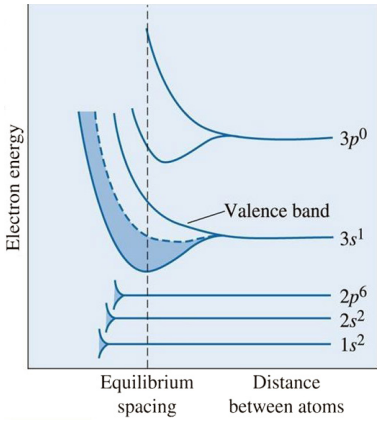

Fig. 2. Splitting of energy levels of a sodium atom (Na); the interatomic distances are marked on the axis of abscissa, and the energy values are marked on the axis of ordinates [1]

Valence electrons in a metal gradually occupy states inside the band, starting from the lowest located energy levels and upwards, two electrons per each state. The band can accommodate 2N electrons. If in a given crystal there are less than 2N valence electrons (e.g. in sodium, there are exactly N valence electrons), then the band is only partially filled. Such a band is referred to as a conductive band. This means that in an electric field, electrons can move inside the band – they are conductors of current. If a crystal contains such a number of electrons that the allowed energy bands are completely filled or completely empty, then the electrons cannot move in an electric field, and the crystal behaves like an insulator[8].

In the ground state (i.e. in the state corresponding to the temperature of absolute zero), the energy level occupied by electrons (fermions[9]) to a certain maximum value of energy is called the Fermi energy E_F (above the Fermi energy, the energy states are empty). Thus, the band of conductivity is occupied to a certain value of energy – the E_F energy. In the case of sodium, the Fermi energy is equal to about half of the value of the valence band.

In order to fully describe the behaviour of electrons forming electron gas in a metal, one has to consider the influence of positive ions arranged in a periodic crystal lattice. For the sake of simplicity, let us start with a one-dimensional case. Let us imagine an infinitive (one-dimensional) crystal represented by a chain of equidistant atoms (Fig. 3), i.e. a crystal with a fixed "a" lattice.

[8] Electrical insulator, dielectric – a material whose resistivity is greater than 10^7 Ωm (in the case of metals, it is at a level of 10^{-8}–10^{-6} Ωm) [2].

[9] Fermions are particles having a multiple of a half spin.

Fig. 3. Infinitive (one-dimensional) crystal represented by a chain of equidistant atoms

If we induced in such a chain an elastic wave of the length λ described by the wave vector $\vec{\mathbf{k}}$, it would propagate along the crystal carrying the momentum $\vec{\mathbf{p}} = \hbar\vec{\mathbf{k}}$ where $k = \frac{2\pi}{\lambda}$.

Now the kinetic energy of the free electron can be recorded as:

$$E = \frac{p^2}{2m} = \frac{1}{2m}(\hbar k)^2 = \frac{\hbar^2 k^2}{2m}. \tag{3.1}$$

Thus, the diagram of kinetic energy as a function of a wave vector is a parabola. Taking into account the fact that regularly distributed atoms (ions) create a variable potential for the moving electron, the energy image will change. By modifying the Schrödinger equation, we can state that all electrons described by vectors $\vec{\mathbf{k}}$ differing by a total multiple of $2\pi/a$ carry the same momentum. This means that in the diagram E_k on $|\vec{\mathbf{k}}|$, one has to divide the energy curve into zones corresponding to different ranges of values of $\vec{\mathbf{k}}$ and move the corresponding segments of the curve $E_k(|\vec{\mathbf{k}}|)$ to the first zone, i.e. to $\vec{\mathbf{k}}$ lying in the range $\left(-\frac{\pi}{a}, +\frac{\pi}{a}\right)$ (see Fig. 3).

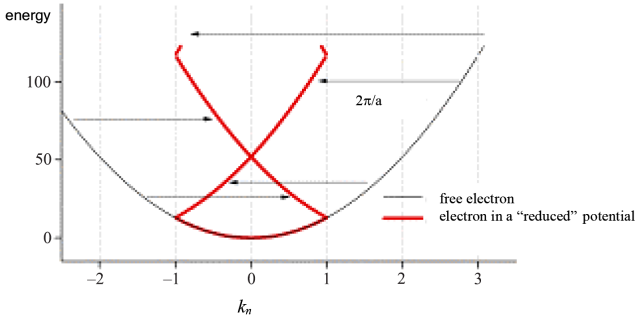

Fig. 4. Diagram E_k of a free electron and an electron in the potential reduced to the first Brillouin zone $\left(-\frac{\pi}{a}, +\frac{\pi}{a}\right)$ (energy is presented in arbitrary units)

The quantum calculus, taking into account the existence of the periodic potential in the points where atoms (ions) are placed, i.e. in lattice nodes (lattice points), shows that within the boundaries of zones ($\pm n \cdot 2\pi/a$), vector discontinuities appear $\vec{\mathbf{k}}$. Bearing in mind that a wave diffraction may occur on a crystal lattice, the Bragg condition[10] will take the form of:

[10] The Bragg condition is a relation linking the geometry of a crystal with the wavelength of incident radiation.

$$k = \pm n\frac{\pi}{a}. \tag{3.2}$$

Thus, the first reflection occurs for $k = \pm\pi/a$. On the other hand, a wave deflection can occur when:

$$\left|\Delta k\right| = \frac{2\pi}{d_{hkl}} = 2k\sin\Theta = \frac{4\pi}{\lambda}\sin\Theta = \left|\vec{\mathbf{G}}\right|, \tag{3.3}$$

where Θ is the angle of incidence or the angle between the direction of the primary rays and the plane of the crystal (note that the angle Θ is defined differently than in optics). The vector $\vec{\mathbf{G}}$ is a reciprocal lattice vector. From the formula (3.3), it follows that:

$$\lambda = 2\cdot d_{hkl}\cdot\sin\Theta. \tag{3.4}$$

The reciprocal lattice vector $\vec{\mathbf{G}} = h\vec{\mathbf{A}} + k\vec{\mathbf{B}} + l\vec{\mathbf{C}}$ introduces reciprocal lattice vectors defined by reciprocal vectors with the following relationships:

$$\vec{A} = 2\pi\frac{\vec{b}\times\vec{c}}{\vec{a}\cdot\vec{b}\times\vec{c}} \quad , \quad \vec{B} = 2\pi\frac{\vec{c}\times\vec{a}}{\vec{b}\cdot\vec{c}\times\vec{a}} \quad , \quad \vec{C} = 2\pi\frac{\vec{a}\times\vec{b}}{\vec{c}\cdot\vec{a}\times\vec{b}}, \tag{3.5}$$

where the denominator expressions are the volume of the crystal lattice cell.

A simple cell of a reciprocal lattice cell is, for historical reasons, referred to as first Brillouin zone. Thus, the area $\left(-\frac{\pi}{a},+\frac{\pi}{a}\right)$ is also referred to as a first Brillouin zone. In a one-dimensional case, $G = h \cdot A = h \cdot (2\pi/a)$. The reflection at the Brillouin zone boundary causing the discontinuity of the vector $\vec{\mathbf{k}}$ can be explained by the phenomenon of interference. If the Bragg condition is met, the wave propagating in one direction is reflected and propagates in the opposite direction. Each subsequent reflection changes the propagation direction to the opposite. By superposing these waves, one can create two different standing waves; a ψ^+ wave being the sum and a ψ^- wave being the difference of the current waves. The energy states corresponding to both waves are different. The average energy of the ψ^+ wave is less than that of the current wave, while the average energy of the ψ^- wave is greater than that of the current wave. The difference in the energy of both waves E_g determines the value of the energy gap, i.e. the difference in value between two solutions for $k = -\pi/a$ and $k = +\pi/a$.

For a regular simple lattice, the first and second Brillouin zones are relatively straight; they have the shape of a cube and of a rhombic dodecahedron, respectively (see Fig. 6).

A schematic image of energy bands in a solid is represented in the Fig. 7, showing horizontally positioned bands. Their interpretation is limited to identification of the area that represents the permitted bands and which area represents the forbidden energy area.

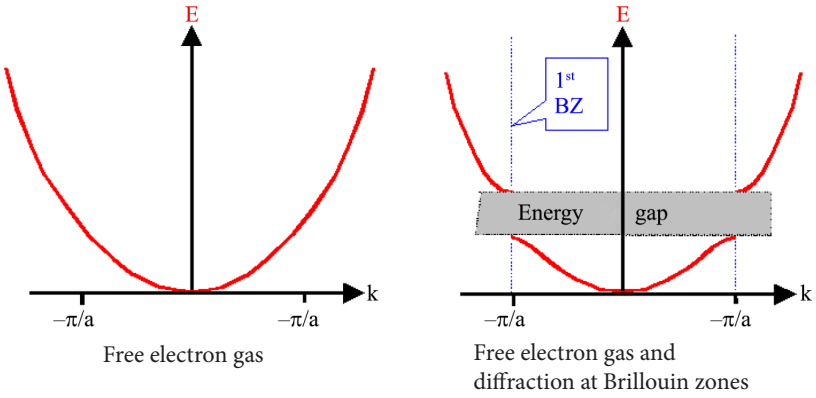

Fig. 5. Schematic diagram illustrating the energy gap E_g [3]

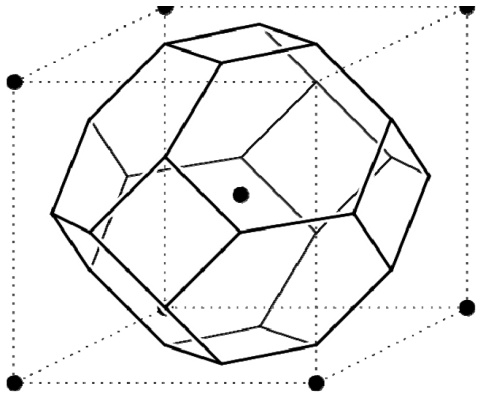

Fig. 6. Schematic drawing of Brillouin zones; a cube and a rhombic dodecahedron [4]

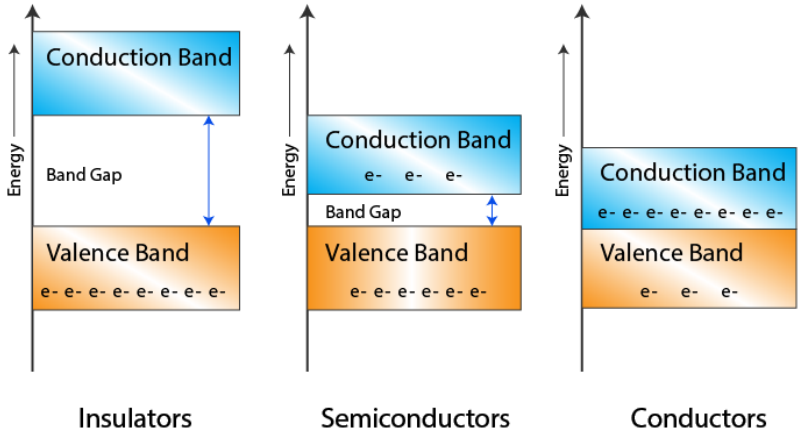

Fig. 7. Schematic drawing of energy bands [5]

At a temperature of 0°K, electrons occupy the lowest energy states. The highest band containing electrons is called the valence band, and the (permitted) band above it is called the conductive band. Depending on the manner of occupation and the mutual positions of the bands and the freedom of movement of electrons, crystals are divided into insulators (dielectrics), semiconductors and conductors (metals).

In insulators and "pure" semiconductors[11] at a temperature of 0K, the lower (valence) band fully occupied by electrons is separated from the completely empty higher (conductive) band by the energy gap. In the conductive band, there are no charge (current) carriers, which results in their lack of conductivity. In the valence band, the lack of conductivity is a consequence of occupation of all possible energy states; consequently, it is impossible to change the state.

As shown in Fig. 6, the difference between an insulator and a semiconductor is based on the size of the energy gap; in insulators, the value of the energy gap is so high that even at room temperatures, the thermal excitations are not high enough to enable some electrons from the valence band to "jump" to the conductive band. It is assumed that the value of the energy gap in insulators is at a level of 10eV[12]. In semiconductors, the authors of the band theory (the 1930s), estimated the value of the energy gap to be less than 2.5eV, although, currently, there is knowledge of a gap equal to 6eV (6.2eV at 300K in aluminium nitride).

In metals, the band containing non-localised electrons is partially filled, or, as shown in Fig. 6, the valence band is superimposed on an empty conductive band. In both cases, the motion of electrons, i.e. the flow of current, is possible.

The structure discussed herein refers to ideal crystals that do not contain any dopants or defects in the structure of the crystallographic lattice. In reality, this never happens. The inclusion of these elements in the band structure model leads to the conclusion that in a real structure, one should observe additional energy levels. Two types of such levels lying within the energy gap are particularly important: a donor level close to the conductive band and an acceptor level close to the valence band.

These bands, appearing as a result of the doping effect, play a special role in semiconductors.

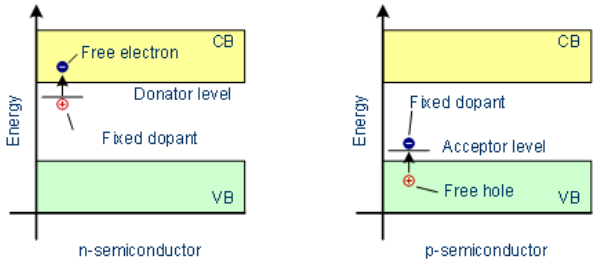

Fig. 8. Schematic drawing of energy bands in a doped structure (VB – valence band, CB – conductive band) [6]

[11] There are also so-called doped semiconductors.

[12] 1eV = 1.602×10^{-19}J.

Semiconductors

Semiconductors can be divided into intrinsic and doped. Intrinsic semiconductors are those that have a large energy gap between the conductive band and the valence band at an absolute zero temperature. As the temperature increases, electrons are thermally excited from the valence band to the conductive band. These electrons can participate in electrical conductivity (type *n* conductivity). However, the unoccupied states, which were formed in the valence band and are referred to as "holes", can also conduct electricity. The "holes" are fully-fledged positive carriers of current (on equal terms with electrons), and one can call them a positive hole charge (without quotation marks; hole instead "hole"); we are then dealing with conductivity of the *p* type. The mechanism of type *p* conductivity differs from the type *n* conductivity in that the free energy state (hole) can be occupied by another electron from the neighbouring atom, which fills the hole and creates another one. As one can see, the motion of a hole is actually annihilation and creation of subsequent holes. The hole as such does not move (unlike an electron), but it is assigned a certain effective mass resulting from the interaction of electrons with the crystalline field of atoms.

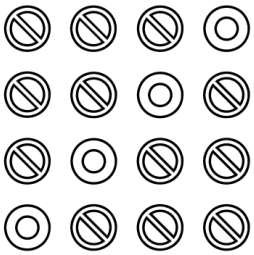

Fig. 9. Schematic drawing of hole conductivity (type *p*); the electron (the crossed circle) moves to the right, implying a virtual movement of the hole (ring) to the left

Doping is a very effective action; the addition of 1 boron atom to 10^5 atoms of silicon at room temperature results in a thousand-fold increase in the electrical conductivity of pure silicon.

Let us consider the influence of dopants in silicon and germanium. These elements crystallise in a tetrahedral structure. Each atom creates four bonds to its four nearest neighbours. If a five-value dopant atom (for example arsenic or antimony) is inserted into a crystalline lattice in place of the base atom, its one valence electron remains free (the remaining four form a bond). Such ionised dopant atoms are called *donors*. The resulting redundant electrons can move freely through the crystalline lattice – like in a metal. Similarly, if the dopant is an atom of the third group, having three external electrons (for example indium or gallium), then the fourth electron, at the cost of a small amount of energy needed to fill the bond, can be taken from the valence band. In the valence band, a conductive hole will be created. This type of a dopant is called an *acceptor*.

The donor level (Fig. 8) lies very close to the conductive band, i.e. about 0.01eV below the bottom level of the conductive band with the gap of 1eV (for comparison, the thermal energy k_BT at 20°C is equal to k_BT = 0.026eV). The acceptance level is about 0.01eV above the valence band.

The presence of additional energy bands makes it easier to excite electrons to the conductive band, because they have to cross a smaller energy gap.

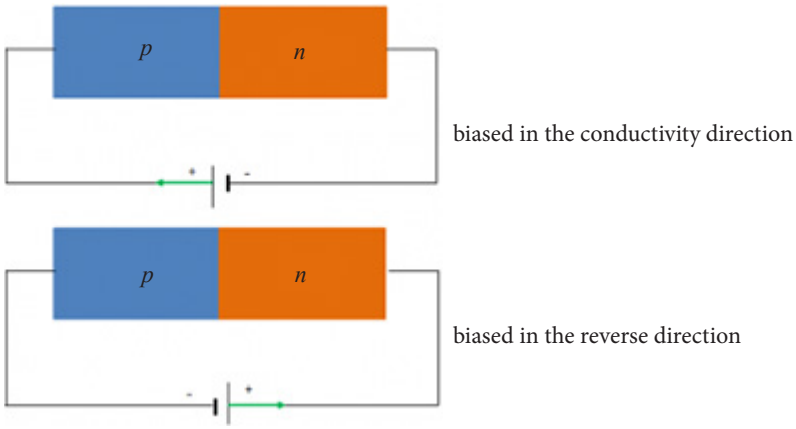

Fig. 10. Drawing of the *p-n* junction biased in the direction of conductivity and the reverse direction [7]

The boundary of the bond between two conductive areas (type *p* and *n*) is called the *p-n* junction. The width of this junction is at the level of 10^{-7}-10^{-6}m. In the area of the *p-n* junction, electrons move from the semiconductor of the *n* type to the semiconductor of the *p* type, while holes move in the opposite direction. Thus, the direction of applied voltage polarises the bond to form a barrier (negative potential applied to the area of the *p* type) or in the direction of conductivity (at opposite polarisation). One should keep in mind that the resistance of a polarised junction in the barrier (reverse) direction increases significantly, but the current (relatively weak) will flow through it. For example, with a conductive current of 100mA, it will be 10pA in the case of a silicon diode or 100nA in the case of a germanium diode.

References

[1] https://slideplayer.com/slide/4661608/15/images [access: 26.04.19].
[2] https://eng.libretexts.org/@api/deki/files/1735 [access: 26.04.19].
[3] https://i.stack.imgur.com/fHbOG.gif [access: 26.04.19].
[4] Strobl K., *Improvements for Vachaspati-Vilenkin-type Algorithms for Cosmic String and Disclination Formation*, arXiv:hep-lat/960808, 1996, PACS: 02.70.Rw 11.10.Lm 61.72.Lk.
[5] https://cdn1.byjus.com/wp-content/uploads/2019/03/Energy-band-diagram-03.png [access: 26.04.19].
[6] https://www.halbleiter.org/images/fundamentals/doping/baender-dotiert.gif [access: 26.04.19].
[7] https://www.watelectronics.com/wp-content/uploads/ [access:26.04.19].

4. DIELECTRIC SPECTROSCOPY METHOD[13]

Dielectric spectroscopy (DS) (also commonly referred to with the acronym DR[14]) or broadband dielectric spectroscopy (BDS) is a particularly attractive research method for substances whose molecules have one or more polar groups in their structure. The development of electronics in recent years has made it possible to observe and analyse dielectric relaxation processes in the frequency range from 10^{-4} Hz to 10^{12} Hz, unattainable for other measurement techniques, making dielectric spectroscopy a unique way to study the dielectric properties of materials and the reorientation dynamics of the molecular electrical dipole moment in the soft phases of matter, which, in addition to mesomorphic phases, include complex liquids, polymers, colloids, dendrimers, glasses and biological systems, as a function of both frequency and amplitude of the applied electric field.

The dielectric spectrum, i.e. the dependence of the complex dielectric permittivity ε^* on the frequency of the electric field and temperature, contains a lot of information, the analysis of which enables qualitative and quantitative comparison of experimental results with theoretical predictions.

An electric dipole with a certain degree of freedom of orientation knocked out of the equilibrium position by an electric field impulse returns to its original state after some time – the relaxation process is observed. If this simple model is extended to the entire volume of the analysed dipole system (e.g. a capacitor filled with a dielectric), and the electric field impulse is replaced with an alternating external field $E(t)$, then the reaction of the system to the disturbance $E(t)$ will be the appearance of macroscopic polarisation $P(t)$, described by the equation:

$$P(t) = \int \phi(t - t')E(t')dt', \tag{4.1}$$

where $\phi(t)$ is the dielectric response function of the system as measured with a dielectric spectrometer.

The relaxation times characterising the molecular relaxation processes cover a wide range of values, which means that the apparatus used in dielectric spectroscopy should cover at least 14 measuring decades (from the frequency ranges in which

[13] Wojciech Otowski – own materials [1] and references cited therein.

[14] The symbol of the DR method is a commonly used abbreviation in literature based on the English term *dielectric relaxation*.

the selected measuring methods can be used 10^{-3}Hz to 10^{10}Hz). This creates specific experimental problems. With such a wide frequency spectrum, it is not possible to use a single measuring technique (Fig. 1).

At subhertz and hertz frequencies, which are required, for example, for relaxation tests in polymers, but also for glassy states in liquid crystals, the capacitor discharge method is used. It consists in observation of the discharge current of a capacitor filled up with a dielectric. In this frequency range, the conductivity of the sample very strongly disturbs the measured spectrum. This effect may quantitatively exceed the measured signal many times over.

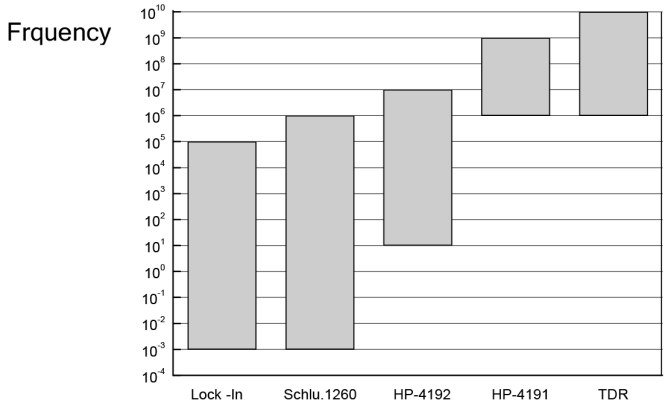

Fig. 1. Schematic representation of the frequency ranges within which selected dielectric measurement methods can be used

Bridge methods are used in the range from about a dozen or so hertz to about 10 MHz. A capacitor filled with a dielectric is one of the arms of a Schering bridge. The Schlumberger-1260 set is a classic example of this type of equipment used in the range from hertz to megahertz. If, for interpretation reasons, it is necessary to obtain results ranging from tens of hertz to tens of gigahertz, the HP-4192 set is used. This impedance meter enables a smooth transition to gigahertz frequencies by directly switching the measurement set to a similar type set, the HP model 4191. Schlumberger bridges and HP sets are typical combined resistance meters $Z(\omega)$. They measure the impedance of a sample placed at the end of a 50 Ω coaxial transmission line. The measuring cell is a flat parallel capacitor with gold-plated electrodes in the form of discs of a small diameter (usually 3 mm), separated with 50 μm silicone spacers. The capacitor is designed to be placed in a commercial holder. This way of combining the technical conditions of the device with the requirements of the experiment ensures that an accuracy of not less than 97%, as stipulated by the manufacturer, is maintained. All the bridges mentioned above are usually connected "on-line" with a computer, which enables direct analysis of data and for obtaining results in real time. The theoretical function of the dependence ε' and ε" on frequency is shown in Fig. 2.

Currently, bridge sets are also used in the range from megahertz to gigahertz. In this case, however, the measurement method is different from that used for megahertz bridges. The system measures the combined conductivity of a sample placed at the end of a transmission line as a function of frequency. The classic method used in this frequency range is the waveguide method. When the size of the sample is comparable to the measuring wavelength, which occurs starting from 0.1 GHz, it is possible to determine the properties of the dielectric from the interaction between the wave transmitted by the transmission line, i.e. the waveguide, and the sample placed in this line. A measurement of the impedance of a hollow waveguide and a waveguide filled with a dielectric provides the data needed to calculate the complex dielectric permittivity. However, this method has two main disadvantages. The thickness of the sample must be at a level of several millimetres (comparable to the length of the measuring wave), which results in relatively large volumes of the substance used in the experiment – several cm^3. The second disadvantage is the need to use a new waveguide when changing the frequency of the measuring field to another. A given transmission line has dimensions that are closely related to the length of the measuring wave. A sample can only be measured at one selected frequency. Each change in frequency requires the use of a new portion of the measured substance. Of note are the high accuracy of this method and the high quality of the results obtained.

The measuring methods described above provide information about the properties of the dielectric as a function of frequency. Another measurement technique, called Time Domain Spectroscopy (TDS), is also used to measure the parameters of a dielectric substance as a function of time. This is a method used in the range from a few megahertz to a dozen or so gigahertz. A modification of this method is the so-called Time Domain Reflectometry (TDR) technique. A TDR kit consists of a short rise time tunnel diode, a broadband digital oscilloscope and a computer for data collection and analysis. The rectangular voltage impulse generated by the diode is stored in the memory of the oscilloscope. At the same time, the same impulse, previously divided in the so-called head, transmitted by a semi-rigid waveguide line, reaches its free end, where the tested dielectric is placed. The signal is reflected from the sample and returns in the same line to the oscilloscope, where it is subtracted from the primary impulse. The complex dielectric constant is calculated from the formula:

$$\varepsilon^* = \varepsilon' - i\varepsilon'' = \frac{c}{i\omega d} \cdot \frac{V_0 - R}{V_0 + R} \cdot f(z), \tag{4.2}$$

where c is the speed of light, and V_0 and R are the Laplace transform of the incident impulse $v_0(t)$ and the reflected impulse $r(t)$, respectively. The function $f(z)$ is a high-frequency correlation coefficient that must be determined each time by calibration measurements of substances with known dielectric parameters. The TDR method makes it possible to perform very fast measurements in a wide frequency range. However, it is necessary to pay attention to the problem that occurs when the transformation from a time domain

to a frequency domain is performed. Cutting off a series to a finite number of terms in a Fourier transform, which is necessary for numerical reasons, often causes a value to appear – especially the real component ε^* – which differs by several orders of magnitude from the expected values. At the same time, even a slight disturbance of the data obtained in the time domain can seriously affect the calculations done by the Fourier transform.

The measuring cell used for TDR measurements is a coaxial capacitor. It is the natural end of the transmission line, which guarantees the correct adjustment of the capacitor to the parameters of the system. This shape of the cell allows one, after placing it in a magnetic field, to obtain a perpendicular and semiperpendicular-semiparallel orientation.

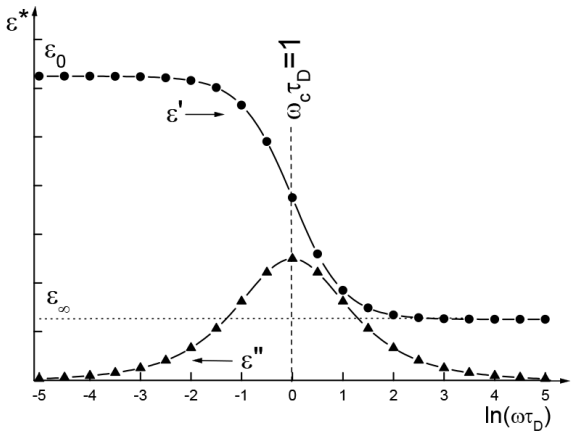

Fig. 2. Schematic diagram of dispersion ε' and dielectric absorption (dielectric losses) ε'' as a function of relative frequency $\Omega \equiv \omega\tau_D$ (the axis of abscissa represents the logarithm Ω)

Why is dielectric spectroscopy such an important measuring technique?

- Firstly, it is an excellent method of characterising phases and phase transitions;
- Secondly, dielectric spectroscopy is a unique way to study the reorientation dynamics of molecular electrical dipole momentum, especially in mesomorphic phases;
- Thirdly, dielectric spectroscopy enables the measurement of material properties, such as the frequency dependence of anisotropy of conductivity and dielectric permittivity, viscosity, elastic constants and the influence of temperature on the above-mentioned properties;
- Fourthly, dielectric spectroscopy is a very versatile technique; measurements can be performed on samples of different thicknesses, from μm to mm; one can use a commercial glass measuring cell (a flat capacitor) with electrodes of the ITO type, and one can measure samples with homeotropic or planar orientation of the director (which distinguishes SD from optical measurements where a homogeneous arrangement of the optical axis is required);
- Fifthly, the dielectric experiment can be fully automated.

The measuring cell in SD is a flat parallel-plate capacitor. This element of the measuring circuit consists of two parallel plates, each with a surface area of S, placed at a distance of d from each other. When a capacitor is connected to the voltage U, an electric field $\vec{\mathbf{E}}$ will appear between its plates (the electric field can be visualised by a vector field whose "trajectories" lines always originating from the positive charge and terminating at the negative charge).

The value of the field is equal to:

$$E = \frac{U}{d} \quad \left[\frac{\mathrm{V}}{\mathrm{m}}\right]. \tag{4.3}$$

When calculating the capacitance C_0 of the capacitor with a vacuum between its plates (actually, it is air, but the assumption of the identity *air≡vacuum* is, in this case, justified[15]), one gets:

$$C_0 = \frac{Q}{U} = \frac{Q}{Ed} = \frac{Q}{\frac{Qd}{\varepsilon_0 S}} = \frac{\varepsilon_0 S}{d} \quad [\mathrm{F}], \tag{4.4}$$

where Q is the value of the charge collected on the plate (on each plate, there is a charge of the same value but with opposite signs – Fig. 3), ε_0 is the dielectric permittivity of vacuum ($\varepsilon_0 = 8.85\ 10^{-12}$ [C^2/Nm^2]).

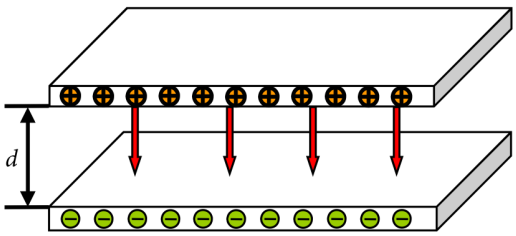

Fig. 3. Flat parallel-plate capacitor charged with Q (d – distance between parallel plates (electrodes))

Thus, the value of capacitance can be determined based on electrical or geometrical values. Having filled the space between the plates of a capacitor with a dielectric (e.g. a liquid crystal – Fig. 4), one will observe polarisation processes occurring in the dielectric. The dipoles are arranged (in the case of a polar dielectric) or formed in the electric field (of a capacitor), or both effects take place simultaneously. One must keep in mind that the phenomenon of polarisation (arrangement of the direction of molecular dipoles) occurs in the entire volume of the dielectric, i.e. a volumetric effect takes place.

[15] Relative permittivites of air at room temperature under 1 kHz is 1.00058986±0.00000050.

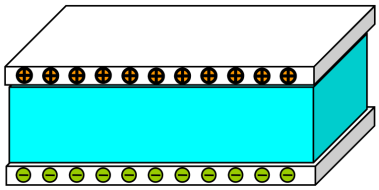

Fig. 4. Flat parallel-plate capacitor (charged) filled with a dielectric

The only difference between a spatial charge generated by polarisation of a free charge is that the former cannot move. The effect of this additional charge is expressed by the polarisation vector $\vec{\mathbf{P}}$ equal to the sum of dipole moments per volume of the dielectric. Because the dipole moment is measured in [Cm], the polarisation unit is [Cm/m^3], i.e. [C/m^2].

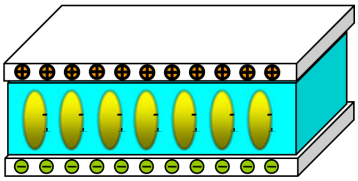

Fig. 5. Polarised capacitor filled with a dielectric

A polarised dielectric induces surface charges on the plates of a capacitor, the sign of which is opposite to the polarising charge, i.e. the same as that of the primary charges (Q). Assuming that the value of the polarisation vector $\left|\vec{\mathbf{P}}\right|$ is directly proportional to the strength of the field $\left|\vec{\mathbf{E}}\right|$ causing the polarisation, one obtains:

$$P = \chi \varepsilon_0 E, \tag{4.5}$$

where χ is the dielectric susceptibility.

If a capacitor remains connected to the voltage U, then its capacitance increases $(1 + \chi)$ times, where $(1 + \chi)$ is a material constant called a dielectric constant (in literature, the designation $(1 + \chi) = \varepsilon$ is also used):

$$C = (1+\chi) C_0 = \varepsilon C_0. \tag{4.6}$$

Dielectric relaxation is the process of gradual return to the state of equilibrium of a system composed of polar molecules with a certain degree of freedom of reorientation when a disturbance such as an alternating electric field $E(\omega) = E_0 e^{i\omega t}$ is removed (where E_0 is the amplitude, and $\omega = 2\pi f$ is the circular frequency).

The observed relaxation is described by the formula:

$$\frac{dP(t)}{dt} = -\frac{P(t)}{\tau}, \tag{4.7}$$

where the τ parameter is the macroscopic relaxation time.

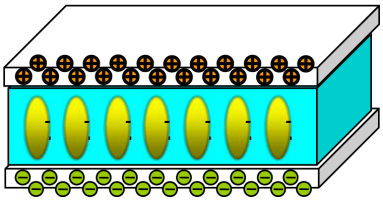

Fig. 6. Polarised capacitor filled with a dielectric – the figure shows surface charges, the sign of which is opposite to the polarisation charge

In the above formula, the effect of interactions between identical reorienting dipoles in a viscous environment is neglected.

Under the assumption of fulfilment of the linear relationship between polarisation *P* and variable field *E*, one obtains:

$$P = \chi^*(\omega)\varepsilon_0 E(\omega) = \left(\varepsilon^*(\omega) - 1\right)\varepsilon_0 E(\omega), \tag{4.8}$$

where

$$\chi^*(\omega) = \chi'(\omega) - i\chi''(\omega) \text{ and } \varepsilon^*(\omega) = \varepsilon'(\omega) - i\varepsilon''(\omega). \tag{4.9}$$

One must keep in mind that the possible phase shift between the polarisation vector and the electric field vector is contained in the frequency dependence of dielectric susceptibility (or dielectric permittivity).

For systems described by the relaxation equation, the dependence of the complex dielectric permittivity on the frequency, $\varepsilon^*(\omega) = \varepsilon'(\omega) - i\varepsilon''(\omega)$, where ε' (real part) means dielectric dispersion, and ε'' (imaginary part) means dielectric absorption, is the following:

$$\varepsilon^*(\omega) - \varepsilon_\infty = \frac{(\varepsilon_s - \varepsilon_\infty)}{1 + i\omega\tau} = \frac{(\varepsilon_s - \varepsilon_\infty)}{1 + i\left(\dfrac{\omega}{\omega_{\max}}\right)} = \frac{(\varepsilon_s - \varepsilon_\infty)}{1 + i\left(\dfrac{f}{f_{\max}}\right)}, \tag{4.10}$$

where the parameter ε_∞ is the value of dielectric permittivity within high frequencies ($\omega \to \infty$), also called the (optical) dielectric constant, and the parameter ε_S is the value of dielectric permittivity within low frequencies ($\omega \to 0$), also called static dielectric permittivity, $f_{\max} = \omega_{\max} / 2\pi = (2\pi\tau_{\max})^{-1}$ determines the maximum absorption, and $\tau_{\max}$ is the macroscopic relaxation time (note that the relaxation equation is also fulfilled by dielectric susceptibility). The parameter ε_∞ specifies relaxation-free inductive polarisation and is not associated with orientation polarisation, which determines dielectric relaxation. In other words, within the high frequency limits, the dipole does not reorient quickly enough to contribute to the dielectric response function. The difference $(\varepsilon_S - \varepsilon_\infty)$ is a measure of the effective dipole moment, taking into account the influence of the molecular environment.

At this point, it should be mentioned that polarisation of the dielectric material is caused by several mechanisms, such as:

- electron polarisation – related to deformation of the electron cloud of atoms, there is a displacement of negative charges of the electron cloud in relation to electrically positive nuclei and the formation of an electric dipole;
- atomic polarisation – related to the relative shift of the centre of charge mass within the lattice;
- ionic polarisation – the result of relative ion dispersion in the crystal lattice;
- dipole polarisation (also called orientation polarisation) – a result of arrangement of permanent dipoles along the direction of an external electric field.

The simplest response function describing the evolution of a system after the application of a disturbance (an electric field impulse) is the exponential function of the following form:

$$\phi(t) = \exp\left(-\frac{t}{\tau}\right), \tag{4.11}$$

where τ is the above-mentioned macroscopic relaxation time.

This relaxation, which is characterised by only one relaxation time, is called Debye relaxation (after the physicist Peter Debye). The model relaxation characteristic for dynamic polarisation with only one relaxation time is the dielectric response of an ideal, noninteracting dipole aggregation to an alternating external electric field.

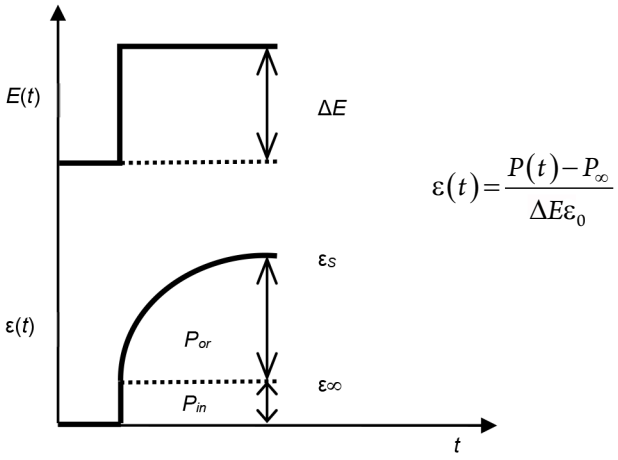

Fig. 7. Schematic image of a polar dielectric reaction to an electric field impulse. $\varepsilon_\infty = \varepsilon\ (\omega \to \infty)$ is the value of dielectric permittivity within the limits of high frequencies and determines non-relaxable inductive polarisation P_{ind}; P_{or} is an orientation polarisation, which conditions dielectric relaxation; and $\varepsilon_S = \varepsilon\ (\omega \to 0)$ is the value of dielectric permittivity within the limits of low frequencies

A simple transformation (multiplication of the denominator of the expression for the combined dielectric permittivity by the conjugate number $(1 - i\omega\tau)$ makes it possible to separate the combined function into the real part and the imaginary part:

$$\varepsilon' - \varepsilon_\infty = \frac{\varepsilon_S - \varepsilon_\infty}{1 + (\omega\tau_D)^2} \qquad \varepsilon'' = \frac{\varepsilon_S - \varepsilon_\infty}{1 + (\omega\tau_D)^2} \cdot \omega\tau_D. \tag{4.12}$$

As has been mentioned, the real part describes dielectric dispersion, i.e. the dependence of dielectric permittivity on the relative frequency ($\Omega \equiv \omega\tau_D$) of the measuring field, and the imaginary part describes the dielectric absorption, i.e. the dependence of dielectric losses on the relative frequency Ω of the measuring field.

Fig. 2 shows that dielectric losses ε'' become zero for both low and high frequencies, and the maximum value is reached at the *critical frequency* $\omega_C = 1/\tau_D$. By measuring ε' and ε'' as a function of the external field frequency ($\varepsilon' = \varepsilon'(\omega)$, $\varepsilon' = \varepsilon'(\omega)$), one can determine the time of dielectric relaxation τ_D.

In a real experiment carried out in the frequency range from hertz to megahertz, bridge methods are used. A capacitor filled with a dielectric is one of the arms of a Schering bridge. The quantity measured by the bridge is the combined conductivity (admittance):

$$Y = G + iB = \frac{1}{Z} = \frac{1}{R + iX} = G + i\omega C \quad [\mathrm{S}], \tag{4.13}$$

where G is conductance, B is susceptance, Z is impedance (hindrance – complex resistance), R is resistance, X is reactance, and C is the capacitance of the measured capacitor.

Conductance G can be linked to ε'':

$$\varepsilon'' = \frac{G}{\omega C_0}, \tag{4.14}$$

and susceptance B can be linked to ε':

$$\varepsilon' = \frac{C}{C_0}, \tag{4.15}$$

where C_0 is the capacity of an empty capacitor (air capacitor).

The presented image of dielectric relaxation has been simplified to describe one mono-time process called the Debye process. In experimental reality, there are usually several processes observed in different frequency ranges. An example is the four different processes shown in Fig. 8. The figure shows that if the critical frequencies differ by at least an order of magnitude, it is possible to separate the mods precisely. We can assume that relaxation processes contribute to dielectric permittivity in an additive manner. Consequently, the complex dielectric constant can be expressed with the following equation[16]:

$$\varepsilon^*(\omega) = \varepsilon_\infty + \sum_k \frac{\Delta_k}{1 + i\omega\tau_{Dk}} \text{ where } \sum_k \Delta_k = \sum_k (\varepsilon_s - \varepsilon_\infty)_k = 1. \tag{4.16}$$

[16] $(\varepsilon_S - \varepsilon_\infty)$ may be called relaxation process amplitude.

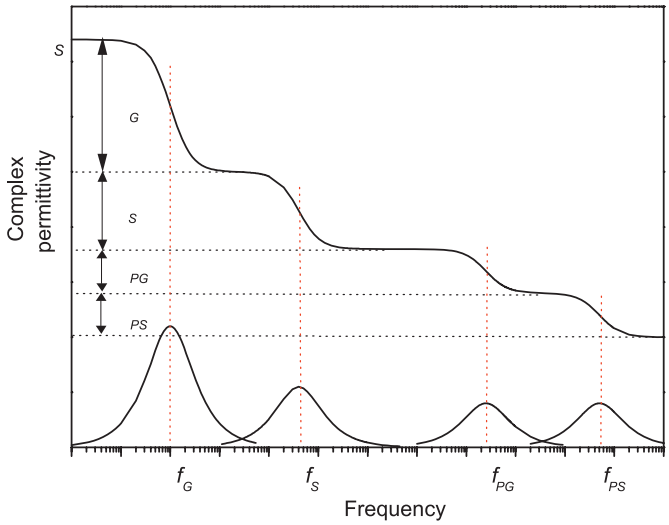

Fig. 8. Complex dielectric constant as a function of the frequency of the measuring field. The figure shows four modes corresponding to four different relaxation processes

It should be emphasised that the Debye relaxation model describes quite correctly an undisturbed three-dimensional rotational diffusion characterised by a single relaxation time. In most of the studied systems, fluctuations of the local molecular structure and the molecular environment cause a situation where only few molecular movements meet these conditions. The experimental results have shown that the Debye formula can only be used in certain cases. In order to achieve better compliance of the phenomenological description with the results of dielectric spectroscopy, the Debye relaxation model was modified by introducing additional empirical parameters. One of the most commonly used modifications is the so-called Cole-Cole equation introduced in 1941:

$$\varepsilon^*(\omega) = \varepsilon_\infty + \frac{\varepsilon_S - \varepsilon_\infty}{1 + (i\omega\tau_D)^{1-\alpha}}, \tag{4.17}$$

where $0 \le \alpha < 1$.

The above formula cannot be derived analytically, but the parameter α, called the relaxation time distribution parameter, is commonly interpreted as a measure of the symmetrical relaxation time distribution around the value of τ_D.

In the case of $\alpha = 0$, there is the so-called Debye equation (Debye-type process), and the Cole-Cole diagram is a semi-circle (Fig. 9a), whereas in the case of $0 < \alpha < 1$, the diagram is an arc of a circle with the centre located below the axis ε' (Fig. 9b). In such a case, the relaxation time is determined using the following relationship:

$$(\omega\tau_D)_i^{1-\alpha} = \frac{v_i}{u_i}. \tag{4.18}$$

The empirical relaxation time distribution parameter α is expressed by the value of the angle θ formed by the axis ε' and the radius of the circle led to the point $\varepsilon_\infty(\theta = \frac{1}{2}\alpha\pi)$.

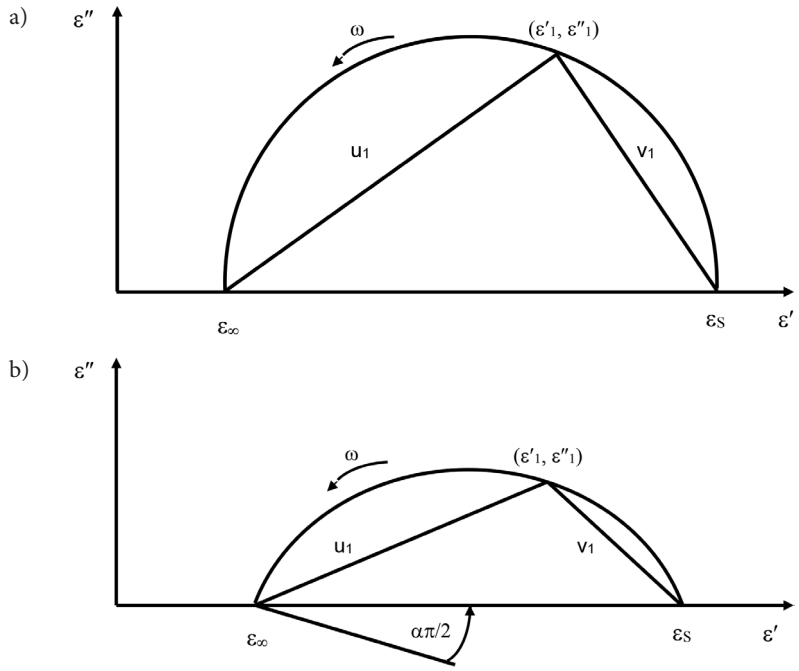

Fig. 9. Cole-Cole Diagrams: typical diagram for a Debye process (a), a relaxation process in which the parameter $\alpha \neq 0$ (b)

Fig. 10 shows the boundary cases of the Cole-Cole diagrams and their associated relaxation time distribution functions.

There are also asymmetrical distributions described empirically with additional parameters. One of them, expressed in the formula below, was proposed by Cole and Davidson in 1951:

$$\varepsilon^*(\omega) = \varepsilon_\infty + \frac{\varepsilon_S - \varepsilon_\infty}{(1 + i\omega\tau_D)^\beta}, \tag{4.19}$$

where $0 < \beta \leq 1$.

In 1966, Havriliak and Negami introduced an even more complicated modification to Debye's formula in the following form:

$$\varepsilon^*(\omega) = \varepsilon_\infty + \frac{\varepsilon_S - \varepsilon_\infty}{\left(1 + (i\omega\tau_D)^\delta\right)^\gamma}, \tag{4.20}$$

where $0 < \delta \leq 1$ and $0 < \gamma \leq 1$.

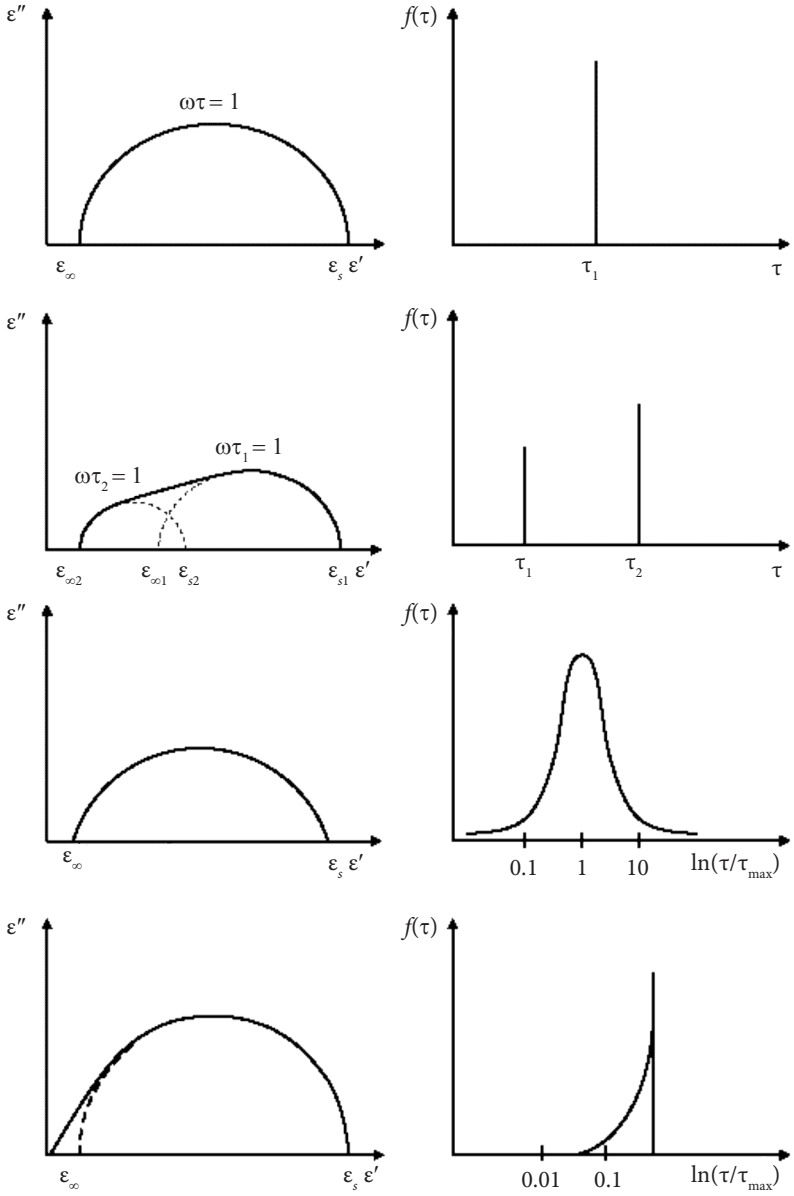

Fig. 10. Cole-Cole diagrams (border cases) and their assigned dielectric relaxation time distribution functions. From the top, the first distribution corresponds to the Debye-type process, the second corresponds to the two Debye-type processes, the third corresponds to the Cole-Cole model, and the fourth corresponds to the Cole and Davidson model

The assumption of stochasticity of the process described by parametric distributions is still maintained. It should be emphasised that increasing the number of fitting parameters leads to better compatibility of the model with experimental results; however, it causes an increase in the number of problems associated with molecular interpretation of the data obtained.

In systems where the condition of linear system response to an applied disturbance is fulfilled, a very important issue is to check whether the response function satisfies the Kramers-Kronig condition. The Kramers-Kronig relation is a mathematical relationship between the real and the imaginary part of a complex function. In the case of SD, the relationship between the real (ε′) and the imaginary (ε″) part of complex dielectric permittivity ε^* is as follows:

$$\varepsilon'(\omega)-\varepsilon_\infty=\frac{1}{\pi}\oint\frac{\varepsilon''(\Omega)}{\Omega-\omega}d\Omega \text{ and } \varepsilon''(\omega)=-\frac{1}{\pi}\oint\frac{\varepsilon'(\Omega)-\varepsilon_\infty}{\Omega-\omega}d\Omega. \tag{4.21}$$

When $\omega \to 0$ and $\varepsilon'(0) = \varepsilon_S$, the function $f(\Omega)$ reaches singularity, and an additive real segment appears, which leads to the modification of the equation for ε'' to the following form:

$$\varepsilon''(\omega)=-\frac{1}{\pi}\oint\frac{\varepsilon'(\Omega)-\varepsilon_\infty}{\Omega-\omega}d\Omega+\frac{A}{\omega}. \tag{4.22}$$

As a consequence of this change, we conclude that the segment A/ω describing the effect of conductivity and revealed within the low frequency limits ($\omega \to 0$) does not have its share in the real component of the complex dielectric permittivity.

Local field models

The electric fields acting on the molecule of a dielectric can be described as a local field. This is always a superposition of an external field applied to a dielectric and a certain "reaction" field that was created in the nearest vicinity of a molecule. The problem of a theoretical description is difficult. Therefore, below are presented the basic local field models proposed by Lorentz, Onsager, Kirkwood and Fröhlich, as well as Bordewijk and de Jeu (who extended the Kirkwood-Fröhlich model onto liquid crystals).

Lorentz local field model

To calculate the local field, Lorentz placed a molecule of a dielectric in the middle of a sphere with a radius that is large compared to the intermolecular distances but small compared to the size of the dielectric (the so-called semi-macroscopic cavity). This made it possible to obtain the formula for the field:

$$\vec{\mathbf{E}}_p = \frac{\vec{\mathbf{P}}}{3\varepsilon_0}, \tag{4.23}$$

where ε_0 is the dielectric permittivity of a vacuum, derived from charges evenly distributed on the surface of the cavity. Lorentz assumed that the fields of interactions with the nearest neighbours cancel each other in gases and liquids due to random movements of molecules, and in crystals, due to high symmetry $\vec{\mathbf{E}}_m = 0$.

The final formula describing the Lorentz local field is given as the following expression:

$$\vec{\mathbf{E}}_{lok} = \frac{\varepsilon_s + 2}{3}\vec{\mathbf{E}}. \tag{4.24}$$

Thus, in the case of non-polar gases and liquids, the deformation polarity looks like this:

$$\vec{\mathbf{P}}_\infty = \varepsilon_0\left(\varepsilon_\infty - 1\right)\vec{\mathbf{E}} = N_0\alpha_\infty\vec{\mathbf{E}}_{lok}, \tag{4.25}$$

where $\vec{\mathbf{P}}_\infty$ and α_∞ are the polarisation and the deforming polarisability, respectively.

After simple transformations, one obtains the Clausius-Mossotti formula, which makes it possible to determine the deforming polarisability on the basis of measurements of the dielectric constant:

$$\frac{\varepsilon_\infty - 1}{\varepsilon_\infty + 2} = \frac{N_0\alpha_\infty}{3\varepsilon_0}, \tag{4.26}$$

where $N_0 = \rho\frac{N_A}{M}$ (N_A – Avogadro number, M – molar mass, ρ – density).

Onsager local field model

In 1936, L. Onsager presented a local field model for dipole dielectrics. In a dielectric, it separated a spherical cavity of a molecular size with a polarisable point dipole inside. The dielectric on the outside of the cavity was treated as a continuous and homogenous medium. Onsager assumed that the local field is a superposition of the cavity field $\vec{\mathbf{G}}$ created by an applied field $\vec{\mathbf{E}}$ and appearing as a reaction of the field system $\vec{\mathbf{R}}$:

$$\vec{\mathbf{E}}_{lok} = \vec{\mathbf{G}} + \vec{\mathbf{R}} = \frac{3\alpha_s}{2\varepsilon_s + 1}\vec{\mathbf{E}} + \frac{2\left(\varepsilon_s - 1\right)}{\left(2\varepsilon_s + 1\right)}\frac{\mu}{4\pi\varepsilon_0 a^3}, \tag{4.27}$$

where μ is the total dipole moment, and a is the radius of the cavity.

The Onsager model can be used to derive the Onsager equation having the following form:

$$\frac{(\varepsilon_s - \varepsilon_\infty)(2\varepsilon_s + \varepsilon_\infty)}{\varepsilon_s (\varepsilon_\infty + 2)^2} = \frac{N_0 \mu^2}{9\varepsilon_0 k_B T}, \tag{4.28}$$

where N_0 is the number of identical molecules per unit volume that have effective dipole moments μ, k_B is Boltzman's constant, and T is the temperature.

The above equation makes it possible to calculate the dipole moments of molecules in pure liquids and in solutions with non-polar solvents. In his local field model, Onsager took into account long-range dipole-dipole interactions (which was not done by Lorentz) but omitted short-range interactions (e.g. interactions of hydrogen bonds). Onsager's theory was "corrected" by Kirkwood and Fröhlich.

W. Maier and G. Meier used the local field model suggested by Onsager to describe nematic liquid crystals. The Maier-Meier theory combines the main components of the tensor $\hat{\varepsilon}$ with the main components of the dipole moment $\vec{\mu}$ and the local field coefficient:

$$\varepsilon_0 (\varepsilon_{s\parallel} - 1) = hFN_A \left[\left(\alpha_l + F \frac{\mu_l^2}{k_B T} \right) \langle \cos^2 \theta \rangle + \left(\alpha_t + F \frac{\mu_t^2}{k_B T} \right) \langle \sin^2 \theta \rangle \right], \tag{4.29}$$

$$\varepsilon_0 (\varepsilon_{s\perp} - 1) = \frac{1}{2} hFN_A \left[\left(\alpha_l + F \frac{\mu_l^2}{k_B T} \right) \langle \sin^2 \theta \rangle + \left(\alpha_t + F \frac{\mu_t^2}{k_B T} \right) \langle 1 + \cos^2 \theta \rangle \right], \tag{4.30}$$

where F is the reaction field coefficient, h is the cavity coefficient, and μ_l and μ_t are components of the permanent dipole moment along the direction of the long l and short t axes of the molecule, and $\varepsilon_{s\parallel}$, $\varepsilon_{s\perp}$ are components measured, respectively, parallel and perpendicular to the director.

Kirkwood-Fröhlich local field model

Onsager, in his field model, did not take into account short-range intermolecular forces, which are the cause of correlation of orientation of neighbouring molecules. These correlations were taken into account in the theory developed by H. Fröhlich and J.G. Kirkwood.

Fröhlich considered the intermolecular interaction by considering a semi-macroscopic cavity containing N molecules (where N is a number that is small enough to treat the problem microscopically but large enough to apply statistical laws). Kirkwood, in turn, considered the correlations between the orientations of the dipole moments of neighbouring molecules by introducing the parameter g.

The equation they proposed looks like this:

$$\frac{(\varepsilon_s - \varepsilon_\infty)(2\varepsilon_s + \varepsilon_\infty)}{\varepsilon_s(\varepsilon_\infty + 2)^2} = \frac{N_0}{9\varepsilon_0 k_B T} g\mu^2, \tag{4.31}$$

where g is the Kirkwood-Fröhlich correlation coefficient defined by the following formula:

$$g = 1 + \sum_{i \neq j} \langle \cos\theta_{ij} \rangle, \tag{4.32}$$

where θ_{ij} is the angle between the directions of permanent dipole moments of molecules i and j.

The g parameter indicates whether and how the orientations of neighbouring dipoles are interdependent. When $g = 1$, this means that the orientations of the dipoles are uncorrelated (the Kirkwood-Fröhlich formula turns into the Onsager formula), when $g < 1$, the dipoles assume an anti-parallel orientation, and when $g > 1$, the dipoles tend to be parallel.

The g coefficient goes up to 1 as the temperature rises. An increase in temperature (increase in the energy of movements) weakens the inter-dipolar correlations.

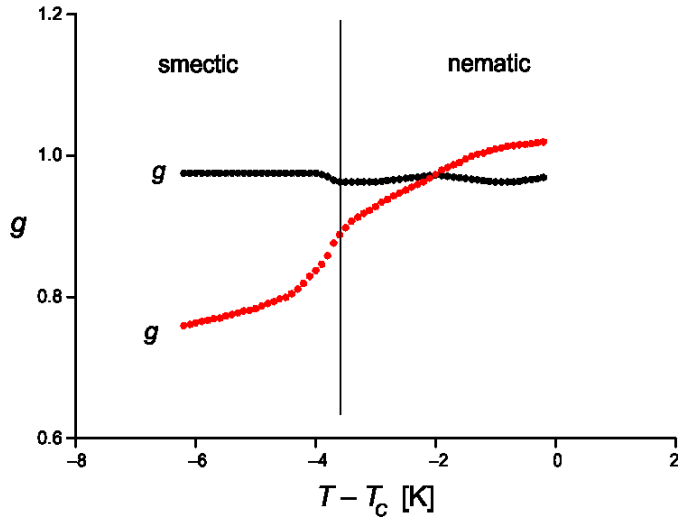

Fig. 11. Example of the temperature dependence of the correlation coefficient

Local field model for liquid crystals – de Jeu and Bordewijk

P. Bordewijk was the first to define an ellipsoidal cavity rather than a spherical cavity in his calculations of the local field. Nevertheless, Kirkwood-Bordewijk's extended theory makes it possible to calculate, in a transparent manner, the relation between microscopic values and the macroscopic field $\vec{\mathbf{E}}$ only in two extreme cases: for an ideal arrangement ($\alpha_{\parallel} = \alpha_1$, $\alpha_{\perp} = \alpha_t$) and for isotropic distribution of the tensor of polarisability ($\alpha_1 = \alpha_t$).

Further improvements were made by de Jeu and Bordewijk. In 1978, they presented an equation that is an extension of the Kirkwood-Fröhlich theory to cover anisotropic systems (e.g. liquid crystals). Starting from the experimentally observed proportionality between the birefringence – $\Delta\varepsilon_{\infty} = \Delta n^2 = n^2_{\parallel} - n^2_{\perp}$ – and the order parameter S – $\Delta\varepsilon_{\infty} \sim N_0 \cdot S$ – they proposed a linear relationship between the macroscopic electric field $\vec{\mathbf{E}}$ and the field inside a polarised dielectric $\vec{\mathbf{E}}_i$. In case of diamagnetic susceptibility, where a linear relationship with the order parameter was also found, the relationship – $(\chi_{\parallel} - \chi_{\perp}) = (\chi_1 - \chi_t) \cdot S$ – suggests that the field "acting" on the molecule can be identified with the macroscopic field. Hence, the above conclusion about the linear relationship is described by the formula $\vec{\mathbf{E}}_F \equiv \vec{\mathbf{E}}_i = \hat{K} \cdot \vec{\mathbf{E}}$ where $\hat{K}$ is the second rank tensor.

The final form of the formula they proposed is the following:

$$\frac{\left(\varepsilon_{0_\lambda} - \varepsilon_{\infty_\lambda}\right)\left(\varepsilon_{0_\lambda} + \left(\varepsilon_{\infty_\lambda} - \varepsilon_\lambda\right)\Omega^{\varepsilon}_{\lambda}\right)}{\varepsilon_{0_\lambda}} = \frac{N_0}{\varepsilon_p k_B T} g_\lambda \left\langle \left(\mu_d\right)^2_\lambda \right\rangle, \tag{4.33}$$

where $\lambda \equiv$ l, t; (l – direction of the long axis of the molecule, t – direction of the short axis of the molecule), $\Omega_\lambda^{\varepsilon}$ is a tensor coefficient dependent on the shape of the cavity and the dielectric anisotropy, and g_λ is the de Jeu-Bordewijk anisotropic correlation coefficient.

The molecular dipole $\mu^2_d = \mu^2_l + \mu^2_t$ is defined in relation to molecular coordinates l and t:

$$\left(\vec{\mu}_d\right)_\lambda = \hat{K}_\lambda \cdot \vec{\mu}_\lambda \;\; \lambda \equiv \text{l}, t. \tag{4.34}$$

In the above formula, $\hat{K}_\lambda$ is a second rank tensor with the main components defined by the following formulas:

$$K_l = \left(1 - \frac{1}{\varepsilon_p} N_0 \alpha_l \Omega^{sh}_l\right)^{-1}, \tag{4.35a}$$

$$K_t = \left(1 - \frac{1}{\varepsilon_p} N_0 \alpha_t \Omega^{sh}_t\right)^{-1}. \tag{4.35b}$$

An important feature of this model is the introduction of an effective polarisation dependent through Ω_i^{sh} on the local structure of the medium:

$$\Omega_l^{sh} = 1 - w + \frac{1}{2} w\left(w^2 - 1\right) \cdot \ln\left(\frac{w+1}{w-1}\right), \tag{4.36a}$$

$$\Omega_t^{sh} = \frac{1}{2}\left(1 - \Omega_l^{sh}\right), \tag{4.36b}$$

where $w^2 = a^2/(a^2 - b^2)$, while a and b are, respectively, the length and the width of the ellipsoid.

Ultimately, the transverse and longitudinal components of a molecular dipole are expressed by the following formulas:

$$\left\langle \left(\mu_d\right)_{||}^2 \right\rangle = \frac{1}{3}\left(\left(\mu_d\right)_l^2 \left(1 + 2S\right) + \left(\mu_d\right)_t^2 \left(1 - S\right)\right), \tag{4.37a}$$

$$\left\langle \left(\mu_d\right)_{\perp}^2 \right\rangle = \frac{1}{3}\left(\left(\mu_d\right)_l^2 \left(1 - S\right) + \left(\mu_d\right)_t^2 \left(1 + \frac{S}{2}\right)\right). \tag{4.37b}$$

It should be emphasised that the issues discussed herein concerned the description of monomolecular dynamics processes.

References

[1] Wojciech Otowski. *Molecular motion in liquid crystals as seen via dielectric spectroscopy*, [in:] *Dielectric Properties of Liquid Crystals,* Transworld Research Network, monograph edited by Z. Galewski and L. Sobczyk, Vol. 37/661 (2), 2007, 1–33.

5. ROTATIONAL MOTION MATTER – SELECTED PROBLEMS[17]

Since time immemorial, people have been observing movement. It was Aristotle who formulated the first laws of the movement. Having a certain rather intuitive notion of force, he created the foundations of dynamics. His erroneous concepts survived until the 17th century, and it was only the works of Galileo and Newton that led to the formulation of the laws of movement that are accepted today. Dynamics, a word of Greek origin, remained and, with the development of knowledge and measuring instruments, became synonymous with phenomena related to all forms of movement. On the one hand, we talk about the dynamics of "macro" objects, such as planets and stars, and on the other hand, we analyse the dynamics of molecules and atoms, for example the dynamics of a crystal lattice.

Types of molecular motion

The term "dynamics" in broadly defined molecular systems can refer to both molecular motions and, for example, to hydrodynamic effects[18]. From the point of view of the following chapter, it is important to analyse reorientation movements of entire molecules and molecular groups.

Below is defined, uniformly for the entire paper, the different types of molecular movements: translation, orientation and internal:

- translational (progressive) movement leads to relocation of the centre of mass of the molecule as a whole;
- orientation motion is the rotation of the entire molecule around a chosen reference system. These rotations can be almost free or partially hindered and limited to torsional movements. These movements concern a model molecule, which cannot always be identified with a physical molecule, and are commonly referred to as molecular movements. The term "intermolecular movements" is sometimes used to distinguish it from the following intramolecular movements;
- internal movement is, in the case of molecules with a complex chemical structure, the motion of one or more molecular groups that perform

[17] Wojciech Otowski – own materials and references cited therein [1].

[18] Complementary material on the dynamics of molecules in Polish is contained in the book *Chemical Physics* [5].

intramolecular reorientations independently of the movement of the entire molecule. The term "intramolecular movement" is also used for this type of movement.

The definitions presented above apply to a single molecule, the motion of which is determined by its surrounding neighbours. The second group of movements are collective processes or correlated movements of many molecules. On a time scale, they are, by their nature, slower than molecular (monomolecular) processes. Using the classical division into crystalline phases, liquids and gases can be attributed to the occurrence of different types of movements in each of them. In a crystal, collective processes are present – these are vibrations (of low amplitude) of atoms or molecules. In liquids, reorientation motions are observed, for example, stochastic translation motions. In gases, there are both undisturbed rotation and rare collisions that limit the full freedom of translation.

An interesting example of collective processes is the two modes existing in the low-frequency relaxation area of ferroelectric liquid crystals – the Goldstone mode and the "soft" mode. Relative reorientation of the molecule in relation to the selected reference system (e.g. a molecular system) can also occur as a result of a collective process that changes the direction of the director $\vec{\mathbf{n}}$ (an electroconvection phenomenon).

Isotropic rotational diffusion: the Debye model

In the comments to and descriptions of many molecular processes, the reader may find the term "Debye relaxation" or "Debye process". Let us explain the concept (see chapter 4, page 71 of [1]).

In all molecular systems with a defined degree of freedom of reorientation, a continuous, chaotic movement of molecules is observed; the movement is progressive, rotational or oscillating. This stochastic sequence of steps that change the orientation of a molecule is called Brownian motion. The theoretical explanation of their essence was provided in the works of Marian Smoluchowski and Albert Einstein (1905–1906). The authors have shown that the Brownian motions are the result of the thermal movement of atoms and molecules postulated by the kinetic theory of matter. Using the idea of Brownian motions, Peter Debye (1929) proposed a diffusional model of molecular reorientation. The essence of the model is the assumption that the reorientation movement of the molecule is a three-dimensional, spherically isotropic, unhindered rotational diffusion subject to the laws of classical mechanics. The duration of each stochastic diffusion step is so short that the molecule does not perform a full rotation in its course – it changes its orientation only slightly (infinitesimal). The stochastic effect results from the assumption that collisions of molecules eliminate any interdependence of the movement. By solving the rotational diffusion equation, one can calculate the relaxation time of the diffusing molecules.

According to the model's assumption, it is a single time characteristic of the system called macroscopic relaxation time τ, dependent on the temperature in an activating manner. The diffusion equation is a differential equation. It describes the change in time of density of the probability $P(\vec{\mathbf{R}},t)$, specifying that molecules are at the t moment in the volume element dR^3 in the space point described by the vector $\vec{\mathbf{R}}$, which is a set of coordinates necessary to determine the position and orientation:

$$\frac{\partial P\left(\vec{\mathbf{R}},t\right)}{\partial t} = \hat{D}\left(\vec{\mathbf{R}}\right)\cdot P\left(\vec{\mathbf{R}},t\right). \tag{5.1}$$

The rotational diffusion operator $\hat{D}$ can be additively enlarged by components taking into account e.g. molecule collisions. It should be emphasised here that the diffusion equation does not provide a correct description of reorientation in times shorter than ω_g^{-1}, where $\omega_g^2 = k_B T/I$, where I is the moment of inertia of a given molecule. For example, for most liquid crystal molecules, the limit is 10 ps.

Despite the limitations introduced to the Debye model, and especially the condition of free reorientation, it turns out that many experimental results obtained even for anisotropic systems, such as liquid crystals, allow one to define the corresponding movements as Debye processes, i.e. those characterised by a single time of relaxation (mono-time processes).

Tsu-Wei Nee and Robert Zwanzig proved (qualitatively and quantitatively) that the mono-time process is one of the possible motions resulting from the model of two-dimensional rotational diffusion that they proposed. The authors assume in their model, firstly, that the motion takes place on the surface of a cone and, secondly, that reorienting molecules with rigidly bound dipoles produce a time-dependent electric field in their environment. As a result of dielectric losses, the energy of the field is dissipated in space, which causes the effect of friction and braking of reorienting dipoles. This way of describing the molecular process leads to the occurrence of a relaxation time distribution. In this case, the diffusion operator consists of two components $\hat{D} = \hat{D}_O + \hat{D}_C$, where $\hat{D}_O$ is the classic operator of the evolution of the system in the absence of friction, and $\hat{D}_C$ is the collision operator taking into account any fluctuations resulting from the interaction with the environment. From a molecular standpoint, this two-dimensional reorientation concerns the internal motion of a part of the molecule in relation to the selected bond. However, if the internal movements are strongly hindered, and there is a reorientation of the entire (almost) rigid molecule whose movement is weakly hindered, then the result is a Debye process. It should be emphasised that the authors assume that the rotating molecules "slide" perfectly in relation to the environment. Thus, the kinetic energy of spherical molecule rotation is diffused only as a result of dielectric friction, and viscosity does not affect motion.

Hubbard conducted a theoretical analysis of the assumption made by Nee and Zwanzig. Taking into account both the effect of dielectric friction caused by the

environment of the rotating molecule and viscosity, the author demonstrated that in the case of an ideal slip and at the zero frequency limit of an electric field, the dispersion function describing the reorientation described above is a function typical for the Debye process, which confirms the correctness of the assumption made. Thus, under certain specific conditions, the system of reorienting mutually interacting molecules can be described as a mono-time rigid rotator model. Hubbard and Wolynes also analysed the solution of the diffusion equation when the diffusion operator consists of two components. An important conclusion of the analysis is that the effect of dielectric friction decreases with the increase in the number of L, which is an index of the Y_{Lm} function describing the orientation of molecules. However, in the case of dielectric spectroscopy where $L = 1$, it is necessary to take into account the discussed effect. The second observation is the induction by dielectric friction of a relaxation time distribution, which can be described as a multi-exponential decay function. Hubbard and Wolynes also concluded that when the interaction between molecules (rotating dipoles) is very strong, and the environmental configuration is quasi-static, the diffusion process responsible for the reorientation goes into a jump process. Thus, a simple description with the Debye formula is incorrect.

In 1967, Fatuzzo and Mason suggested a model similar to the deliberations presented by Nee and Zwanzig. It seems, however, that the form of presentation and the manner of obtaining the results by Nee and Zwanzig are much simpler and more direct than the Fatuzzo and Mason model.

It should be emphasised that translation motion can greatly reduce the distribution of relaxation times. Nee and Zwanzig demonstrated that long-range orientation correlations responsible for dielectric friction (η_{DF}) are frequency dependent, which leads to a departure of the relaxation process from the form of the Debye process. However, the inclusion of the translation mode in η_{DF}, in the microscopic hydrodynamic theory of relaxation, reduces the above-mentioned time distribution described by the multi-exponential decay function. This was the solution suggested by Bagchi and Chandra. The authors introduced the p' coefficient that additively modifies the translation diffusion tensor. When $p' = 0$, the translation effect is ignored as it was by Nee and Zwanzig. Obtaining the Debye process type behaviour requires, according to the authors, that p' be equal to e.g. 0.3 for water or 0.7 for methanol.

Anisotropic rotational diffusion

The diffusion equation presented above (Eq. 5.1) is a very attractive way to describe molecular dynamics. However, considering both the anisotropy of the reorienting object and the anisotropy of the medium in which the object is located creates problems in the mathematical description of the issue. The anisotropic diffusion formula has to be analysed not generally but for selected special cases.

In the case of nematic and smectic phases, the anisotropic diffusion equation has the following form:

$$\frac{\partial P\left(\vec{\mathbf{R}},\Omega,t\right)}{\partial t} = -\hat{D}_A \cdot P\left(\vec{\mathbf{R}},\Omega,t\right), \tag{5.2}$$

where, as before, P is the probability density. The vector $\vec{\mathbf{R}}$ determines the position, and the set of Euler angles Ω determines the orientation of the model molecule. The anisotropic diffusion operator $\hat{D}_A$ consists additively of translational and rotational components – $\hat{D}_A = \hat{D}_T + \hat{D}_R$. In the nematic phase, P is independent of $\vec{\mathbf{R}}$ – $P\left(\vec{\mathbf{R}},\Omega\right) \equiv P\left(\Omega\right)$ – and we are dealing with the rotation as in the case of magnetic or dielectric relaxation. On the other hand, however, transport phenomena occurring over long distances observed, e.g. using the spin echo technique, described by the translation operator, average the reorientation movement. In general, the rotational-translation coupling effect of $\hat{D}_T\left(\Omega\right)$ should be taken into account when analysing the neutron spectra, because in this case, the spectral function depends on the position and the orientation.

In the smectic phase A, due to the heterogeneous density of the medium along the normal to the smectic planes (axis Z), it is not possible to develop $P\left(\vec{\mathbf{R}},\Omega\right)$ into a functional series. Additionally, a strong rotational-translational coupling prevents such an analysis of the diffusion equation, because the frequency-dependent tensor rotational operator $J(\omega)$ has, in addition to a rotational component $\hat{J}^R(\omega)$, a translation component $\hat{J}^T(\omega)$:

$$\hat{J}(\omega) = \hat{J}^R(\omega) + \hat{J}^T(\omega). \tag{5.3}$$

Diffusion equation and internal motions

The diffusion equation can also take into account internal motions. The simplest form of description of an internal motion is to treat it as a jump between conformational equilibrium positions. For one degree of freedom, the matrix W of the passage from the minimum 'm' to the minimum 'n' through the saddle point 's' is expressed by the formula:

$$W_{m\to n} = \left(\frac{D_s\left|U_s\right|}{2\pi k_B T}\right)\exp\left(\frac{E_m - E_s}{k_B T}\right), \tag{5.4}$$

where D_s – diffusion tensor, U_s – conformational potential, E_i ($i \equiv m,s$) – free energy.

The general form of the diffusion equation for molecules with multiple degrees of freedom takes the following form:

$$\frac{\partial}{\partial t} P(\Phi,\Omega,t) = \left(\hat{D}^i + \hat{D}^r\right) \cdot P(\Phi,\Omega,t), \tag{5.5}$$

where Φ describes the internal coordinates, and Ω describes the external coordinates that define the orientation in the laboratory system. $\hat{D}^i$ and $\hat{D}^r$ are, respectively, the tensor describing the reorientation of the entire molecule and the tensor describing the reorientation of its fragments. The potential acting on the molecule with internal degrees of freedom in the anisotropic phase can be expressed in the following form:

$$U(\Phi,\Omega) = U^{tors}(\Phi) + U^{mf}(\Phi,\Omega), \tag{5.6}$$

where $U^{tors}(\Phi)$ is the twist component, and $U^{mf}(\Phi,\Omega)$ is the component describing the anisotropic interaction with the environment. The above formula can be broken down into the sum of components coming from different units, such as e.g. functional molecular groups:

$$U^{mf}(\Phi,\Omega) = U^{core}(\Omega) + \sum_i U^i(\Phi,\Omega), \tag{5.7}$$

where $U^{core}(\Phi)$ and U^i describe, respectively, the energy of the body of the molecule and the energy of its *i*-th fragment, taking the following form:

$$\begin{aligned} \frac{U^{core}}{k_B T} &= E_1 D_{00}^2(\Omega) \\ \frac{U^i}{k_B T} &= E_2 D_{00}^2(\Omega_i) \end{aligned} \tag{5.8}$$

where E_1 and E_2 are, respectively, the strength of the external molecular field acting on the body and the *i*-th fragment of the molecule.

Ferrarini et al. [2] made numerical estimates of the spectral densities of the NMR signal for 4-pentyl-4′-cyanobiphenyl (5CB). They assumed two coupling states and that the ratio of the components of the anisotropic diffusion tensor are $D_{\|}/D_{\perp} = 10$. In the first state, they assumed the existence of a coupling between the movement of the body (inter motion) and the internal movements (intra motions). In the other state, they assumed there was no such coupling. The calculations made it possible to conclude that the coupling effect becomes significant when the diffusion movement of the molecule, as a whole, is slower than the frequency of the conformational jumps.

Diffusion equation and molecular biaxiality effect

Let us consider a molecule that, from the point of view of symmetry, can be considered as biaxial. We will have to deal with such an effect when analysing, for example, disc--like molecules, where, in order to fully define their degree of order, one has to take into account the parameters S and D.

The parameter S is the mean value of the Legendre polynomial P_2:

$$S = \left\langle \frac{1}{2}\left(3\cos^2\theta - 1\right)\right\rangle = \left\langle P_2 \right\rangle, \tag{5.9}$$

where the angle θ is the angle between the axis of symmetry of the elongated molecule and the axis of symmetry of the mesophase, and the parenthesis < > is the statistical-mechanical average. In the description of the arrangement with the so-called Saupe array, the D parameter corresponds to the following expression:

$$D = \left\langle \frac{3\left(l_X^2 - l_Y^2\right)}{2} \right\rangle, \tag{5.10}$$

where $l_i = l_X, l_Y, l_Z$ are the director's directional cosines relative to the molecular axis of the reference system.

Diffusion equation and local field effect

It should be emphasised that the presented applications of the diffusion equation for the analysis of molecular dynamics were related to the reorientation of a selected *model* molecule placed in an anisotropic environment. It can be stated that the "solvent" molecules form an anisotropic molecular potential field acting on the model molecule of the dissolved substance. The "solvent" also determines the form of the diffusion tensor used to describe the dynamics.

When considering the problem of the molecular field, the idea appears for recording the potential in the following form:

$$U\left(x, X\right) = U_0\left(x\right) + U_0\left(X\right) + U_\infty\left(x, X\right), \tag{5.11}$$

where the x and X coordinates determine the position relative to the solved substance system and the solvent system. The component $U_\infty\left(x, X\right)$ describes the interaction of these two systems. In the case of dielectric spectroscopy where dipole molecules $\vec{\mu}$ are involved, the coupling effect between the model molecule oriented in relation to the laboratory system and the "solvent" appears as dielectric friction. An analogy can be seen with the effect of braking of the reorientation of electric dipoles introduced

by Tsu-Wei Nee and Zwanzig. In literature, the following expression is used for the time of relaxation of model molecules of a solution in the isotropic phase:

$$\tau_L \approx \frac{\left\{\tau_R + \left(\frac{2\Delta E_S}{k_B T}\right)\tau_S\right\}}{L(L+1)}, \tag{5.12}$$

where $\tau_R = (D_R)^{-1}$ and τ_S is the correlation time for fluctuations of solvent polarisation. The interaction energy ΔE_S is a function of the volume V occupied by the model molecule, the ε_s static dielectric permittivity and the ε_∞ (optical) dielectric constant of the solvent:

$$\Delta E_S = \frac{\mu^2}{V}\left(\frac{\varepsilon_s - 1}{2\varepsilon_s + 1} - \frac{\varepsilon_\infty - 1}{2\varepsilon_\infty + 1}\right), \tag{5.13}$$

In literature on this subject, this issue is often referred to as the problem of local field. Knowledge of the local field makes it possible to determine the relationship between the macroscopic and microscopic parameters of a dielectric. However, one must keep in mind that the macroscopically measurable values describing a dielectric are statistical in nature and are the result of many complex processes, whose inclusion in the model(s) qualitatively and quantitatively describing a given dielectric substance is often impossible. This entails the need to introduce various assumptions limiting the generality and applicability of the results obtained.

Onsager separated a spherical macro-cavity in a dielectric with a polarisable point dipole inside. He assumed that the local field is a superposition of the cavity field $\vec{\mathbf{E}}_C$ (created by an applied field $\vec{\mathbf{E}}$) and the field $\vec{\mathbf{R}}$ appearing as a reaction – $\vec{\mathbf{E}}_{loc} = \vec{\mathbf{E}}_C + \vec{\mathbf{R}}$. In his calculations, however, he did not take into account intermolecular short-range interactions, assuming that the environment of the cavity is a homogeneous and continuous medium with dielectric permittivity of ε_0. The theory proposed by Fröhlich and Kirkwood had no such limitation. Fröhlich took the intermolecular interaction into account by considering a macro-cavity with many molecules in it. Kirkwood took into account the degree of correlation between the orientations of the dipole moments of the neighbouring molecules by introducing the parameter g, referred to as the Kirkwood-Fröhlich correlation coefficient:

$$g = 1 + \sum_{i \neq j} \left\langle \cos \Theta_{ij} \right\rangle, \tag{5.14}$$

where Θ_{ij} is the angle between the directions of permanent dipole moments of molecules i and j. When $g < 1$, dipoles tend to be antiparallel, $g > 1$ means a tendency to parallel dipoles correlations, and $g = 1$ means that the orientations of all dipoles are completely random. As a result, they obtained the formula:

$$\frac{(\varepsilon_0 - \varepsilon_\infty)(2\varepsilon_0 + \varepsilon_\infty)}{\varepsilon_0 (\varepsilon_\infty + 2)^2} = \frac{N_0}{9\varepsilon_p k_B T} g\mu^2, \tag{5.15}$$

called the Kirkwood-Fröhlich formula, where ε_p means the dielectric permittivity of vacuum, $N_0 = \rho N_A / M$ is the number of identical molecules in the volume unit having effective dipole moments $\vec{\mu}$, T is the temperature, k_B is the Boltzman constant, ρ is the density, N_A is the Avogadro number, and M is the molar mass. The expression $g\mu^2$ is often referred to as the effective dipole moment – $\mu^2_{eff} = g \cdot \mu^2$:

$$g_{||} = \frac{\left\langle \sum_k (\mu_{||})_i (\mu_{||})_k \right\rangle}{\mu_l^2}, \tag{5.16a}$$

$$g_{\perp} = \frac{\left\langle \sum_k (\mu_{\perp})_i (\mu_{\perp})_k \right\rangle}{\mu_t^2}, \tag{5.16b}$$

where the summation extends to all molecules different from the selected molecule *i*, and the components of the dipole moment μ_l and μ_t are defined, respectively, as parallel and perpendicular to the long molecular axis *L*.

Other values, such as dielectric permittivity, become a second order tensor ε_{ij}, where *i, j* are permutations of the axes (*X, Y, Z*) of a selected macroscopic (laboratory) coordinate system. Bringing this tensor to a diagonal form results in:

$$\check{\varepsilon} = \begin{bmatrix} \varepsilon_\perp & & \\ & \varepsilon_\perp & \\ & & \varepsilon_{||} \end{bmatrix}, \tag{5.17}$$

where $\varepsilon_{\parallel} = \varepsilon_{ZZ}$ $\varepsilon_\perp = (\varepsilon_{XX} + \varepsilon_{YY})/2$ and ε_{XX}, ε_{YY}, ε_{ZZ} are the components measured along the axes *X, Y, Z*. The main components of the tensor $\varepsilon_{||}$ and $\varepsilon_\perp$ can be measured, respectively, parallel and perpendicular to the director $\vec{\mathbf{n}}$. Of note is the fact that dielectric anisotropy in liquid crystals was observed by Jeżewski as early as in 1924. He measured the first two liquid crystals, oriented with an electric field, from the homologous series *p*-anisotropy: PAA and PAP.

W. Maier and G. Meier developed the theory of static dielectric permittivity (MM theory), combining the main components of the tensor $\hat{\varepsilon}$ with the main components of dipole moment $\vec{\mu}$ and the local field, which resulted in an expression for dielectric anisotropy:

$$\Delta\varepsilon = \varepsilon_{||} - \varepsilon_{\perp} = \frac{1}{\varepsilon_p} N_0 FhS\left[\Delta\alpha + \frac{F}{2k_B T}\mu^2\left(3\cos^2\beta - 1\right)\right] = \frac{1}{\varepsilon_p} N_0 FhS\left[\Delta\alpha + \frac{F}{k_B T}\left(\mu_l^2 - \frac{1}{2}\mu_t^2\right)\right], \tag{5.18}$$

where F is the coefficient of the reaction field, h is the coefficient of the cavity, $\Delta\alpha = \alpha_l - \alpha_t$ is the anisotropy of the tensor of polarisability, and S is the parameter of order.

Correlation function

The system of molecules is a dynamic system, with a continuous, chaotic thermal movement of mesogens. However, one can imagine that it is an external factor that causes an additional disturbance. Assuming that we are dealing with dipole molecules, it is their interaction with the external electric field that will cause a change of the energy state of the system. Removing the external factor will enable the system to return to the state of equilibrium in a finite but non-zero time. The return process is called the *relaxation process*. By tracing in time the behaviour of a chosen physical value, for example the dipole moment, one can, in some cases, determine the time of return of the system to its original state; this time is called *relaxation time*.

One of the forms of the description of the "return process" is an analysis of the molecular correlation function of the physical value A. By measuring the response function of the system at $t = 0$, and later at $t = t_1 > 0$, one can express the fluctuation of the correlation of the value A by means of the correlation function $C_A(t)$. The C_A function is defined as the average of the product of the value of A at the initial moment $t = 0$ multiplied by the value at the moment $t = t_1 > 0$:

$$C_A(t) = \left\langle A_i(0) A_j(t) \right\rangle. \tag{5.19}$$

When $i \neq j$, then the function $C_A(t)$ is called the mutual correlation function. If $i = j$, then this is autocorrelation of the same molecule in different time moments. The autocorrelation function reaches its maximum at the moment $t = 0$, when the value A is compared with itself. It is more convenient to use the normalised autocorrelation function:

$$C_A(t) = \frac{\left\langle A(0)A(t) \right\rangle}{\left\langle A(0)A(0) \right\rangle}. \tag{5.20}$$

According to the ergodic hypothesis, i.e. the assumption that the averaging of all the elements of a set is the same as the averaging of time for the selected element of

the set and the assumption that the system remains in the state of thermodynamic equilibrium for negative times ($t < 0$), the correlation functions can be expressed with the formula:

$$C_A(t) = \lim_{T\to\infty} \frac{1}{T} \int_0^T A(\tau)A(t+\tau)d\tau, \tag{5.21}$$

where T is the time interval in which the averaging was performed.

The correlation function is associated with its integral characteristics, called the correlation time τ_A of the value A:

$$\tau_A = \int_0^\infty C_A(t)dt. \tag{5.22}$$

If a molecule makes random jumps over a potential barrier under the influence of sudden fluctuations in energy, one can speak of a stochastic process. Let us assume that there is a molecular system with two equal equilibrium positions and that at the moment $t = 0$ all molecules of this system are in the first position. Over time, the molecules will jump to the second position. This process will continue until the equilibrium is reached, i.e. until the degree of occupancy of the first and second position is the same. In relation to the entire set of molecules, one can describe the above phenomenon with the formalism of the correlation function. There will be a connection, an identity correlation, of the state from before the given moment of time with the state from the present moment, because, in the system, there is a memory about the occurring phenomena. This memory will decrease (asymptotically) to zero. The correlation function can be considered in this case as the probability of finding the quantity A in any point of space at moment t if the specific quantity was in another point of space at moment $t = 0$.

In the general case of non-normalised correlation functions of physical properties, mathematical formalism boils down to the averaging of Legendre's polynomials (so-called spherical harmonics):

$$C_L(t) = (2L+1)\left\langle P\left(\cos\Theta_0\right)\cdot P\left(\cos\Theta_t\right)\right\rangle, \tag{5.23}$$

where Θ_0 is the angle measured at $t = 0$, and Θ_t is the angle measured at $t = t_1 > 0$. $L = 1$ is the correlation function studied in dielectric measurements, and $L = 2$ corresponds to the correlation function in the nuclear magnetic resonance method (NMR).

The microscopic normalised correlation function of a single permanent dipole moment $\vec{\mu}$ whose length $|\vec{\mu}| = \mu$ does not depend on time ($\mu(0) = \mu(t)$) is defined as:

$$C_\mu(t) = \frac{\langle \mu(0)\mu(t)\rangle}{\langle \mu(0)\mu(0)\rangle}. \tag{5.24}$$

In the nematic or smectic phase A, assuming the orientational order, i.e. considering a rigid molecule, the correlation function $C_A(t)$ will be limited to the averaging of the values of angle Θ.

This results in the function:

$$C_\mu(t) = \frac{\langle \mu(0)\mu(t) \rangle}{\langle \mu(0)\mu(0) \rangle} = \frac{\langle \mu^2 \cdot \cos(\Theta(t)) \rangle}{\mu^2} = \langle \cos(\Theta(t)) \rangle, \tag{5.25}$$

which describes the fluctuation of the deviation of the dipole moment from the axis of symmetry.

In the general case, when the orientation has to be described by three Euler angles $\Omega \equiv (\theta, \varphi, \psi)$, the correlation function $C_A(t)$ will be limited to the statistical averaging of the relevant elements of the Wigner matrix:

$$M^L_{pq}(t) = \left\langle D^L_{pq}(\Omega(0)) \cdot D^{L'}_{p'q'}(\Omega(t)) \right\rangle. \tag{5.26}$$

Due to the orthogonality of the Wigner function, the components describing mutual correlations disappear. It can be assumed that $L = L'$, $p = p'$, $q = q'$.

Solution of the diffusion equation for the nematic phase

In 1973, Nordio, Rigatti and Segre proposed a theory known in literature as the NRS theory. Let us analyse the solution of the nematic phase diffusion equation proposed by this theory, which is presented below.

The nematic phase diffusion equation takes on the following form:

$$\frac{\partial}{\partial t} P(\Omega, t) = \hat{L}\hat{D}_N(\Omega)\left[\hat{L} + \frac{1}{k_B T}\hat{L}U(\Omega)\right]P(\Omega, t), \tag{5.27}$$

where $\hat{D}_N(\Omega)$ is the diffusion tensor, and $\hat{L}$ is the operator of infinitely small (infinitesimal) rotations around the long axis of symmetry, formally equal to the quantum-mechanical angular momentum operator (for $\hbar = 1$). $U(\Omega)$ is the (potential) energy that the molecule overcomes when changing its orientation.

Wigner functions $D^L_{pq}(\Omega)$ $(p, q = 0, \pm 1)$ create a matrix representation of the rotation operator and are therefore most frequently used to mathematically describe the problem:

$$\begin{aligned} L^2 D^L_{pq}(\Omega) &= L(L+1) D^L_{pq}(\Omega), \\ L_z D^L_{pq}(\Omega) &= -q^2 D^L_{pq}(\Omega). \end{aligned} \tag{5.28}$$

If a transformation is made into a molecular system (orthogonal *xyz*) with an longitudinal axis (||) and a twice degenerated transverse axis (⊥), in which the tensor $\hat{D}_N(\Omega)$ has the form of a diagonal matrix with the main components $D_{zz} = D_{||}$, $D_{xx} = D_{yy} = D_{\perp}$, then the solution of the diffusion equation is reduced to the problem of the eigenvector:

$$\hat{D}_N \psi_n(\Omega) = \alpha_n \psi_n(\Omega). \tag{5.29}$$

The calculation of the average for angular variables takes the following form:

$$\left\langle D^L_{pq}(0) D^{L',*}_{p',q'}(t) \right\rangle = \sum_{n \neq 0} \left\langle \psi_0 \left| D^L_{pq} \right| \psi_n \right\rangle \exp(-\alpha_n t) \left\langle \psi_n \left| D^{L',*}_{p',q'} \right| \psi_0 \right\rangle. \tag{5.30}$$

This definition of the problem leads to the diffusion equation in the form of:

$$\frac{\partial P}{\partial t} = D_{\perp} \left[\nabla^2_{\Omega} P + \frac{1}{2k_B T} \left\{ \nabla^2_{\Omega} PU + P\left(\nabla^2_{\Omega} U\right) - U\left(\nabla^2_{\Omega} P\right) \right\} \right], \tag{5.31}$$

where $\nabla^2_{\Omega} = -\left(L^2 - \left(\frac{D_{\text{II}}}{D_{\perp}} - 1 \right) L^2_z \right)$.

The operator's own functions ∇^2_{Ω} are matrix elements $D^L_{pq}(\Omega)$ with eigenvalues of $L(L + 1) + (k - 1)p^2$, where $k = D_{\parallel}/D_{\perp}$.

If the potential U is expressed as a series of Wigner matrix elements:

$$\frac{U}{k_B T} = U_2 P_2(\cos\theta) + U_4 P_4(\cos\theta), \tag{5.32}$$

(see the nematic potential of HJL) and the mesophase symmetry $D_{\infty h}$ (which happens in nematic phases), and the uniaxial symmetry of molecules are taken into account, then a general solution of the diffusion equation taking into account the components derived from the mutual correlations, after averaging for angular variables, takes the following form:

$$\left\langle D^L_{pq}(0) D^{L',*}_{p',q'}(t) \right\rangle = \sum_k A^k_{pq} \exp\left(-\frac{t}{\tau^k_{pq}} \right), \tag{5.33}$$

where $\tau^k_{pq} = \left(D_{\perp} \alpha^k_{pq} \right)^{-1}$ and A^k_{pq} are coefficients proportional to the dielectric increment. The value τ^k_{pq} is interpreted as the correlation time.

Ferrarini et al. [2] have made a numerical evaluation of the model presented herein. An important conclusion is that the correlation time assigned to the D^1_{00}

component is strongly dependent on the order parameters. Calculations made with one component in the above development have demonstrated that this approximation is correct for all forms of potential. A numerical analysis made it possible to draw further conclusions. The potential recorded in the above form provides three timescales describing dynamic phenomena. The first interval of very short scale, decreasing rapidly with the increase in the height of the potential, connected with the non-steady movement inside the well of the potential limited by angles $\theta = 0$ and $\theta = \pi$. The second interval of mean time scale assigned to the Wigner matrix elements with $p = q$ and corresponding to the uniaxial rotation around the long axis of symmetry. It should be emphasised here that the symmetry of the system imposes the condition $\tau_{pq} = \tau_{qp}$, which is fulfilled only when $D_{\|} = D_{\perp}$. The third interval of very long times, which characterises the disappearance of the components $D^1_{00}(\Omega) \equiv P_1(\cos\theta) = \cos\theta$, is connected with 180° jumps over the potential barriers. In molecular terms, this jumps process is called an Arrhenius process, i.e. it demonstrates activation behaviour. Fig. 1 shows the relationship between the value $\alpha^1_{pq} = \left(D_{\perp}\tau^1_{pq}\right)^{-1}$, i.e. the frequency of dielectric relaxation normalised to the perpendicular component of the diffusion tensor. This relationship was drawn on admission in the potential of the ratio $\frac{U_4}{U_2} = -\frac{1}{3}$ (see Eq. 5.32).

All calculations were made with $D_{\|}/D_{\perp} = 1$. As one can see, the inverse of time τ_{00} strongly decreases with the increase of the order parameter S, regardless of the form of the potential, which is in accordance with the previously formulated conclusion. The remaining components are less dependent on the change S. Assuming that $S = 0.5$ and $D_{\perp} \sim 10^8 s^{-1}$, Nordio and Segre calculated the critical frequency $f_C(p = q = 0) = (2\pi\tau_{00})^{-1}$ for the reorientation described by the component D^1_{00}, which takes place in the area of megahertz frequencies. For the D^1_{01} component, the critical frequency is in the gigahertz area. As can be seen from Fig. 1, the correlation times $\tau_{pq} = \tau_{qp}$ ($p = 0$, $q = 1$) and τ_{pq} ($p = q = 1$) are weakly dependent on the form of the potential.

Fig. 2 shows the effect of anisotropy of the diffusion tensor on α^1_{pq}. In relation to the values calculated from $D_{\|}/D_{\perp} = 1$, it is necessary to make a shift by the factor of $[(D_{\|}/D_{\perp}) - 1]q^2$. The figure shows that as tensor anisotropy increases, the difference $\left|\alpha^1_{01} - \alpha^1_{00}\right|$ increases. This fact suggests good separation of relaxation areas attributed to the components D^1_{01} and D^1_{00}.

Of note are the numerical estimations of the influence of steric effects on the NRS theory presented by Kozak and Mościcki (Table 1) [3]. By calculating the relaxation times τ_{pq} and the coefficients A_{pq} (p, q = 0.1), they took into account the steric component in the nematic potential by introducing the parameter X, which is the ratio of the length to the width of rod-like molecules. In the case of the nematic potential of dispersion forces without a steric component, the change of parameter X caused a slight change of the time τ_{00}. With an increase in the parameter X by about one and a half times ($X = 1.67$), Kozak and Mościcki achieved an increase of

τ_{00} 1.88 times. However, when the potential was increased by a steric component, the change of the parameter X as mentioned above (X = 1.67) caused a jump of the time τ_{00} by an order of magnitude (increase about 52 times).

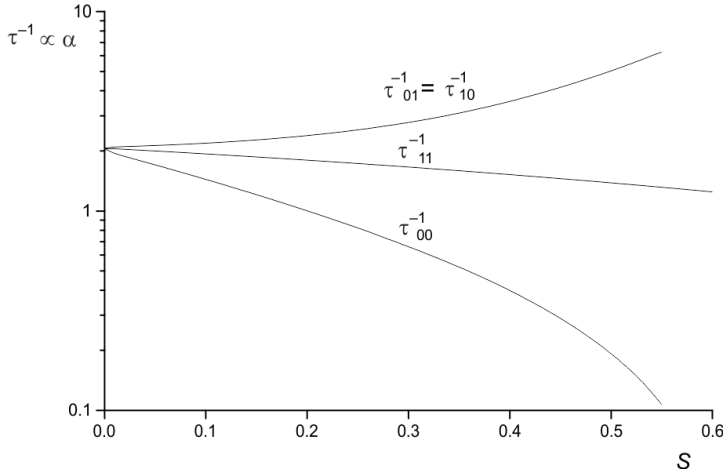

Fig. 1. Dependence of $(\tau^1_{pq})^{-1}$ on the parameter $S = \langle P_2 \rangle$

The impact of the steric effect on the other times was smaller. The comparison of the times τ_{00} of the first six substances of the *p*-azoxyanisole series collected in Table 1 may be a certain evaluation of the correctness of this model. The comparison shows that the increase in the parameter X by about 1.6 times, resulting from the change in the chemical structure of subsequent molecules of the *p*-azoxyanisole series, causes a six-fold increase in the time τ_{00}. It seems that in the case of *p*-azoxyanisole series molecules, the impact of the steric effect through nematic potential is small.

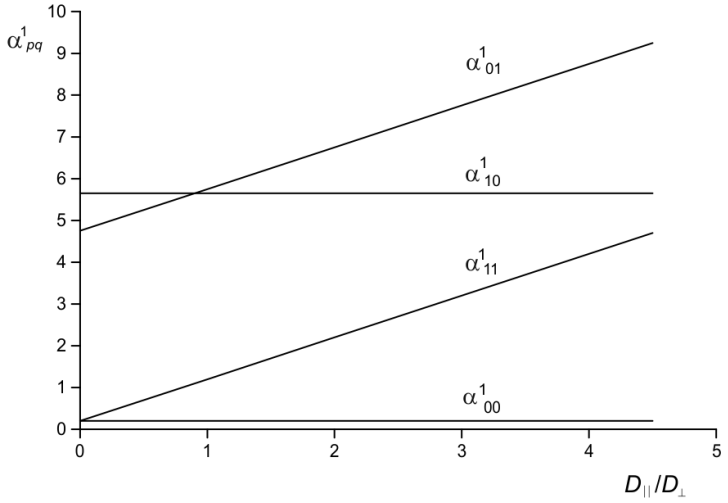

Fig. 2. Dependence of α^1_{pq} on anisotropy of the diffusion tensor $D_{\parallel}/D_{\perp}$

Table 1

The relaxation times τ_{00} and the parameter X of the first six ($n = 1 \div 6$) substances of the homologous *p*-azoxyanisole series (nOAOB) [3]

nOAOB	t_{00} [ns] (at $T = T_C - 10$K)	$X = a/b$
1	4	2.7
2	7	3.0
3	14	3.4
4	15	3.7
5	42	4.2
6	25	4.5

Diffusion equation and internal motions

The diffusion equation can also take into account internal motions. The simplest form of description of an internal motion is to treat it as a jump between conformational equilibrium positions. For one degree of freedom, the matrix W of the passage from the minimum m to the minimum n through the saddle point s is expressed by the formula:

$$W_{m\to n} = \left(\frac{D_s |U_s|}{2\pi k_B T}\right) \exp\left(\frac{E_m - E_s}{k_B T}\right), \tag{5.34}$$

where D_s – diffusion tensor, U_s – conformational potential, E_i ($i \equiv m, s$) – free energy.

The general form of the diffusion equation for molecules with multiple degrees of freedom takes the following form:

$$\frac{\partial}{\partial t} P(\Phi, \Omega, t) = \left(\hat{D}^i + \hat{D}^r\right) \cdot P(\Phi, \Omega, t), \tag{5.35}$$

where Φ describes the internal coordinates, and Ω describes the external coordinates that define the orientation in the laboratory system. $\hat{D}^i$ and $\hat{D}^r$ are, respectively, the tensor describing the reorientation of the entire molecule and the tensor describing the reorientation of its fragments. The potential acting on a molecule with internal degrees of freedom in the liquid crystal phase can be expressed in the following form:

$$U(\Phi, \Omega) = U^{tors}(\Phi) + U^{mf}(\Phi, \Omega), \tag{5.36}$$

where $U^{tors}(\Phi)$ is the twist component and $U^{mf}(\Phi, \Omega)$ is the component describing the anisotropic interaction with the environment. This expression can be spread out

into the sum of components from different units, such as e.g. functional molecular groups:

$$U^{mf}\left(\Phi,\Omega\right)=U^{core}\left(\Omega\right)+\sum_{i}U^{i}\left(\Phi,\Omega\right), \tag{5.37}$$

where U^{core} and U^{i} describe, respectively, the energy of the body of the molecule and the energy of its *i*-th fragment, taking the following form:

$$\begin{aligned}\frac{U^{core}}{k_BT}&=k_1D_{00}^{2}\left(\Omega\right)\\ \frac{U^{i}}{k_BT}&=k_2D_{00}^{2}\left(\Omega_i\right),\end{aligned} \tag{5.38}$$

where k_1 and k_2 are, respectively, the intensity of the external molecular field acting on the body (k_1) and on the *i*-th fragment of the molecule (k_2).

Ferrarini et al. made numerical estimates of the spectral densities of the NMR signal for the 4-pentyl-4'-cyanobiphenyl (5CB) [2]. They assumed the ratio of $D_{\parallel}/D_{\perp}=10$ and two states. In the first state, they assumed the existence of a coupling between the movement of the body (inter motion) and the internal movements (intra motions). In the other state, they assumed there was no such coupling. The calculations made it possible to conclude that the coupling effect becomes significant when the diffusion movement of the molecule as a whole is slower than the frequency of the conformational leaps.

Kozak and Wróbel demonstrated that within the framework of the NRS theory, it is possible to take into account internal movements [4]. The movement of one final chain is treated as a sequence of diffusion steps in a potential with the symmetry of a cone, whose axis of symmetry coincides with the direction of the director, leading to the appearance of a discrete distribution of relaxation times. The theoretical relaxation spectrum obtained by the authors consists of seven components. Two components are the result of the movements of the entire molecule. The others originate from internal movements, such as rotation around the long axis of the chain, precession around the axis of the cone and "rattling" in the area of the cone. Of course, the predicted relaxation spectrum must also include components resulting from the coupling of basic movements with internal movements. It should be emphasised that a numerically correct distribution of the real spectrum into seven modes will, however, encounter serious difficulties in interpretation. The critical frequencies of internal movements fall within one value range – the gigahertz area. Therefore, it is not possible to unambiguously assign the times τ_i to the above-mentioned reorientations. In Chapter 5.5 of [1], the distribution of dielectric spectroscopic spectra was performed within the basic NRS theory. The difference between the predictions of the NRS theory and the experimental results was interpreted as coming from internal movements, which were treated as a global reorientation. The "amplitude" of all internal movements in

the case of the 3OAOB molecule discussed in Chapter 5.5 of [1] is only 6% of the total increment. This value confirms the impossibility of separating (in this case) the five modes suggested by Kozak and Wróbel [4]. Similar values of increments caused by global internal movements are also observed for other liquid crystals.

References

[1] Otowski W., *Dynamika molekuł termotropowych ciekłych kryształów w świetle badań relaksacji dielektrycznej*, Cracow University of Technology Kraków 2008 (in Polish)

[2] Ferrarini A., Nordio P.L. and Moro G.J., *The Molecular Dynamics of Liquid Crystals*, NATO ASI Series, Series C, vol. 431, 1994, p. 41.

[3] Kozak A. and Mościcki J.K., *Mol.Cryst.Liq.Cryst.Letters*, 5 (6), 195, 1988.

[4] Kozak A. and Wróbel S., *Zeszyty Naukowe Politechniki Łódzkiej*, 538, 249, 1989 (in Polish).

[5] *Fizyka Chemiczna*, edited by J.M. Janik, PWN, Warszawa 1989 (in Polish).

6. NANOSTRUCTURES

Nanotechnology is a science that deals with the creation of nanostructures, i.e. structures on the level of individual atoms and molecules, in order to control structures at the molecular level. Nanomaterials are structures containing *nanoparticles*. So the question is: What are nanoparticles?

Nanoparticles are intermediate structures between atoms and molecules and macroscopic objects. As defined by the European Commission (Brussels, 18 October 2011 – According to the recommendation adopted by the European Commission), *[…] "nanomaterials" are materials in which the dimension of the main ingredients ranges from one – 1 nm – to one hundred billionth parts of a meter – 100 nm. The definition adopted currently is based on the size of the particles in the material and not on hazards or risks. According to the definition, a "nanomaterial" means a natural, incidental or manufactured material containing particles, in an unbound state or as an aggregate or as an agglomerate and where, for 50% or more of the particles in the number size distribution, one or more external dimensions is in the size range 1–100 nm* (see Fig. 1).

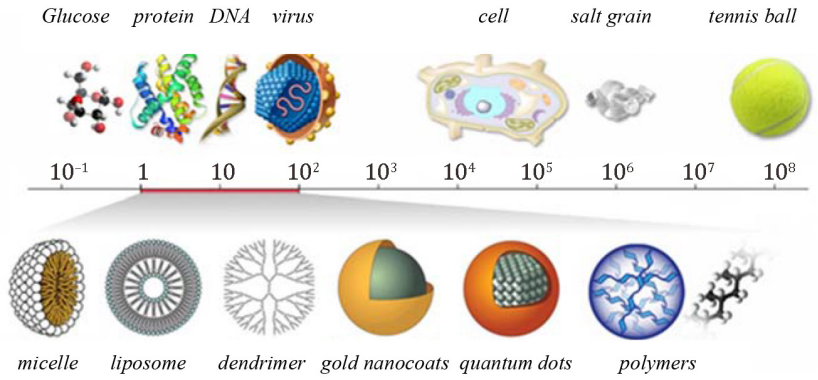

Fig. 1. Comparison of dimensions of molecular systems [1]

For comparison, 1 nanometre = 10^{-9}m. The unit often used to describe the dimension of a crystal or of phenomena occurring on the atomic scale, which is not an SI unit, is 1 Å (angstrom) equal to 10^{-10}m. Thus, 1 nm is equal to 10 Å. This means that along a one--nanometre section, one can place about 20 hydrogen atoms (assuming that the radius of a hydrogen atom in the ground state is equal to about 0.0529 nm) or about 17 O_2 atoms, which confirms that nanoparticles are atomic scale systems – for comparison, the diamond

lattice constant $a = 3.56$ Å $= 0.356$ nm, the copper lattice constant $a = 3.615$ Å $= 0.3615$ nm, and the diameter of human hair is approx. 100,000 nm, which is one million Å (see, for instance, the size comparison in Fig. 2).

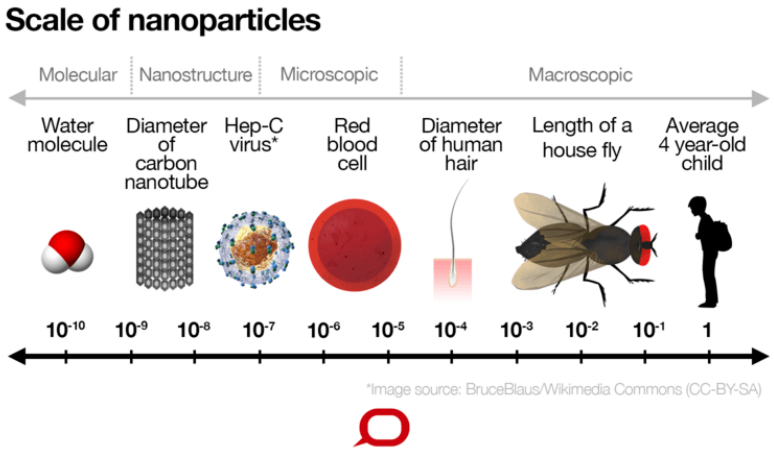

Fig. 2. Size comparison from man to a water molecule [1]

In the understanding of a physicist, nanoscience describes how structures organised at the level of individual molecules are created by using specialised nanomachines.

This statement is close to the theses presented in Richard Feynman's (1959) lecture titled "There's Plenty of Room at the Bottom". The lecture, given on 29 December 1959 during the annual meeting of the American Physical Society at the California Institute of Technology (Caltech), became an announcement of nanotechnology. The associated paper was first published in February 1960 [2]. Richard Phillips Feynman (born on 11 May 1918 in New York, died on 15 February 1988 in Los Angeles), an American physicist-theorist, recognised in 1999 as one of the top ten physicists of all time. He was one of the main creators of quantum electrodynamics and a Nobel Prize winner in physics in 1965 for independent creation of relativistic quantum electrodynamics.

Feynman (1959) considered the problem of what it takes to fit the 24-volume "Encyclopaedia Britannica" on a pinhead. He presented the concept of miniaturisation and the possibilities provided by a technology that can operate at the nanometre level.

The concept or definition of *nanotechnology* was also dealt with by other scientists. A number of definitions are given below:

- Norio Taniguchi's[19] 1974 definition presented in the work titled "On the Basic Concept of 'NanoTechnology'" [20]: *Nanotechnology is a technology that leads to very high accuracy and extremely small dimensions, i.e. a precision of 1 nm.*

[19] Norio Taniguchi, who was a professor of Tokyo University of Science, coined the term nano-technology in 1974 to describe semiconductor processes. The European Society for Precision Engineering and Nanotechnology presented Professor Taniguchi with its 1st Lifetime Achievement Award in Bremen, May 1999.

- A. Franks' 1987 definition presented in the work titled "Nanotechnology" [3]: *Nanotechnology involves the production of elements with dimensions or dimensional tolerances in the range of 0.1–100 nm.*
- Definition from Wikipedia: *Nanotechnology is the general name for a whole set of techniques and methods of creation of various structures of nanometric sizes (10–1,000 nm), i.e. at the level of individual molecules.*
- Sefinition from Netpedia: *Nanotechnology – the science of micromachines, i.e. miniature devices made of single atoms; Nanobots (microscopic, autonomous or remotely controlled robots) working under the control of nanocomputers (computers with molecular size systems) can be widely used in medicine and science of the future.*
- Definition from the web page "trilog" [4]: *Nanotechnology is a revolution in the field of materials whose structures and elements exhibit peculiar and perfectly developed physical, chemical and biological properties, in which the processes taking place are caused by their nano-dimensions. The primary objective of nanotechnology is to exploit these properties by achieving control on the atomic and molecular level of molecules to develop effective ways to produce and use them.*
- Definition of The Royal Society & The Royal Academy of Engineering, presented in "Nanoscience and Nanotechnologies: Opportunities and Uncertainties": *Nanoscience is the science of natural phenomena and manipulation of materials on the level of atoms and molecules and in macromolecular sizes, where properties differ significantly from those of large scale. Nanotechnologies are projects, characterizations, productions, and applications of structures, devices and systems through the control of shapes and sizes on a nanoscale.*
- Definition from the book "A Gentle Introduction to the Next Big Idea" [5]: *Nanoscience is the study of the fundamental properties of molecules and molecular structures that have at least one dimension from 1 to 100 nanometres. These structures are known as nanostructures. Nanotechnology is a way of applying these nanostructures in useful machines on the nanoscale.*
- Definition from the book "Nanoscale Science and Technology" [6]: *Nanotechnology is the term for the design, production and use of materials having one or more dimensions in the range from 1 to 100 nm.*

Nanoparticles have properties different from those of particles made up of the same atoms but with a size of micrometres and larger; e.g. nanocrystals (nanometric-sized crystals) can have melting points several hundred degrees lower than the melting point of larger crystals. Their crystalline structure may be different, e.g. they may have a smaller lattice constant. This is probably a result of the ratio of the number of atoms on the surface to the number of atoms in the volume in nanocrystals, which causes the surface energy to have a key influence on the stability of the crystal. A model nanocrystal contains 3 x 3 x 3 = 27 atoms. There is only one atom in the volume, thus there are 26 atoms (**96%**) on the surface.

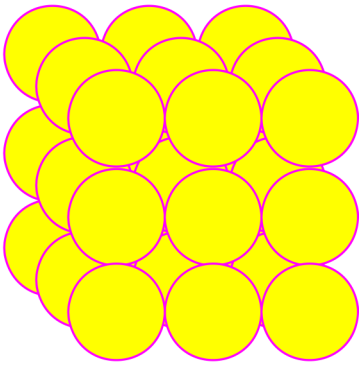

Fig. 3. A model nanocrystal contains 3 x 3 x 3 = 27 atoms

If the edge of a crystal is 1,000 times longer (1 μm), the crystal would contain:

$$5{,}000 \times 5{,}000 \times 5{,}000 = 125{,}000{,}000{,}000 \text{ atoms},$$

of which in volume there would be:

$$4{,}998 \times 4{,}998 \times 4{,}998 = 124{,}850{,}059{,}992 \text{ atoms},$$

and on the surface, there would be only:

$$(125{,}000{,}000{,}000 - 124{,}850{,}059{,}992) = 149{,}940{,}008 \text{ atoms},$$

which is 0.12% of all atoms $\left(\frac{149940008}{125000000000} = 0.12\%\right)$.

Thus, the dominating role of the surface in relation to the volume makes it possible to disregard gravitational effects resulting from the volume and the mass. It is possible to place many nanoparticles on a small surface or in a small volume and to build complex and multifunctional nanostructures out of them. An example is the "atomic" IBM logo presented in 1989 (Fig. 4). A scanning tunnel microscope was used to place 35 single xenon atoms on a chilled nickel crystal substrate. Atoms were, for the first time, precisely aligned on a flat surface.

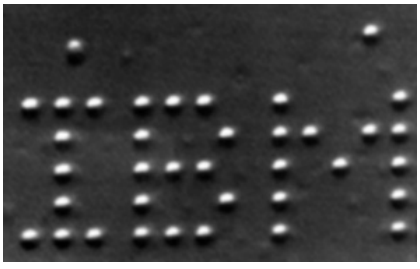

Fig. 4. The "atomic" IBM logo [7]. The electrical and optical properties are controlled by quantum effects; these properties can be changed in a controlled way by changing the size of nanoparticles

The extraordinary properties of matter in the form of nanoparticles open up new possibilities of application in practically all fields of technology, biology and medicine. Many methods of effective and reproducible manufacturing of nanomaterials with full control of their structure have already been developed. Special nanostructures are nanotubes, fullerenes and quantum wires. Nanotubes are hollow nanoparticle structures; carbon tubes are currently the most popular. These are excellent heat conductors and are extremely durable and non-stretchable. They are in the form of cylinders with diameters from 1.0 to 1.5 nm. A nanotube is a one-dimensional structure (like a quantum wire), as described below.

Multi-walled carbon nanotubes have a thermal conductivity five times higher than that of copper and are characterised by excellent electrical conductivity and high mechanical strength, up to 20 times higher than that of steel.

The largest demand for nanotubes in recent years has been in the polymer segment. In these materials, they improve the mechanical properties of the composites obtained. The second most important area of application of nanotubes is the electrical and electronics sector. The share of CNT (carbon nanotubes – Fig. 5) is steadily increasing in applications such as solar cells, semiconductors, transistors, touch sensors, ultraconductive copper and electromagnetic devices.

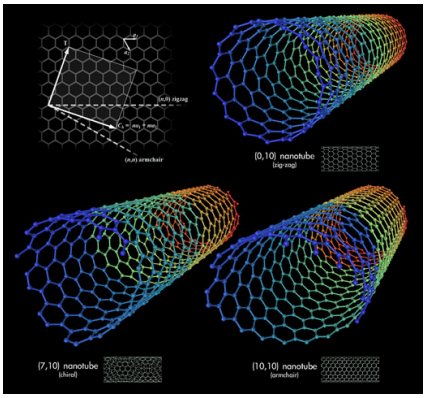

Fig. 5. Nanotubes [8]

In a solid crystal, the motion of electrons and holes is not limited in space – no translation symmetry disturbance in two directions (spatial).

As mentioned above, a nanotube is a one-dimensional structure. This term results from a disturbance in the symmetry of translation in two directions (spatial) and not from the geometry of the structure. Just like fullerenes, they are zero-dimensional structures, so-called quantum dots. The figure below shows that carbon atoms form a spatial geometric structure (empty inside) of the Buckyball type, i.e. complex surveying domes composed of pentagons and hexagons (Fig. 6). However, since the motion of the carrier is limited by the potential barriers in all three dimensions, fullerenes are considered to be a zero-dimensional nanostructure.

Low-dimensional structures (nanostructures) make it possible to limit (partially or totally) the movement of the carriers:

- 3D means a solid crystal;
- 2D means a quantum well (makes it possible to limit the movement of the carriers to a plane);
- 1D means a quantum wire (a system that limits the movement of electrons or holes to one direction);
- 0D means a quantum dot (movement of the carrier is limited in three dimensions).

In order for spatial limitation of the movement of carriers to exist, the depth of a well (or the size of a quantum dot) must be comparable to the length of the de Broglie wave, which usually means sizes at the level of 10 nm.

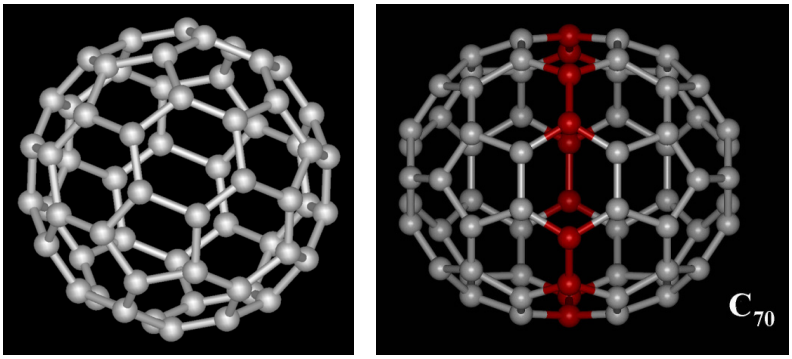

Fig. 6. Fullerenes – left side: C_{60}, right side: C_{70} [9]

There is already a commercial market for the manufacture of products using nanomaterials. Clothing and footwear containing silver nanoparticles with bactericidal and neutralising effects have already been manufactured (Fig. 7).

Fig. 7. Thermoactive shirt with silver ions

The first medicine containing nanoparticles of albumin approved for use in the USA (in 2005) was Abraxane®. It was demonstrated that encapsulation of albumin nanoparticles improves their therapeutic effect in the treatment of breast cancer (Fig. 8).

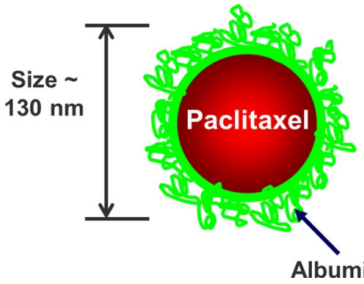

Fig. 8. Diagram of the Abraxane® drug containing albumin nanoparticles [10]

Another surprisingly interesting example of the use of nanoparticles (although apparently unintentional) is the chalice, which is now located in the British Museum in London (Fig. 9). The chalice was probably made in the 4th century AD. The patterns on the vessel tell the story of the King Lycurgus, who is caught in a thicket of vines. It is a punishment for the transgression committed against Dionysus, the Greek god of wine.

The unique properties of the cup were first noticed in the 1950s, when the vessel was placed in the museum. Only in 1990, thanks to the observation of the glass under a microscope, did scientists guess how the colours change.

Fig. 9. The Lycurgus Cup (4th century AD) [11]

The chalice was created about 1,600 years ago, using a process of deposition of very fine gold and silver particles in the glass. The diameter of the nanoparticles is about 50–70 nm. When illuminated at the front, the chalice is light green (jade), when the light source is placed inside or behind it, the colour changes to ruby red (Fig. 10).

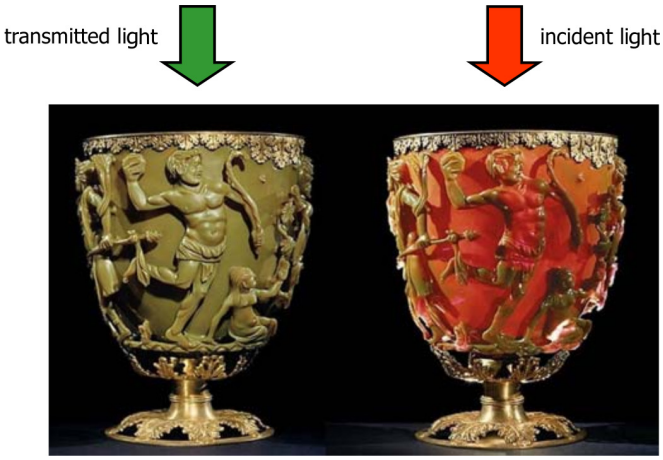

Fig. 10. Lycurgus Cup in incident and transmitted light [11]

Ancient Romans created the so-called dichroic glass, in which a play of two colours can be observed. Such glass, allowing a given colour to pass through, reflects its complementary colour. After application of several dozen layers of nanoparticles, the colour differs depending on the angle of observation and the direction of incident light.

Gold and silver nanoparticles of a certain diameter strongly diffuse light of wavelengths corresponding to green (550 nm). However, when the cup is illuminated from behind, the green colour is absorbed and the observer sees only the red colour, which is a complement to the green (it lies on the opposite side of the colour circle (colour wheel)).

The Dichroic glass used nowadays was developed by NASA researchers for use in the mirrors of satellites. Dichroic glass is used in the production of lasers, sunglasses, lighting, fibre optics, stained glass and as filters in photography. It is characterised by resistance to weather and abrasion and by colours that never fade. This material is used in everyday technology [11].

Gold-coloured windows of stained glass in medieval churches purify the air in the sunlight and are one of the earliest examples of the use

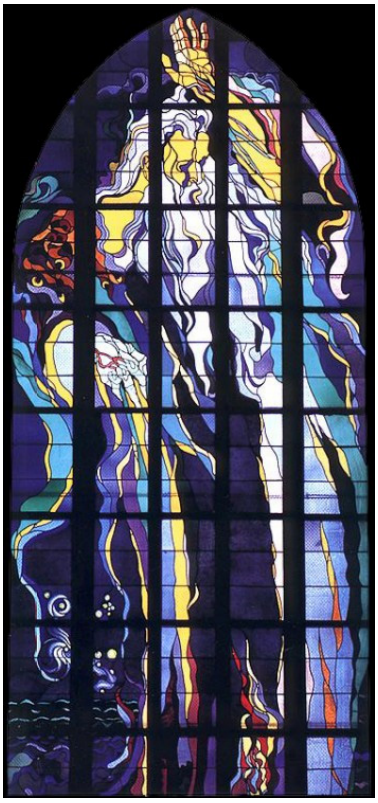

Fig. 11. The God Father stained-glass window, Franciscan Church in Cracow, designed by Stanisław Wyspiański [13]

of nanotechnology. Medieval glaziers used gold nanoparticles to produce glass of different colours, depending on the particle size, whereas the best-known example is ruby-coloured glass [12].

Professor Zhu Huai Yong, from Queensland University of Technology in Australia, who studies old stained glass, discovered that gold-coloured glass does not change its colour, but it is also a nanocatalyst that decomposes air pollutants under the influence of light [12] (see, for instance, the old stained glass window in Fig. 11).

Tiny gold particles become very active thanks to the energy supplied by the Sun and can break down volatile organic compounds, among other things. The decomposition of pollutants results in small amounts of carbon dioxide. According to Professor Zhu, gold nanoparticles are a very economical catalyst. Under the influence of light, only the gold nanoparticles heat up, leaving their surroundings cool. They could potentially be used in many chemical processes.

Gold is chemically inert, but gold nanoparticles show strong catalytic properties. For example, gold nanoparticles on a titanium dioxide substrate very actively oxidise carbon monoxide (Fig. 12).

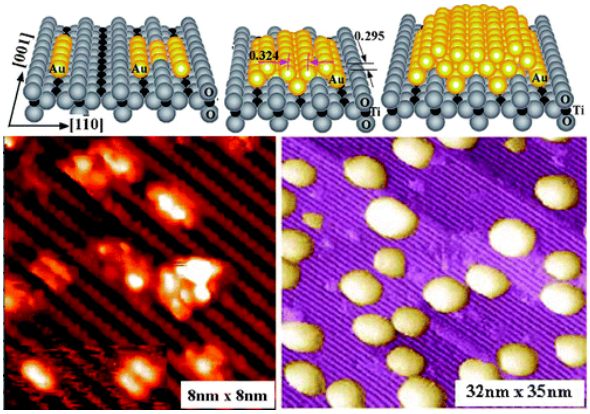

Fig. 12. Catalytically active gold on ordered titania supports. Schematic structural models for 1-D, 2-D and 3-D structures with two- and three-atomic-layers thick Au particles on the TiO_2 [110] and STM images showing gold nanoparticles on TiO_2 (direction [110]); 2nm Au = very active, 10nm and bulk Au = completely inactive) [21]

Gold nanoparticles, which form a solid colloidal solution in glass, exhibit a different colour than the colour known for solid metal because of the so-called plasma surface resonance, i.e. a specific interaction of plasmons (collective vibrations of free electrons) located near the surface of the metal with incident visible light. Quantum effects cause the wavelength of absorbed radiation to be strongly dependent on the curvature of the surface, i.e. on the size of Au nanoparticles. The surface of gold nanoparticles can be easily functionalised (by attaching specific receptors or antibodies), so that they can be used to detect specific cells or antigens. Due to their specific electron and optical properties, functionalised gold nanoparticles are used for imaging of lesions at the

level of organs, tissues and individual cells using optical or electron microscopy. An additional functionalisation of the surface of Au nanoparticles and drug molecules enables their application in targeted therapy, in which therapeutic substances are delivered in a controlled, selective way to cells or tissues constituting the outbreak of a disease. Functionalised gold nanoparticles can be used to destroy cancer tissue by heating it with IR radiation (Fig. 13). The gold nanoparticles with short DNA chains attached to them enable identification of a given DNA sequence in a sample. Gold nanoparticles accumulate in this region; the interactions between gold nanoparticles change the absorption of surface plasmons (a red sample becomes blue) [11].

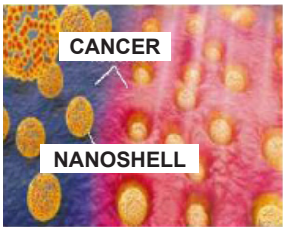

Fig. 13. Functionalised gold nanoparticles [11]

A common feature of all nanoparticles is the predominant share of surface atoms or molecules in the total number of atoms. In a cube of iron with a side of 1 cm, there is only approx. 10^{-5}% of the total number of atoms; in a cube with a side of 10 nm, surface atoms would already represent 10% of the total number of atoms; in a cube with a side of 1 nm, every iron atom would be on the surface.

The percentage of surface atoms as a function of change of the diameter of palladium clusters is presented in Fig. 14.

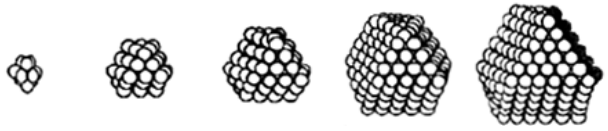

Number of shells around one central atom	1	2	3	4	5
Number of atoms	13	55	147	309	561
Percencage of atoms at the surface	92	76	63	52	45

Fig. 14. Percentage of surface atoms as a function of change of the diameter of palladium clusters [15]

Nanotechnology-based medicines have been approved by the Food and Drug Administration of the United States (FDA) and have been used for several years. One of them is DOXIL® – a liposome preparation of doxorubicin, recommended for use in the case of Kaposi sarcoma and in cases of breast and ovarian cancer resistant to treatment [16].

The group of nanopreparations also includes other chemotherapeutic agents, such as Eligard®, Genexol®, Opaxio® or Zinostatin Stimalamer®. Another example is an anti-cancer drug containing gemcitabine, based on gold nanoparticles that act as a "drug delivery" system.

A study conducted by the Nanobiotechnology Department of the Warsaw University of Life Sciences demonstrated the anti-cancer properties of graphene nanoplates in the treatment of brain tumours (multiform glioma) and documented that platinum nanoparticles are equally effective and significantly less toxic compared to traditional cis-platinum. The synergistic action of both factors (platinum nanoparticles deposited on graphene flakes) was found to be the most effective against cancer.

Silver has also been used in medicine, although as a heavy metal, it is very controversial. Robert Burrell created the first Acticoat™ (Smith and Nephew, London, UK) approved product to treat wounds, burns, ulcers, epidermal necrosis and pemphigus. Silver nanoparticles and their antibacterial properties are used in the production of medical instruments: the Silverline catheter (Spiegelberg GmbH and Co. KG, Hamburg, Germany) and the ON-Q Silver Soaker™ (I-Flow Corporation, CA, USA).

When antibiotics were not yet known, silver compounds were widely used in medicine, and during wars, one of the most effective methods of wound healing was to put silver coins on wounds. The destructive effect of silver on microorganisms has been confirmed in numerous studies. Colloidal silver, according to EMSL tests (Analytical, Inc. Microbiology Division), kills such microorganisms as: *Aspergillus niger*, *Candida albicans*, *Escherichia coli*, *Escherichia coli* 0157H7, methicillin-resistant *Staphylococcus aureus* (MRSA), *Pseudomonas aeruginosa*, Staphylococcus aureus (ut13), *Trichophyton rubrum (ut15), vancomycin-resistant Enterococcus faecalis* (VRE) and vancomycin-resistant *Staphylococcus aureus* (VRSA).

The negative effects of antibiotics can be partially offset by the introduction of antibacterial preparations based on Ag nanoparticles. Silver not only has antibacterial properties but also anti-inflammatory properties, and it seems that it also has anti-cancer properties.

Methods of nanoparticle production can be divided into two groups (Fig. 15):

- bottom-up methods;
- top-down methods.

Bottom-up methods consist in building nanometric structures from single atoms or particles. Top-down methods consist in the fragmentation of a micrometric structure into a nanometric scale.

The bottom-up method, as mentioned above, consists in the composition of the desired nanostructure from blocks, which are chemical molecules, most often organic molecules capable of self-organisation. We owe the concept of this method to, among others, Richard Feynman, who, in his famous lecture, mentioned the possibility of building nanostructures from single atoms.

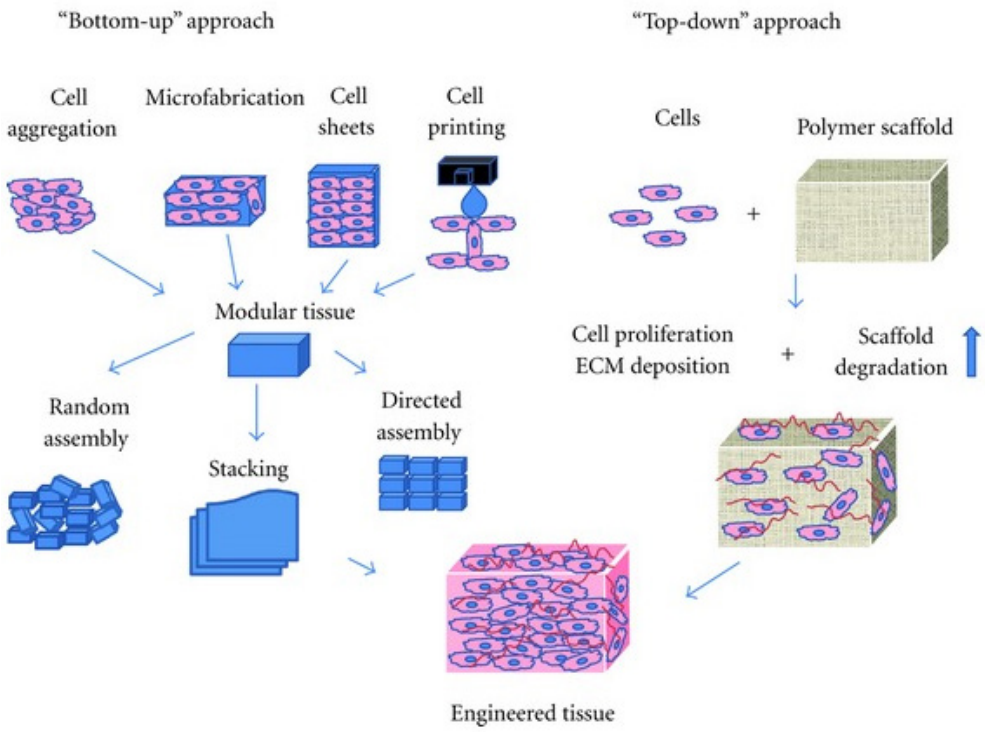

Fig. 15. Methods of nanometal production: top-down, bottom-up [17]

Bottom-up methods include:

- sedimentation from the gaseous or liquid phase;
- nanocrystallisation from the amorphous phase;
- consolidation of nanopowders;
- co-precipitation of nanoproducts in solutions;
- application of reagents layer by layer (the Langmuira-Blodgett technique);
- decomposition of organic precursors;
- synthesis in hydrothermal conditions;
- reagent hydrolysis and subsequent condensation;
- surface redox exchange;
- spraying in vacuum.

The bottom-up method was inspired by phenomena occurring inside living organisms. An example of such a phenomenon is self-organisation, i.e. spontaneous formation of complex structures from smaller elements. The mechanism enabling such behaviour is the entire system's tendency to achieve the minimum energy state (free energy or other thermodynamic potential). As a result, there is no need for outside interference. The process runs according to the laws of physics. Fig. 16 presents a molecular man consisting of 14 carbon monoxide molecules arranged on a metal substrate and depicted with the use of a scanning tunnel microscope [18].

The top-down method consists in fragmentation of the micrometric structure to a nanometric scale. For example, in the case of nanometals, the most important of these methods are the large plastic deformation methods.

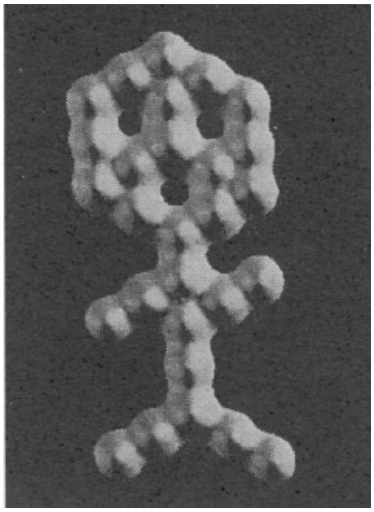

Fig. 16. A molecular man consisting of 14 carbon monoxide molecules arranged on a metal substrate and depicted with the use of a scanning tunnel microscope [18]

Silver vessels for serving meals and drinks protected against the proliferation of bacteria in the food. At present, silver nanoparticles can be found in fabrics (underwear, socks, bandages), cosmetics (powders, deodorants) and even household appliances (refrigerators, washing machines). However, these products quickly lose their nanoparticle silver coating during use, and the particles are released into the environment and, therefore, can penetrate into the human body. Excessive amounts of silver in the body are not healthy. There are known cases of people who, due to uncontrolled absorption of silver by the body, fell ill with argyria (called "silver poisoning"). Thus, for medical reasons, silver nanoparticles have been replaced with zinc (II) oxide, which, in addition to its bactericidal properties, also has a desiccant effect.

Silver poisoning – argyria (from the Greek word *ἄργυρος* – silver) – is a set of symptoms caused by unintentional absorption or deliberate intake of silver compounds (usually silver dust). The main symptom is a change in skin colour to blue or grey in areas exposed to sunlight. The discoloration may affect some areas of the skin or the entire surface of the skin. This condition may be temporary and cease after the absorption or intake of silver stops. The research results gathered by the Environmental Protection Agency indicate that apart from greying of the skin, an increased content of silver in the body does not cause any disease effects, especially cancer (according to Wikipedia). Consequently, its use in fabrics (bandages, plasters) also makes it possible to dry the wound and speed up healing. However, due to

unexplored side-effects, these products are not allowed to be sold in all countries. Nanoparticles of zinc (II) oxide are also used by dentists to fill tooth tubules (4 μm).

Nanoparticles made of chemical compounds (metal oxides, e.g. ZnO, SnO_2) forming crystal lattices are used as carriers of drugs in the body. The catalytic properties of titanium(IV) dioxide are used in self-cleaning coatings (glass, plates, fabrics, films, car mirrors, paints for household appliances, etc.), in flue gas (NOx reduction), water (e.g. pesticide decomposition) and sewage cleaning/purification/treatment processes, etc., and as a catalyst for organic synthesis in the production of antibacterial materials and for the production of photovoltaic cells and solar batteries. Titanium (IV) dioxide is able to absorb UV light and is therefore used in the production of varnishes for wood, automotive and aerospace topcoats, stains, printing inks, laminates, parquet coatings and protective waxes. In such coatings, it plays an important role in making the surface weatherproof and preventing loss of gloss and chalking. In addition, it reduces the receptivity of the surface to scratches and abrasion. It does not affect the colour of the surface (it is transparent), and its share by weight does not exceed 5%. The absorption of UV by titanium (IV) oxide also allows for its application in the production of transparent plastics, agrotechnical films, packaging films, protective films for food (extending the expiry date, limiting the speed of decomposition of vitamins) and cosmetic products (protective creams, sunbathing creams, UV filters) [11]. The development of nanotechnology is increasing the number of nanostructures in the environment, and the lack of data on the harmfulness of nanoparticles to human health and the environment is leading to legislative changes and a tightening of the criteria for placing new products containing nanoparticles on the market. Research into the safe use of nanoparticles is therefore crucial for the development of nanotechnology. All hazards that have both a direct and indirect impact on the environment and on people can significantly slow down or even stop the development of nanotechnology.

There is no research and information on how nanoparticles behave in the natural environment and how they directly affect human body cells or after accumulation in the body. It is important to know the magnitude of these risks. For example, do they cause mutations and protein replication processes or apoptosis? Apoptosis (meaning a *falling of leaves* in Greek) is a natural process of programmed cell death in the body. Thanks to this mechanism, worn out or damaged cells are removed from the body. This is a positive process of controlled cell suicide. It was also found that copper (II) oxide and silver nanoparticles were deadly to soil microorganisms, while zinc (II) oxide nanoparticles inhibited their growth and reduced their reproductive capacity. The toxicity of nanoparticles decreased with the increase of their aggregates. It was found that the toxicity of some nanoparticles also depends on the presence of other compounds, e.g. the toxicity of copper nanoparticles to crustaceans decreased with the content of organic carbon in the water in which the crustaceans lived. Dr Enda Cummis from the Irish UCD Institute of Food and Health created a list of nanomaterials

according to the degree of risk they pose to the environment and human health. Silver and titanium (II) oxide nanoparticles in surface waters represent a moderate to high ecotoxicological risk. In 2009, the most dangerous nanoparticles and the groups of organisms most sensitive to their effects were identified. This was done by reviewing available scientific reports in terms of toxicity of nanoparticles to particular species of bacteria, algae, crustaceans, nematodes, yeasts, ciliophorans and fish – organisms that are most often the first links in the food chain. The group of nanoparticles evaluated included titanium (IV) oxide, copper (II) oxide, nanotubes, C60 fullerenes, zinc (II) oxide and silver:

- zinc (II) oxide and silver were determined to be extremely toxic – LD50 < 0.1 mg/l;
- C60 fullerene and copper (II) oxide were determined to be highly toxic – LD_{50} = 0.1–1 mg/l;
- nanotubes were determined to be toxic – LD_{50} = 1–10 mg/l;
- titanium (IV) oxide was considered to be among the least toxic – LD_{50} = 10–100 mg/l.

Lethal dose, LD (Latin *dosis letalis*, DL) – the toxicity of a substance or the harmfulness of ionising radiation.

For toxic substances, the most commonly used designation is LD_{50}; this is a conventional value:

- LD_{50} – a dose that causes the death of half of the irradiated specimens within 30 days;
- LD_{100} – a dose causing the death of all irradiated specimens within 30 days [19].

In the considerations related to nanoparticles, the problem of their toxicity arises. Nanomaterials are often characterised by different properties compared to their equivalents on a "macroscopic" scale, which affects their biological properties. Such change is often unfavourable for biological applications due to the cytotoxic effect of nanoparticles. Quite often materials that are normally inert to living organisms exhibit a significant increase in cytotoxicity when the size of the particles forming them is reduced to the nanometric scale. Cytotoxicity may be caused by easier and increased release of heavy metal ions from the surface of such nanoparticles as quantum dots, such as CdSe, CdTe and PbS. Cytotoxicity of nanomaterials may also be caused by the porosity of nanoparticles, their tendency to agglomerate, their significant chemical affinity to many biological structures or the increased chemical reactivity of their surface. Physical and mechanical factors, such as size comparable to or smaller than biological structures, also play an important role. By forming stable suspensions in the air, nanomaterials form harmful dusts, which, when inhaled by humans, can cause pneumoconiosis or lung cancer. Due to their small size, nanoparticles can be absorbed by some cells of living organisms as a result of endocytosis and can accumulate as a result of adhesion to proteins, cell membranes and other biological structures. These processes can cause cell and tissue damage through increased oxidative stress, ion channel blockage or mechanical damage to the cell membrane. These factors can also interfere with cell

proliferation (in biology, proliferation means cell multiplication), resulting in cell death or uncontrolled growth that can lead to neoplastic lesions.

The structural properties of nanoparticles are not the same for all materials. An increase of the surface area, and thus of the surface energy, along with an decrease of the particle size are connected with a decrease of the distance between atoms. This relationship applies to clusters of metal atoms, e.g. copper. An inverse relationship, where a reduction in particle size causes an increase in the distance between them, has been observed in semiconductors and metal oxides. The adoption of certain structures, which are stable only on the nanometric scale is not fully described. The thermal properties are also unclear. It was found that the influence of surface energy on the thermal properties of the material causes a decrease in the melting temperature of gold nanoparticles in comparison with the melting temperature of the microcrystalline material. There are also known reports stating that smaller particles have higher melting temperatures. The mechanical properties of nanoparticles are also different from those of their macroscopic analogues (carbon compounds – nanotubes). Mechanical strength is affected by the number of defects occurring in the material, and the probability of their occurrence decreases with the size of the material. Increasing the surface-to-volume ratio causes some surface atoms to bond with their neighbours, which results in magnetic properties – ferromagnetism. Magnetic nanoparticles are often composed of only one domain, and they may exhibit so-called superparamagnetism. Reducing the size of particles affects the electron structure of the system. The ionisation potential is higher in small atomic clusters and directly influences the reactivity of nanoparticles. When the size of the system is reduced, the orbital energy or the position of bands (solids) influences the highest occupied molecular orbital (HOMO) of the valence band or the lowest unoccupied molecular orbital (LUMO). The difference between these levels influences the emission and the absorption and thus changes the optical properties of nanoparticles, e.g. colloidal gold is red and changes into yellow as the aggregates grow. When the system decreases and becomes comparable to the wavelength of de Broglie electrons, the discrete nature of electron states becomes apparent, e.g. conductive materials become insulators.

References

[1] https://www.wichlab.com/research [access: 20.10.19].
[2] Feynman R P., *There's Plenty of Room at the Bottom*, "Engineering and Science", 23(5), 1960, 22–36.
[3] Franks A., *Nanotechnology*, J. Phys. E., 1987.
[4] https://www.triolog.pro.wp.pl [access: 20.10.19].
[5] Ratner D. and Ratner M., *A Gentle Introduction to the Next Big Idea*, Pearson Education Inc., New Jersey 2003.
[6] Kelsall R. W., Hamley I.W., Geoghegan M. (eds.), *Nanoscale Science and Technology*, Wiley, New York 2005.
[7] https://en.wikipedia.org/wiki/IBM_(atoms) [access: 20.10.19].
[8] https://inteng-storage.s3.amazonaws.com/images [access: 20.10.19].
[9] https://66.media.tumblr.com [access: 20.10.19].
[10] https://www.openi.nlm.nih.gov [access: 20.10.19].
[11] https://materialyinzynierskie.pl [access: 20.10.19].
[12] https://www.ekologia.pl [access: 20.10.19].
[13] https://upload.wikimedia.org/wikipedia/commons/4/48 [access: 20.10.19].
[14] Chen M., Goodman D.W., *Catalytically active gold on ordered titania supports*, Chem. Soc. Rev., 37(9), 2008, 1860–1870.
[15] Majeed Z.H. and Taha M.R., *A review of stabilization of soils by using nanomaterials*, "Australian Journal of Basic and Applied Sciences", 7(2), 2013, 576–581.
[16] Laginha K.M., Verwoert S., Charrois G.J.R. and Allen T.M., *Determination of doxorubicin levels in whole tumor and tumor nuclei in murine breast cancer tumors*, "Clinical Cancer Research", 11, 2005, 6944–6949.
[17] https://www.researchgate.net/profile/Judee_Grace_Nemeno/publication/233949725/figure/fig2 [access: 20.10.19].
[18] Zeppenfeld P. and Eigler D.M., *New Scientist*, 129, 20, 1991.
[19] https://en.wikipedia.org/wiki/Lethal_dose [access: 20.10.19].
[20] Taniguchi N., On the Basic Concept of 'Nano-Technology', Proc. Intl. Conf. Prod. Eng. Part II, Japan Society of Precision Engineering, Tokyo 1974.
[21] https://pubs.rsc.org/image/article/2008/cs/b707318f/b707318f-f2.gif [access: 20.10.19].

eISBN 978-83-66531-55-0

Cracow University
of Technology